DE TTK

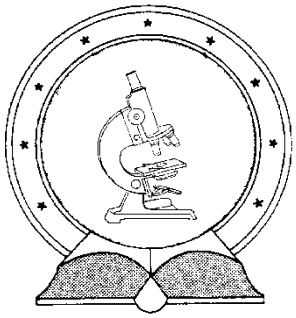

1949

Experimental and Modelling Studies on the Reactions of the Sulfate Ion Radical

Ph.D. thesis

Dóka Éva

Supervisor: *Dr. Gábor Lente*

UNIVERSITY OF DEBRECEN
Chemistry Graduate School
Debrecen, 2016

DE TTK

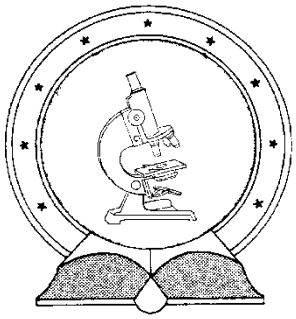

1949

Experimental and Modelling Studies on the Reactions of the Sulfate Ion Radical

Ph.D. thesis

Dóka Éva

Supervisor: *Dr. Gábor Lente*

UNIVERSITY OF DEBRECEN
Chemistry Graduate School
Debrecen, 2016

Ezen értekezést a Debreceni Egyetem Természettudományi Doktori Tanács Kémiai Doktori Iskola K/2 Koordinációs és Analitikai Kémia programja keretében készítettem a Debreceni Egyetem természettudományi doktori (Ph.D.) fokozatának elnyerése céljából.

Debrecen, 2016. május 27.

Dóka Éva

Tanúsítom, hogy Dóka Éva doktorjelölt 2012 - 2015 között a fent megnevezett Doktori Iskola K/2 Koordinációs és Analitikai Kémia programjának keretében irányításommal végezte munkáját. Az értekezésben foglalt eredményekhez és az ezekből született publikációkhoz a jelölt önálló alkotó tevékenységével meghatározóan hozzájárult. Az értekezés elfogadását javasolom.

Debrecen, 2016. május 27.

Dr. Lente Gábor

EXPERIMENTAL AND MODELLING STUDIES ON THE REACTIONS OF THE SULFATE ION RADICAL

Értekezés a doktori (Ph.D.) fokozat megszerzése érdekében
a Kémia tudományágban

Írta: ***Dóka Éva*** okleveles vegyész és alapokleveles matematikus

Készült a Debreceni Egyetem Kémiai Doktori Iskolája
(Koordinációs és analitikai kémiai programja) keretében

Témavezető: ***Dr. Lente Gábor*** egyetemi tanár

A doktori szigorlati bizottság:
elnök: Dr. Kövér Katalin egyetemi tanár (DE)
tagok: Dr. Tóth Ágota egyetemi tanár (SZTE)
Dr. Sóvágó Imre professor emeritus (DE)
A doktori szigorlat időpontja: *2016. március 8.*

Az értekezés bírálói:
Dr. .....
Dr. .....
Dr. .....
A bírálóbizottság:
elnök: Dr. .....
tagok: Dr. .....
Dr. .....
Dr. .....
Dr. .....
Az értekezés védésének időpontja: *2016.* .....

"In the end, everything will be OK. If it's not OK,
it's not yet the end."

/Fernando Sabino/

Acknowledgement

I would like to express my gratitude to all the people who helped me to achieve my goal and successfully finish my doctoral program.

First of all, I am mostly thankful to *Prof. Gábor Lente*, who has been my supervisor throughout my undergraduate and graduate studies, and my first mentor who started my scientific career. He introduced me to the theory and practice of chemical kinetics, as well as numerical modeling. Not only he is an outstanding scientist and a unique creative mind, but also a gifted teacher and a brilliant science writer.

I also thank *Prof. Fábián István*, the head of the Enviromental Reaction Mechanisms research group, for giving me the opportunity to make part of his team from the very beginning of my undergraduate studies and trying to turn my competitive spirit to my own and the group's advantage.

Over the time of my PhD program, I had a chance to carry out research in more than one exciting subjects, in different fields. I could employ my knowledge on solution phase kinetics studying redox biochemistry of thiol proteins. My current supervisor, *Dr. Péter Nagy*, is an inexhaustible source of motivation, who daily teaches me about various aspects of a scientist's life.

Dr. Mihály Bessenyei, my professor of mathematical analysis, was a key person behind my degree in mathematics. His inspiring lectures and personal guidance helped me many times to reach achievements beyond my self-esteem.

I would like to thank the former and current members of the *'D524 lab*', including our guest researchers, for creating a productive and friendly work environment. Special thanks to *Tamás Ditrói*, for his assistance with the laser flash photolysis experiments and MATLAB calculations.

My co-workers at the *Department of Molecular Immunology and Toxicology* supported me enormously in my challenges as a PhD student, never letting me to stop going forward.

I could not list all my friends and the communities I made part of throughout the years in Debrecen and Budapest who enriched my life and shared the happy and the cloudy moments with me. However, I here highlight the very special friendship that connects me to *Ágnes Dávid*.

Significant financial support was provided to me from a number of public foundations, Universitas Alapítvány, Pro Regione – Magyar Vidékért Alapítvány, DETEP Tehetséggondozó Program, Richter Gedeon Centenáriumi Alapítvány and Magyar Kémikusok Egyesülete. I was a grantee of the Apáczai Csere János Doktoranduszi Ösztöndíj within the Nemzeti Kiválóság Program and the Nemzet Fiatal Tehetségeiért Ösztöndíj in the framework of the Nemzeti Tehetség Program.

Last but not least, my family has always been my greatest support. My parents, *Erzsébet* and *Miklós*, truly deserve all of my gratitude for the loving background they created for me and my sister, *Zsuzsa*. My mom was also my first chemistry teacher, who made me love this beautiful field.

No words could thank you, *Peti*, for the last five years together and the great adventures we shared on the way. Your support was an amazing aid in the completion of this thesis.

Table of Contents

1. Introduction

Sulfur (S) is a nonmetallic element in the 16th group of the periodic table, a member of the oxygen family or *chalcogens*. The latter name is a hybrid of the Greek word χαλχος (*khalkos*, meaning *ore*) and the Latinized suffix '*-gen'*, meaning *born* or *produced*. This name implies that the first two elements of the group, oxygen and sulfur are highly frequent components of ores and minerals, oxygen being the most abundant element in the Earth's crust.[1] The chalcophile group within the Goldschmidt classification comprises the elements which are likely to form compounds with sulfur, mainly p and d block metals of soft character.[2,3] Sulfur is ubiquitous in Nature, it occurs mostly in the following forms:

- elemental sulfur in the cap rocks of salt domes or in volcanic eruptions
- H_2S in natural gas and sulfurorganic substances in petroleum
- sulfide ores of metals (PbS, FeS_2, CuS, ZnS, HgS etc.).[1]

Owing to the high abundance of the element, sulfur has been known since the ancient times. It is mentioned several times in the Bible as 'fire and brimstone',[*] in the context of hellfire and eternal misery. Maybe it is the malodorous smell and toxic nature of many sulfur compounds that earned the element such a negative reputation (although pure sulfur does not smell at all). Fire and brimstone also appears in the Greek classics Iliad and Odyssey, although Homer might have mistakenly refer to the smell of sulfur instead of the unpleasant odor of lightning-generated ozone.[4,5] The odor of skunk spray is also due to low molecular weight thiol compounds or mercaptans.

The origin of the name *sulfur* is obscure, the earliest appearances date back to early Latin culture of the first centuries BC. It is known not to be a Greek loan word, since Greek authors called the element *θεῖον* (*theion*, ancestor of the prefix *thio-* for sulfur containing compounds). Conceivably, the word developed from *sulpur* to *sulphur* and finally to *sulfur*. The spelling 'sulphur' persisted, especially in British linguistic environment, even though IUPAC standardized the 'f' spelling a few decades ago, without respect to geographical differences.[6,7]

Owing to its valence electron composition and catenation property, sulfur features versatile redox behavior with significant environmental aspects, biological relevance as well as industrial applications.

[*]The Lord tests the righteous and the wicked, And the one who loves violence His soul hates. Upon the wicked He will rain snares; Fire and brimstone and burning wind will be the portion of their cup. /Psalms 11:5-6/

Sulfur dioxide (SO_2) is one of the so-called criteria air pollutants. Detrimental effects of SO_2 gas necessitated the admission of upper limits of daily exposure, set by EPA (U. S. Environmental Protection Agency), to avoid potential human health and property damage.[8]

SO_2 is a gaseous compound that accumulates in the atmosphere by volcanic activity and from anthropogenic sources such as combustion of fossil energy carriers (due to sulfur contaminations in coal, petroleum and natural gas) and metallurgy.

Upon direct exposure, higher levels of sulfur dioxide cause respiratory irritation, induce bronchoconstriction[9] (shortness of breath due to the constriction of pulmonary airways) and increase the symptoms of asthmatic patients.[10] A slow-releasing SO_2 donor molecule, benzothiazole-sulfinate has recently been discovered, which facilitates the examination of the biological effect of inhaled and endogenously generated SO_2.[11]

On a global level, the major consequence of atmospheric SO_2 is the formation of acid rain or acid deposition.[12-17] Acid rain is rainwater with a pH below the natural value of 5.6, which is a result of the dissolution of atmospheric CO_2. Acidification of rainfall is a relatively modern phenomenon, the consequence of heavy industrialization of the last two centuries. Greenland ice layers from the 1800s have nearly neutral pH values. The pH decrease is aggravated by the formation of sulfuric acid from SO_2 according to eq. (1), the *autoxidation* of hydrated SO_2. Autoxidation is a generic term for the reactions where the reductant is oxidized by elementary oxygen from air. The prefix 'auto' refers to the fact that the oxidant is seldom added deliberately in these processes but is simply taken up from the environment.

$$2\ H_2O{\cdot}SO_2 + O_2 = 2\ HSO_4^- + 2\ H^+ \qquad (1)$$

The lowest pH value measured in rainwater was 1.5, detected in Wheeling, West Virginia, in 1979.[18] Heavy acid rains lead to extended deforestation, destruction of limestone mountains and man-made objects and buildings, such as the Taj Mahal in India, built entirely from marble.

A very interesting and scientifically challenging aspect of the stepwise formation of H_2SO_4 from sulfur and oxygen is the restoration of the Swedish warship *Vasa*, which sank on her maiden journey in 1628 and was conserved underwater until 1961, when the wreckage was salvaged from Stockholm harbor. Today the remains of the ship are exhibited in the Vasa Museet in Stockholm. The water which Vasa sank in was rich in sulfate reducing bacteria. Elementary sulfur, as well as sulfur compounds of intermediate oxidation states accumulated in the oak beams of the ship during the 333 years she spent submerged. Ever since the Vasa was brought to the surface, scientists struggle with the massive acidification of the skeleton because the iron in the bolts catalyzes the overall oxidation of sulfur to sulfuric acid.[19]

An initiative emerged in the field of geoengineering to counteract global warming based on the global dimming effect of stratospheric sulfate aerosols by the reflection of solar radiation. The concept would endorse the application of missiles and aircraft to deliver sulfur dioxide and other sulfur gases in the stratosphere, to act as sulfate precursors and thus increase the albedo (reflectivity) of the planet. However, the reception of such technological measures has been controversial because they do not replace consistent political and social engagement for the reduction of total greenhouse gas emission. In addition, the long-term harmful consequences of the extra sulfur burden are unpredictable.[20-22]

Atmospheric autoxidation of SO_2 drew considerable attention from inorganic chemists, and detailed mechanistic studies revealed that the intermediates of the autoxidation process are of radical nature (mainly $SO_3^{\bullet-}$, $SO_4^{\bullet-}$, $SO_5^{\bullet-}$).

In general, sulfate ion radical ($SO_4^{\bullet-}$) is one of the most broadly studied free radical in the literature, along with hydroxyl radical ($OH^{\bullet}$).[23-25] $SO_4^{\bullet-}$ is a highly reactive transient species with strong oxidizing power $E^{\circ}(SO_4^{\bullet-}/SO_4^{2-}) = 2.43$ V.

Recently, the role of sulfate ion radical in atmospheric aqueous phase chemistry has been investigated by Herrmann and co-workers.[23,26-29] $SO_4^{\bullet-}$ is considered as an oxidant in so-called advanced oxidation processes (AOPs) in water and wastewater treatment, in order to eliminate organic and inorganic contaminants.[30-35] Simultaneously, advanced reduction processes (ARPs) involve UV or ultrasound produced sulfite ion radical ($SO_3^{\bullet-}$) for the reductive degradation of harmful oxidized pollutants.[36] Sulfate ion radical derived oxidation also has biochemical applications. An efficient, tunable footprinting method was developed for monitoring global protein oxidation status. Original FPOP (Fast Photochemical Oxidation of Proteins) utilized $OH^{\bullet}$ as oxidant. The introduction of $SO_4^{\bullet-}$ as a footprinting agent is an improvement due to the slightly lower reactivity and higher target specificity compared to hydroxyl radical.[37]

The present thesis is dedicated to shed further light on the role of sulfate ion radical in the transition metal catalyzed and the iodide ion catalyzed, photoinitiated autoxidation of hydrated SO_2, and more generally, the autoxidation of S(IV). Traditional methods of aqueous solution kinetics are employed, as well as laser flash photolysis for the direct observation of $SO_4^{\bullet-}$. Computational simulations are carried out to study the potential effect of diffusion and spatial inhomogeneities during laser flash photolysis experiments.

2. Literature overview

2.1. Redox chemistry of sulfur

Sulfur has a valence electron configuration of $3s^2 3p^4$. Therefore, it can occur in compounds in (–2) – (+6) oxidation states (even numbers are preferred). Due to the wide range of available oxidation numbers, sulfur exhibits versatile redox chemistry. This section will focus on the redox characteristics of sulfur oxyacids and anions along with the derived sulfuroxy radicals.

Table 1. Sulfur oxyacids, conjugate oxyanions and the related free radicals.

Formula	Name of oxyacid	Oxidation state(s)	Conjugate anion	Related radical
H_2SO_4	sulfuric acid	VI	sulfate, SO_4^{2-} hydrogen sulfate, HSO_4^-	sulfate ion radical,[a] $SO_4^{\bullet-}$
$H_2S_2O_7$	disulfuric acid	VI	disulfate, $S_2O_7^{2-}$	
H_2SO_5	peroxomono-sulfuric acid	VI	peroxomono-sulfate, SO_5^{2-}	peroxomono-sulfate ion radical, $SO_5^{\bullet-}$
$H_2S_2O_8$	peroxodi-sulfuric acid	VI	peroxodisul-fate, $S_2O_8^{2-}$	
$H_2S_2O_6$	dithionic acid	V	dithionate, $S_2O_6^{2-}$	
$H_2S_{n+2}O_6$	polythionic acid	V, 0	polythionate, $S_{n+2}O_6^{2-}$	
$H_2S_2O_3$	thiosulfuric acid	IV, 0, (or II, II)	thiosulfate, $S_2O_3^{2-}$	
(H_2SO_3) $H_2O{\cdot}SO_2$	(sulfurous acid) hydrated sulfur-dioxide	IV	sulfite, SO_3^{2-} hydrogen-sulfite, HSO_3^-	sulfite ion radical, $SO_3^{\bullet-}$
$H_2S_2O_5$	disulfurous acid or pyrosulfurous acid	V, III	Disulfite; commonly known as metabisulfite or pyrosulfite, $S_2O_5^{2-}$	
$H_2S_2O_4$	dithionous acid	III	dithionite, $S_2O_4^{2-}$	

[a]alternative names: sulfate radical anion, sulfate radical

Table 1 gives a brief summary of these kinds of species in the order of decreasing oxidation number.[1] The stabilities of these acids and salts vary on a broad scale, e.g. free acid forms of dithionic, 'sulfurous' and dithionous acids are virtually nonexistent, they are mostly found in solutions and in salts as the conjugate oxyanions.

$H_2O{\cdot}SO_2$ and $SO_4^{\bullet-}$ are of utmost importance in the present thesis, their spectral and chemical features will be discussed in further detail in Sections 2.2 and 2.3. Pyrosulfate salts will be presented therein as a source of S(IV) species and other sulfuroxy radicals ($SO_3^{\bullet-}$, $SO_5^{\bullet-}$) as congeners of sulfate ion radical.

The sulfuroxy species presented in Table 1 participate in various redox equilibria. Standard electrode potentials of a few redox pairs are collected in Table 2.

Table 2. Standard electrode potentials of sulfuroxy ions and radicals

Redox couple[a]	**E° (V)**	**Redox couple[b,c]**	**E° (V)**
S/S^{2-}	-0.476	$SO_2/SO_2^{\bullet-}$	-0.17
S/H_2S_{aq}	0.142		-0.262
$S_2O_6^{2-}/H_2S_2O_3$	0.564		-0.288
$S_2O_8^{2-}/SO_4^{2-}$	2.010		-0.31
$S_2O_8^{2-}/HSO_4^-$	2.123	$SO_3^{\bullet-}/SO_3^{2-}$	0.63
$S_4O_6^{2-}/S_2O_3^{2-}$	0.080		0.72
$H_2SO_3/HS_2O_4^-$	-0.056		0.76
H_2SO_3/S	0.449		0.89
$SO_3^{2-}/S_2O_4^{2-}$	-1.120		0.73 ± 0.01[b]
$SO_3^{2-}/S_2O_3^{2-}$	-0.571	$SO_3^{\bullet-}/HSO_3^-$	0.84
SO_4^{2-}/H_2SO_3	0.172	$SO_4^{\bullet-}/SO_4^{2-}$	2.43
$SO_4^{2-}/S_2O_6^{2-}$	-0.220		2.52-3.08
SO_4^{2-}/SO_3^{2-}	-0.930		2.6
		$SO_5^{\bullet-}/HSO_5^-$	1.1
		$SO_5^{\bullet-}/SO_5^{2-}$	0.81 ± 0.02[b]
		$S_2O_6^{2-}/SO_3^{\bullet-},SO_3^{2-}$	-0.49
		$S_2O_8^{2-}/SO_4^{\bullet-},SO_4^{2-}$	1.39
		$S_4O_6^{\bullet3-}/2S_2O_3^{2-}$	1.07 ± 0.03[b]

a: ref.[38]; b: ref.[39] ; c: ref.[40] and references therein

SO_4^{2-} and HSO_4^- are the most frequent sulfur oxyanions in Nature. These are both very stable species, they are formed as oxidation products of sulfur compounds and during the decomposition of peroxodisulfate ions. Sulfate salts take part in the composition of particulate matter in the atmosphere. However, sulfuric acid, especially in its concentrated form, is a highly reactive, strong oxidizing agent, which is able to dissolve electropositive metals. Disulfuric or pyrosulfuric acid is found in fuming sulfuric acid (also known as oleum, oil of vitriol, or spirit of vitriol), it is formed by the dissolution of SO_3 in H_2SO_4.

Anhydrous peroxomonosulfate ion (H_2SO_5) is also called Caro's acid, it is one of the strongest oxidants known ($E°(HSO_5^-/HSO_4^-)$ = 1.84 V)[40]. Its conjugate anion, SO_5^{2-} is available as the composite salt Oxone® (registered trademark of DuPont), which has been recognized as a 'green' oxidizing agent as its reduction product is sulfate ion and with the possible by-product elementary oxygen.[41,42]

Peroxodisulfate ion ($S_2O_8^{2-}$) is generally used in the form of its water-soluble ammonium or potassium salts. Peroxodisulfate salts are utilized as oxidizing and bleaching agents and to initiate radical polymerization processes. Ammonium persulfate (APS) is the most common initiator in polyacrylamide gel electrophoresis.

$S_2O_8^{2-}$ has very high electrode potentials (see Table 2), thus it is expected to be a strong oxidizing agent, but its redox reactions are quite sluggish due to a kinetic barrier. Silver(I) ion has been proved to be a powerful catalyst of these reactions. They usually take place as chain reactions and their rate determining step is eq. (2), which is a one-electron transfer that produces highly reactive sulfate ion radical.[43-45]

$$Ag^+ + S_2O_8^{2-} = Ag^{2+} + SO_4^{2-} + SO_4^{\bullet -} \quad (2)$$

Dithionate ion ($S_2O_6^{2-}$) exhibits quite poor redox chemistry, it is highly inert under common circumstances. It cannot be protonated in the usual pH range, and it reacts even with strong oxidizing agents only at elevated temperatures. If it participates in a redox reaction, the first step is disproportionation in most cases, where sulfur(VI) and sulfur(IV) are the direct products and the latter can be oxidized rapidly by the oxidizing agent.[46]

Polythionates ($O_3S\text{-}(S)_n\text{-}SO_3^{2-}$ or $S_{n+2}O_6^{2-}$) are relatively stable sulfur oxyanions, containing a chain of zero-valent sulfur atoms as a linker between two SO_3^- groups. Polythionates are frequently found in crater lakes, and they were suggested to serve as efficient markers of forthcoming volcanic eruptions.[47]

Thiosulfuric acid has not been isolated so far, it is only known to exist in thiosulfate salts. $S_2O_3^{2-}$ ion is a medium strong reducing agent. It is extensively used in iodometric measurements in the laboratory practice and as dechlorinating agent in the textile industry.[48]

Dithionous acid is unstable both in its pure form and in aqueous solution, dithionites ($S_2O_4^{2-}$) can be isolated as anhydrous salts. In the presence of water, they disproportionate into sulfite and thiosulfate anions (especially in acidic medium). Sodium dithionite is used as a reducing agent in industrial dyeing procedures and for laboratory purposes as well.[49,50]

2.2. Autoxidation studies of sulfur(IV)

Table 1 and Table 2 in the previous section show that +4 is an intermediate oxidation state of sulfur. SO_2 is generally considered to be a moderate reducing agent, although depending on the reaction partner, it can be an oxidizing agent as well. A well-known example of the latter is the reaction between SO_2 and hydrogen sulfide, which is an important step of the Claus process (patented in 1883), used simultaneously for the desulfurization of crude oils and the production of elementary sulfur.[51]

The major occurrences of S(IV) atoms are sulfur dioxide (SO_2), hydrated sulfur dioxide, $H_2O{\cdot}SO_2$ and its deprotonated forms: HSO_3^- and SO_3^{2-} ions. S(IV) is also found in sulfurorganic molecules, such as sulfonic acids, sulfonates and sulfite esters.[52,53] The formula $H_2O{\cdot}SO_2$ is generally used to denote dissolved sulfur dioxide because there is no experimental evidence of the existence of the fully protonated H_2SO_3 molecule. The acid dissociation constant values for the subsequent deprotonation steps of $H_2O{\cdot}SO_2$ are $pK_{a,1} = 1.86$ and $pK_{a,2} = 6.34$.

The dimerization of sulfite ions into pyrosulfite or metabisulfite ions ($S_2O_5^{2-}$) at higher concentrations is a well-known phenomenon.[54] In aqueous medium, the dimeric anion is in equilibrium with the hydrogen sulfite ion, the $S_2O_5^{2-}$ form only occurs in concentrated solutions ($\geq$ 0.1 M). Therefore, it is convenient to prepare solutions of sulfite ions by dissolving pyrosulfite salts, e.g. $Na_2S_2O_5$.[55] In the subsequent sections of the thesis, the different deprotonated forms of $H_2O{\cdot}SO_2$ will be collectively referred to as 'sulfite ion' or simply S(IV).

The atmospheric autoxidation of S(IV), depicted in reaction (1) is the major source of acid rain formation. SO_2 can easily accumulate in rain droplets, as its water solubility is much higher compared to other atmospheric gases (Table 3).[38] Mole fractions are compared instead of the corresponding Henry's constants because the concentration of SO_2 passes through the limit of validity of Henry's law.[56] The solubility of sulfur dioxide is lower in acidic medium, which provides the basis of the identification of sulfite ions within the Fresenius system.[57]

Table 3. Mole fractions (X) of atmospheric gases in aqueous solutions. p = 1 atm, T = 25 °C[38]

	X
SO_2	2.9×10^{-2}
CO_2	7.1×10^{-4}
O_2	2.5×10^{-5}
N_2	1.3×10^{-5}

The kinetics and mechanism of the process represented by the overall equation shown in eq. (1) drew considerable attention from inorganic chemists, a significant amount of experimental findings have been published on this subject. Catalytic aspects, photochemical phenomena or the role of free radicals in the system have been discussed.

2.2.1. Transition metal ion catalysis in the autoxidation of sulfur(IV)

Numerous studies have revealed the role of transition metal ion catalysis in the oxidation of sulfur(IV) species. Kraft and van Eldik investigated the iron(III) catalyzed autoxidation of sulfur(IV) oxides and considered the possible role of metal-sulfito complexes in the mechanism.[58-61] A detailed kinetic and mechanistic analysis of the Fe(III)–S(IV)–O_2 system was published later on and proved the catalytic effect of iron(III).[62] Brandt and van Eldik examined the influence of pH, the medium and aging in independent experiments.[63] These authors also presented a comprehensive overview of the subject, focusing on atmospheric-relevant processes and mechanisms.[40] According to this summary, the majority of the published reaction mechanisms for the homogeneous transition metal catalyzed autoxidation of sulfur(IV) oxides suggest radical mechanisms that involve steps from the scheme given by Bäckström, who was the first to publish mechanistic observations on reaction (1).[55] He proposed a radical chain mechanism involving sulfoxy radical intermediates, which was supported by the fact that common radical scavengers inhibit the reaction. Fábián and Csordás reviewed the role of metal ions in autoxidation processes from kinetic and mechanistic points of view.[64]

Elding and co-workers examined the catalytic effect of manganese, chromium and vanadium ions, and they observed the emergence of iron-manganese synergism. They even considered gold(III) as a catalyst in S(IV) autoxidation based on a reduction study of Au(III) complexes by sulfite and hydrogen sulfite ions.[65-68] Alexander et al. reported that 9-17% of total sulfate production on Earth can be assigned to oxidation of S(IV) by O_2 catalyzed by Fe(III) and Mn(II).[69]

Coichev and co-workers studied the radical intermediates that are generated in the autoxidation process catalyzed by Co(II) and Cu(II) complexes, and their potential detrimental effects on DNA chains.[70,71] The catalytic effect of Cu(III) tetraglycine complexes on the autoxidation was found and studied by Anast and Margerum.[72] DNA damage examinations were also carried out by Burrows's team with Ni(II) and Mn(II) complexes.[73-75] Pioneering work on free radical induced DNA damage was presented by Clemens von Sonntag.[76]

2.2.2. Photochemical phenomena in the autoxidation of sulfur(IV)

Photoinitiated autoxidation in the presence of iron(II)

The autoxidation processes of sulfur(IV) in acidic aqueous solution have been extensively studied by Kerezsi et al.[55,77-79] They observed that the uncatalyzed or dark reaction is very slow. In the presence of Fe(II), the rate of the reaction increases, but it acts as an auxiliary reducing agent rather than a catalyst. The experiments have been carried out in a diode array spectrophotometer, which is a convenient tool for the simultaneous initiation and detection of the reaction. According to their results, the uncatalyzed autoxidation takes place through excited $H_2O{\cdot}SO_2$ and HSO_5^- intermediates and follows the stoichiometry indicated in eq. (1).[78]

The reaction rate is independent of the concentration of dissolved oxygen in the pH-range 0.0 – 1.67, but shows a well-defined dependence on light intensity and sulfur(IV) concentration.

In the presence of iron(II), the formation of iron(III) ions was detected, which may be interpreted by the simultaneous presence of two additional pathways. Both pathways contain the oxidation of iron(II) into iron(III) by one of the reaction intermediates. Figure 2.1 presents the suggested scheme of the reaction.

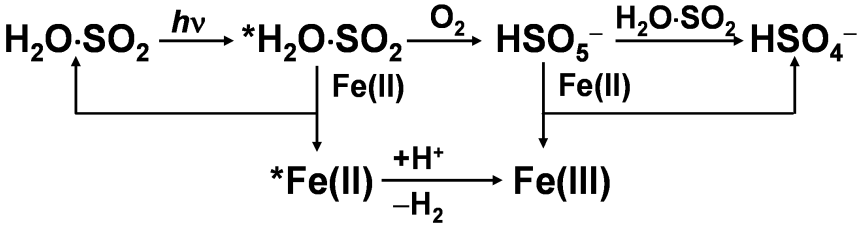

Figure 2.1. Photoinitiated autoxidation of sulfur(IV) in the absence and presence of iron(II) ions in acidic aqueous phase.

Catalysis by iodide ion

Photochemical effects on reaction (1) in the presence of I^- were similarly studied by the same research group.[79] The mechanism proposed by the authors is presented in Figure 2.2. A radical chain reaction occurs, where the absorption of S(IV) and iodide ion initiate the reaction. The rate of the net reaction depends on the concentrations of the components, pH and light intensity in a complex manner. The application of a diode array spectrophotometer allowed the use of the same light beam for excitation and detection as well.

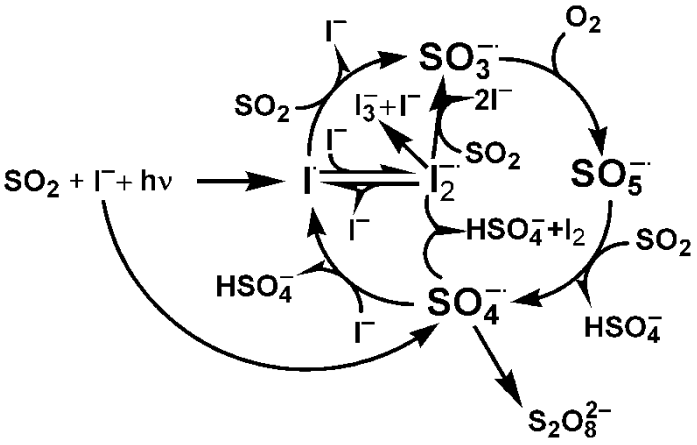

Figure 2.2. Photoinitiated, iodide-catalyzed autoxidation of sulfur(IV) in acidic medium.

Catalysis by cerium(III)

Ce(III) also initiates a chain reaction (Figure 2.3), where the first step is the production of Ce(IV) by light absorption.[77] Sulfite, sulfate and peroxomonosulfate radical anions are included in the mechanism as chain carriers. The reaction rate is proportional to the square root of the light intensity per unit volume. Ce(III) has a synergic effect on other catalytic reactions of sulfur(IV), which has been experimentally proved in Fe(III)–O_2–S(IV) system.

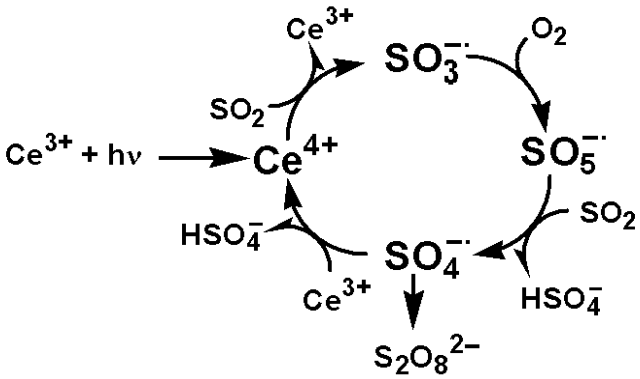

Figure 2.3. Photoinitiated, Ce(III)-catalyzed autoxidation of sulfur(IV) in acidic medium.

2.3. Spectral characteristics of sulfoxy radicals

Ever since the studies of Bäckström,[80-82] it is commonly accepted among the researchers of the field that sulfite autoxidation takes place via a chain reaction with the participation of free radicals as chain carriers. Bäckström applied an inhibition approach, and demonstrated the presence of free radicals by the inhibitory effect of alcohols. He also found that light has an influence on the reaction and he was the first one to suggest a detailed mechanism for the autoxidation process. However, his initial scheme has been refined several times over the decades.[40,65,74,77,83-85]

The real opportunity to examine the reactions of free radicals directly came with the introduction of the laser flash photolysis (LFP) and pulse radiolysis (PR) techniques.[86] Laser technology was invented in the late 1950s and radically transformed the landscape of the experimental studies of fast reactions (in addition to fundamental advances in many other fields). Norrish and Porter shared the Nobel Prize in chemistry with Manfred Eigen in 1967 for their studies of extremely fast chemical reactions.[87-89]

Basically, laser flash photolysis is a method for generating highly reactive intermediates, transient species or free radicals by the excitation of the samples (either in solution or gas phase) by a very short, high energy laser pulse. The concentrations of the transients reach a sufficient level to apply spectrophotometric detection to follow their absorbance over time and thus gaining kinetic information about their reactions.[86,90-95] For a more detailed description of LFP instrumentation used in the present thesis, the interested reader is referred to Section 4.2.2.

The time resolution of flash photolysis has improved significantly over the past decades. In the original method, plasma flash light was able to give a pulse of the order of a few microseconds.[89] The implication of high energy lasers as flash light sources made it possible to achieve nanosecond and subnanosecond time scales. The pulse widths of commonly used lasers lay in the order of 10 ns. Laser pulses may be shortened by Q-switching and mode-locking techniques.[96] Femtosecond spectroscopy operates with extremely short pulses (about 100 fs) nowadays. The Nobel Prize in chemistry in 1999 was awarded to A. Zewail for his results in femtosecond spectroscopy.[97]

Figure 2.2 and Figure 2.3 show the roles of $SO_4^{\bullet-}$, $SO_3^{\bullet-}$ and $SO_5^{\bullet-}$ in the autoxidation mechanisms in the presence of different catalysts. Hereinafter, an overview of the reactivity of these species is given in relation to the autoxidation processes and beyond. For further information, the reader is invited to consult comprehensive collections for transient absorption spectra[98] and published rate constants[99] for a vast number of free radicals.

The reactions of sulfate ion radical ($SO_4^{\bullet-}$) have been extensively studied ever since the 1960s. Dogliotti and Hayon were the first ones to find that flash photolysis of persulfate anion ($S_2O_8^{2-}$) leads to the formation of $SO_4^{\bullet-}$ according to eq. (3).[100,101]

$$S_2O_8^{2-} \xrightarrow{h\nu} SO_4^{\bullet-} \quad (3)$$

They found that $SO_4^{\bullet-}$ has an absorption maximum at 4550 Å (455 nm), a half-life of ~300 μs and shows second order decay with a rate constant of 3.7×10^8 M^{-1} s^{-1}. The broad band around 450 nm in the transient absorption spectrum of the sulfate ion radical has been reproduced by several authors later,[83,102-105] but there are still some discrepancies in the value of the corresponding molar absorption coefficient.

According to the integrated rate law of a second order self-reaction (2A = P), the determination of the second order rate constant from photometric data requires the molar absorption coefficient (ε) of the recombining species. (Second order fitting and the meaning or the parameters are discussed below in Section 4.3.1).

The determination of the molar absorption coefficients of free radicals is not as straightforward as it is for stable absorbing species.[106] In laser flash photolysis experiments, the main difficulty is the inhomogeneous distribution of the transient species in the photolysis cell. The transients are generated along the path of the laser beam, which is getting attenuated when passing through the sample, thus producing a concentration gradient. In order to keep the effect of spatial inhomogeneity at a minimum level, the concentrations of the solutes should be chosen in a way that the measured absorbance would fall below 0.1. On the other hand, the cost of such a low absorption of the solution is the quite poor signal to noise ratio of the laser flash photolysis curves. Generally, 6-10 repeats should be averaged from the same transient absorption curve to obtain a decent kinetic curve that can be fitted within a reasonable error limit. Targeting the analyzing or probe beam right to the front face of the cuvette containing the excited samples is another possibility to deal with the inhomogeneity issue experimentally. Further discussion and some theoretical considerations will be presented in Sections 2.4 and 5.3.

Several direct and indirect methods can be used if transient concentrations need to be estimated from optical absorption data.

i. the transient is formed from a precursor of known concentration
ii. the transient is converted into a new species whose concentration is measurable
iii. transient concentration can be obtained following its build-up over time
iv. the concentration is measured directly and not calculated from absorbance

In methods (i) and (ii), the yield of conversion has to be well known to make a valid estimation.

Dogliotti and Hayon gave a value of 460 ± 25 M^{-1} cm^{-1} for $\varepsilon(SO_4^{\bullet-})$ at 455 nm, which they found to be in good agreement with vacuum UV photolysis results.[100] They used the reaction of $SO_4^{\bullet-}$ with hydrogen carbonate ions (4) to convert the $SO_4^{\bullet-}$ radical quantitatively into carbonate ion radicals, which were known to absorb at 600 nm.[107-111]

$$SO_4^{\bullet-} + HCO_3^- = SO_4^{2-} + CO_3^{\bullet-} + H^+ \quad (4)$$

A molar absorption coefficient value of $\varepsilon(CO_3^{\bullet-})_{600\,nm} = 1830 \pm 30$ M^{-1} cm^{-1} was applied in their calculations. This is an averaged value based on previous results of several authors. Adams, Boag and Michael reported a value of 1800 M^{-1} cm^{-1}, using ferrocyanide dosimetry.[107-109] Weeks and Rabani obtained a similar value, $\varepsilon(CO_3^{\bullet-})_{600\,nm} = 1860 \pm 160$ M^{-1} cm^{-1} from pulse radiolysis experiments and ferrocyanide actinometry.[111] Eriksen, Lind and Merényi later revisited the spectral characteristic of carbonate ion radical, and they also found a good agreement with the former values. From 30 independent PR experiments using thiocyanate (SCN^-) dosimetry, they calculated that $\varepsilon(CO_3^{\bullet-})_{600\,nm} = 1910 \pm 40$ M^{-1} cm^{-1} in air saturated solution at pH 11.4.[112] Considering the comparable data of the above mentioned authors, $\varepsilon(CO_3^{\bullet-})_{600\,nm} = 1830 \pm 30$ M^{-1} cm^{-1} used by Dogliotti and Hayon was a reasonable assumption.

Hayon, Treinin and Wilf carried out a thorough investigation of the autoxidation of sulfite in aqueous solution and improved the chain mechanism of Bäckström by introducing sulfate ion radical as a chain carrier.[83] They reported detailed spectroscopic features for sulfuroxy radicals ($SO_x^{\bullet-}$, x = 2-5). In their study, $SO_4^{\bullet-}$ was generated by the pulse radiolysis of $S_2O_8^{2-}$ ions in the absence of oxygen and found to absorb with a peak at 450 nm. Huie and Clifton revisited the radiolysis and photolysis studies of Hayon et al. and included new rate constants for the reactions of $SO_2^{\bullet-}$ radical.[113] Both groups used a molar extinction coefficient value $\varepsilon(SO_4^{\bullet-})_{450\,nm} = 1100$ M^{-1} cm^{-1} by Roebke et al.[114]

Lesigne et al. irradiated concentrated sulfuric acid solutions to generate sulfate ion radical and found that the radiolytic yield of $SO_4^{\bullet-}$ (denoted as G(SO4) - radiolytic yield (or G-value) is the number of a certain transient species produced (or destroyed) per unit of absorbed energy (generally number or mole per 100 eV)[115]) is linearly dependent on the electron fraction (electron to nucleon ratio[116]) of the solute sulfuric acid.[102] The authors suggested a detailed scheme for the apparent second order decay of sulfate ion radical.

As an interesting cosmological aspect, radiolytic results of sulfuric acid ices were applied to the conditions of Jupiter's moon Europa and it was implied that altering SO_2 concentrations on the chaos terrains are due to the decreased hydration of H_2SO_4.[117]

Tang and co-workers used 248 and 266 nm laser flash photolysis combined with time-resolved long path absorption detection (LFP-LPA) in kinetic and spectroscopic studies of the sulfate ion radical. They created an experimental arrangement where the laser beam passes through the excited solution several times, thus producing longer optical path length. This setting allowed them to minimize the required concentration of $SO_4^{\bullet-}$ and to avoid unwanted side reactions. The determination of the absorbed number of photons per unit volume of the sample was facilitated by a photolysis light source with spatially uniform intensity distribution. They reported that $\varepsilon\Phi = 2770 \pm 170$ M^{-1} cm^{-1} where ε is the molar absorption coefficient of $SO_4^{\bullet-}$, and Φ is the quantum yield of the production of the radical from $S_2O_8^{2-}$ ions. Assuming $\Phi = 2$, the obtained $\varepsilon = 1385$ M^{-1} cm^{-1}, which was close to the middle of the range of previously reported data.[103] This paper also contains a summarizing table (Table 2) comparing all published molar extinction coefficients for sulfate ion radical, ranging from 460 to 1600 M^{-1} cm^{-1}.

According to the results of laser flash photolysis experiments carried out by McElroy, $\varepsilon(SO_4^{\bullet-})_{450\,nm} = 1600 \pm 100$ M^{-1} cm^{-1}.[105,118] He used the oxidation of chloride ion by sulfate ion radical into chlorine molecule anion, and assumed the spectral features of Cl_2^- to be known.

In general, sulfate ion radical is one of the most broadly studied free radicals in the literature, along with hydroxyl radical ($OH^{\bullet}$).[23-25] A comprehensive collection of rate constants for reaction of inorganic radicals was released by the National Institute of Standards.[99] Relevant publications for the reactions of sulfate ion radical studied in the present thesis are going to be cited throughout Section 5.2.

Fundamental work on other sulfuroxy radicals, such as $SO_3^{\bullet-}$ was also conducted by Dogliotti and Hayon. Upon the flash photolysis of Na_2SO_3, they detected a transient species absorbing at 275 nm that they assigned as $SO_3^{\bullet-}$ and assumed that it is one of the products of the primary photoionization of sulfite, as shown in eq. (5).

$$SO_3^{2-} \cdot H_2O \xrightarrow{h\nu} SO_3^{\bullet-} + e_{aq}^- \qquad (5)$$

They identified the 275 nm band as a CTTS transition and provided EPR spectrum of sulfite ion radical. The same spectral behavior was observed during the photolysis of dithionate ($S_2O_6^{2-}$) solutions, suggesting that sulfite ion radical can also be generated by the homolytic

scission of the S-S bond. The identical nature of the transient species from the direct photolysis of SO_3^{2-} and the excitation of dithionate ions is further corroborated by the fact that the observed second order decay rate constants are equal within experimental error ($k/\varepsilon = (3.5 \pm 2.0) \times 10^6$ and $(2.0 \pm 1.0) \times 10^6$ s^{-1} cm, respectively).[119,120]

Pucheault and Ferradini assessed the role of superoxide anion in the autoxidation mechanism by means of γ-radiolysis and concluded that the Haber-Weiss reaction (between superoxide and H_2O_2, producing hydroxyl radicals) has a potential chain propagation role, by increasing the production of sulfite ion radicals.[121]

Sulfite ion radical ($SO_3^{\bullet-}$) has important biochemical relevance as it is the primary product of sulfite oxidation in the body by one-electron mechanism. Two-electron sulfite oxidation to sulfate ions also takes place in humans, catalyzed by the sulfite oxidase enzymes, where the electron acceptor is the Mo^{VI} center of the enzyme.[122,123] A nice summary of the free radical aspects of sulfite oxidation was given by Neta and Huie, including the metabolic fate of inhaled or consumed sulfites.[124] Two possible ways of radical formation out of sulfite is mentioned. The first is the somewhat more obvious one, autoxidation of S(IV) in the lungs and elsewhere in the respiratory system, potentially catalyzed by trace metal ions present. The other considered pathway is the formation of S-sulfocysteine ($RSSO_3^-$) in the blood, and the subsequent reduction to thiolates and sulfite ion radical. Rate constants for $SO_3^{\bullet-}$ and other sulfoxy radicals with organic and biomolecules are collected.

Further kinetic data for the reactions of $SO_3^{\bullet-}$ with different biomolecules was published by Erben-Russ et al.[125-127] $SO_3^{\bullet-}$ was generated by the reaction of sulfite with hydroxyl radicals, in pulse radiolysis experiments and it was reported to absorb at 260 nm. This band overlapped with the absorption of the substrates. Therefore, a competition kinetic method was applied. The carotenoid molecule crocin was found to be the most suitable competing agent at physiological pH. The upper limit of second order rate constants between sulfite ion radical and nucleobases was found to be 1×10^6 M^{-1} s^{-1}, rendering it unlikely that the previously observed DNA damage from sulfite autoxidation is due to direct effect of $SO_3^{\bullet-}$. The lower limit of rate constants with polyunsaturated fatty acids (PUFAs) was estimated to lie in the same range.

Numerous peroxidases are reported to catalyze one electron oxidation of (bi)sulfite,[128-133] confirmed by spin-trapping and ESR spectroscopy.[134] Sulfoxy radicals produced by these processes are suggested to correlate with radical induced protein damage and respiratory irritation by SO_2.

A detailed kinetic and spectroscopic analysis of sulfite anion radical and its decay mechanisms was given by Waygood and McElroy.[135] Laser flash photolysis of sodium dithionate ($S_2O_6^{2-}$) solutions at 193 nm led to the formation of $SO_3^{\bullet-}$ and SO_3^{2-}. They reported that the decay of sulfite ion radical is second order with a limit rate constant of $(4.0 \pm 0.3) \times 10^8$ M^{-1} s^{-1} and takes place by the simultaneous recombination into dithionate ion and self-reaction into sulfite ion and SO_3. The relative rate constant of reaction (6) compared to (7) was found to be 0.8 ± 0.2.

$$SO_3^{\bullet-} + SO_3^{\bullet-} = S_2O_6^{2-} \quad (6)$$

$$SO_3^{\bullet-} + SO_3^{\bullet-} = SO_3^{2-} + SO_3 \quad (7)$$

Warneck and colleagues studied the steady state photolysis of SO_3^{2-} and HSO_3^- at 254 nm and analyzed the possible free radical reactions, rate constants and product distribution in the presence and absence of dissolved oxygen.[136,137]

The literature of peroxomonosulfate radical ($SO_5^{\bullet-}$) is limited compared to the previously discussed congeners, although due to rapid interconversion reactions, the separate investigation of these radicals is barely feasible. Practically all free radical studies connected to S(IV) autoxidation mentioned earlier deal with the parallel occurrence of $SO_3^{\bullet-}$, $SO_4^{\bullet-}$ and $SO_5^{\bullet-}$ radicals, some of them with $SO_2^{\bullet-}$ as well. The radical is most likely generated by the oxygen addition of sulfite ion radical and decays by several radical-radical and radical-stable species reactions. A paper from T. N. Das focuses mainly on $SO_5^{\bullet-}$ radical, re-evaluating its role in sulfite autoxidation chains in liquid hydrometeors.[138] $SO_5^{\bullet-}$ radical shows a weak absorption band between 260-265 nm with a molar absorption coefficient of 1065 ± 80 M^{-1} cm^{-1}.

2.4. Effect of inhomogeneities in fast reaction kinetics

As mentioned in the previous section of this thesis, the inhomogeneous distribution of the transient absorbing species in the sample is a typical characteristic of laser flash photolysis experiments. This fact should be taken into account during the acquisition and processing of transient absorption data. Sample inhomogeneities can lead to distorted conclusions, especially when the kinetic trace detected is not an exponential curve. Whenever possible, setting pseudo-first order conditions is desirable in order to avoid the usage of actual transient concentrations.

Only a handful of papers deal with the experimental and/or mathematical treatment of potential inhomogeneity issues and the resulting errors in kinetic conclusions.

At the dawn of the flash photolysis technique, J. W. Boag analyzed the effect of non-uniform distribution of initial transient concentration along and across the analyzing light beam.[139] He considered first and second order reactions and made an effort to give analytical expressions for the difference between the actual and the experimentally determined rate constants. He assumed certain shapes of the initial distribution (see Figure 2.4) and used practically conceivable parameters, such as total absorbance between 0 and 2 (typically 0.4-0.6), $h > 0.5$, experimental time length at least 4-5 half-life of the observed species. He concluded that first order reactions are less influenced by initial distributions, and with the above parameter values, the difference between $\bar{k}$ (as he assigned the observed rate constant) and k (the actual value) is less than 1%. It is worth noting that he used the linearized versions of the integrated rate laws (which is a source a statistical distortions itself) in his deductions and ignored diffusive motion of the particles within the experimental time.

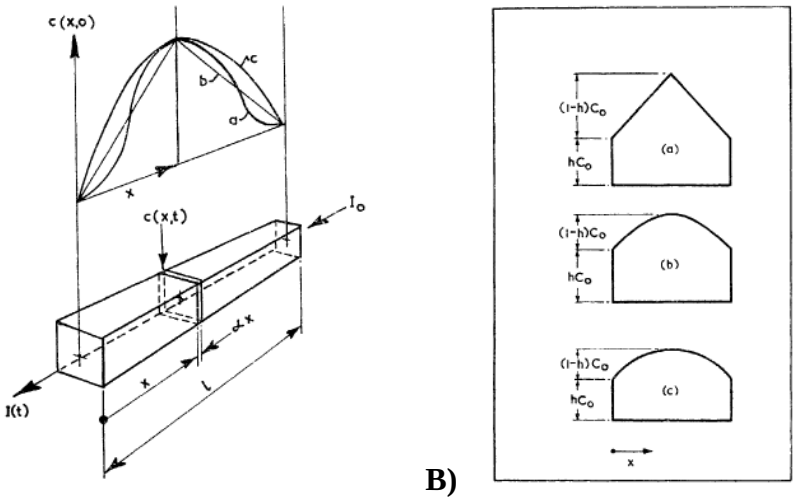

A) **B)**

Figure 2.4. Initial distribution of transient concentration along the analyzing light beam in flash photolysis experiments. **A)** Extreme cases. a = (sine)^2, b = triangular, c = sine distribution; I_0 = incident light intensity; $I(t)$ = exit light intensity at time t. **B)** Expected practical distributions. (a) triangular cap; (b) sine cap; (c) parabolic cap. The parameter h is the ratio between the minimum and maximum of initial concentration ($0 \leq h \leq 1$). Figures adapted from Boag, *Trans. Faraday Soc.* 1968, Figs. 1 and 4.[139]

Bazin and Ebbesen studied the error originating from a poor overlap between the laser beam and the analyzing (or probe) beam in given experimental arrangements of laser flash photolysis. They introduced two kinds of correction factors for such bad overlaps in the laser and probe directions, and provided technical advice on how to detect them.[140]

Instead of considering actual kinetic measurements, they focused on the deviation of the measured absorbance (OD_{exp}) from the real value (OD_{true}). Figure 2.5 shows the possible sources of insufficient overlap between the two light beams.

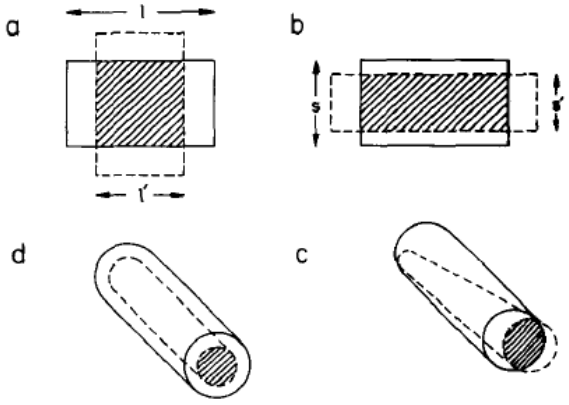

Figure 2.5. Examples of bad overlap situations in laser flash photolysis experiments. The solid line represents the analyzed space, the dashed line delineates the laser beam. The hatched area shows the overlap. (a) and (b): perpendicular, (c) pseudo front face, (d) collinear arrangement. (the reader might notice that the panels are labelled clockwise instead of row-continuously). Figure adapted from Bazin and Ebbesen *Photochem. Photobiol.* 1983, Fig. 1.[140]

The authors assigned *x* and *y* for the fractions not covered by the complementary beams for cases (a) and (b) in Figure 2.5. With the notations of the figure,

$$y = \frac{l - l'}{l} \qquad \text{and} \qquad x = \frac{s - s'}{s}; \qquad 0 \le x, y < 1,$$

and the relation between OD_{true} and OD_{exp} is given in eq. (8).

$$OD_{true} = OD_{exp} \times SF(x,y) \times DF(x) \tag{8}$$

SF values are the scale factors $1/(1 - x)$ and $1/(1 - y)$, the proportionality factors for bad overlap across and along the analyzing direction, respectively. An important outcome of their calculations is that the ratio OD_{true}/OD_{exp} increases with OD_{exp}, and they defined a distortion factor (DF) as the ratio of the relative errors at high and low experimental value.

$$DF = \left(\frac{OD_{true}}{OD_{exp}}\right) / \left(\frac{OD_{true}}{OD_{exp}}\right)_{OD_{exp} \to 0} \tag{9}$$

DF is only a function of *x* and not *y*, in the case of bad overlap along the light path, OD_{true} is always linearly dependent on OD_{exp}. They suggest that DF tends to cause more trouble in data processing, which confirms that it is preferable to work with low absorbance values, as long as the signal-to-noise ratio is acceptable.

Cassidy and Long created a mathematical model to test the validity of experimental rate constants determined under putative pseudo-first order conditions.[141] The underlying chemical

systems were laser flash photolysis studies of CO photodissociation reactions from transition metal carbonyl complexes and the subsequent coupling of the ML_6 and ML_5 forms.

$$M(CO)_6 \xrightarrow{h\nu} M(CO)_5 + CO \quad (10)$$

$$M(CO)_6 + M(CO)_5 \xrightarrow{h\nu} M_2(CO)_{11} \quad (11)$$

Their model implies that $M(CO)_5$ is generated by a laser beam of circular cross section and monitored by a second beam in collinear arrangement, in a cylindrical volume. $M(CO)_5$ concentration decays reaching zero at the far face of the cuvette, and the absorbance can be calculated from Beer's law. They also considered the diffusion of $M(CO)_5$ molecules outside of the monitored volume in the case where reaction (11) is sufficiently slow. Mathematically, this system could be described by two-dimensional diffusion equations coupled to a second order reaction. All diffusion coefficients were supposed to be equal.

It was assumed that $M(CO)_6$ is in high excess compared to $M(CO)_5$ and the second order rate constant of eq. (11) was calculated by the traditional pseudo-first order method (plotting k_{obs} as a function of $[M(CO)_6]$, the obtained slope is k). The percentage differences were given between $\log(k_{calc})$ and $\log(k_{input})$ values, where k were used as an input parameter in the model.

Upon considering different kinds of concentration inhomogeneities and parameter sets, the following conclusions were drawn from their results:

i. when the relative concentration of $M(CO)_5$ was high (violating pseudo-first order conditions), the diffusion outside the cylinder started to interfere below $k_{input} = 10^7\ M^{-1}\ s^{-1}$, causing up to 14% decrease
ii. inhomogeneous distribution along the light path (due to Beer's law) did not cause any distortion, as long as the high excess of $M(CO)_6$ was maintained
iii. when a Gaussian beam profile was used for the excitation pulse, diffusion caused errors below $10^7\ M^{-1}s^{-1}$, at low relative concentration of $M(CO)_6$;
iv. as an interesting complementary information, the pseudo-first order plot for the determination of k_{calc} was always perfectly linear, even if high errors were found between $\log(k_{calc})$ and $\log(k_{input})$. Therefore, the correlation coefficient in this case was not a good indicator for testing pseudo-first order behavior.

The results of the above described model calculations were not compared to experimental data because LFP measurements were carried out with perpendicular arrangement.

Sample inhomogeneity issues can be assessed by experimental approaches as well. Bonneau and co-workers published a detailed manual for the collection and analysis of transient

absorption data and emphasized the importance of correct instrument geometry and inhomogeneous transient distributions. They suggested that a mirror should be placed at the side of the sample opposite to the laser excitation spot in order to reflect the pumping light back and thus increase the absorbed fraction of light and offset inhomogeneities at the same time.[142]

Goez et al. realized the idea above, although they used a solid corner-tube retroreflector instead of a mirror, in order to reduce Beer inhomogeneity (caused by absorption along the light path of the laser).[143] Retroreflectors are less sensitive to alignment imperfections than mirrors and make it possible to carry out measurements at different wavelengths without changing the mirror. The incident and the reflected beams were mixed with the aid of the retroreflector which had double beneficial effect: the total absorbed intensity increased and the Beer inhomogeneity decreased (the former by a factor of 1.45-1.65, the latter 2.6-4.8-fold). They found a very simple relation between these two effects. According to their calculations and measurements, in the presence of the retroreflector, the absorbed intensity increased by a factor of θ, then the total decrease of inhomogeneity equals $2/\theta$-1. Distortions arising from the Gaussian beam profile also improved a little by this method, but the authors pointed out that beam shapers or easier experimental settings could correct for the non-uniformity of the beam.

Solution inhomogeneities tend to cause distortions in stopped flow (SF) measurements as well, although the source if the non-uniform distribution of concentrations is conceptually different than the ones connected to flash photolysis experiments. In the case of the stopped flow technique, the inhomogeneity arises from the fact that the mixture of the reacting components needs a certain time to fill the observation cell (filling time). For very rapid reactions, whose half-life is comparable to the filling time of the instrument, a significant difference can be formed between the front and the far face of the observation cell (see Figure 2.6). Rorabacher and colleagues developed mathematical models to resolve second order rate constants of such rapid reactions, taking into account the concentration gradient under appropriate conditions. First, they treated irreversible second order reactions, choosing an arbitrary 'zero time' of the measurements. They managed to determine a rate constant of 7×10^6 M^{-1} s^{-1} this way.[144] Their model was later improved to remove the reversibility and starting time restrictions and the rate constant limit shifted up by an order of magnitude.[145] Finally, they completed their results by another gradient-corrected approach, where they used the steady state absorbance forming in the flow cell before the cessation of the flow.[146] The resolved rate constants of both methods, as well as a non-corrected second order treatment for the sake of comparison, were carefully analyzed using fast reactions of transition metal complexes as an experimental model. The rate constants of the latter were predicted from the Marcus theory.[147]

As a conclusion, second order rate constants of magnitude up to 10^8 M^{-1} s^{-1} became available from stopped flow measurements for reactions whose half-lives are less than one half of the instrument dead time (the time required for the solution to travel the distance $x + l$ in Figure 2.6).

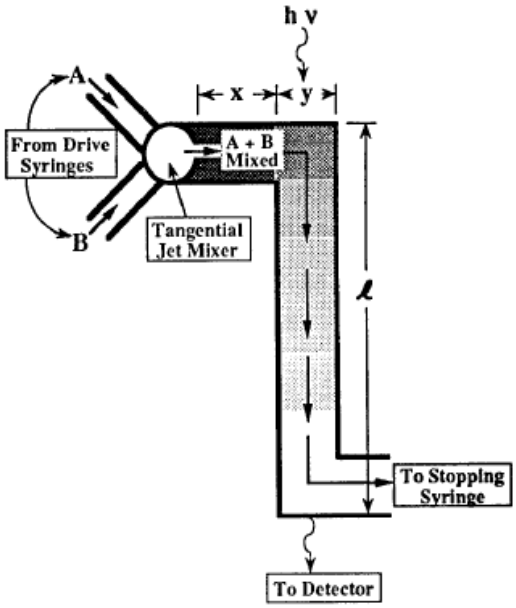

Figure 2.6. Scheme of sample concentration gradient in a stopped flow experiment. Figure adapted from Dunn et al. *J. Phys. Chem.* 1996, Fig. 1.[146]

Considering the sub-nanosecond to millisecond time resolution of the laser flash photolysis technique, it has important overlap with the stopped flow method from the point of view of the order of magnitude of the accessible rate constants. However, the major differences between these techniques still hold, i.e. stopped flow deals with ground state species (even if very short lived), whereas LFP operates with transient species generated by the high energy laser pulse. The laser generation method eliminates the need for manual or instrumental mixing. On the other hand, the 'batch' characteristic of LFP measurements is a technical limitation. The point is that all ground state molecules are located in the cuvette at the moment of the laser pulse. Therefore, the effect of the laser on all components has to be tested individually before observing a radical reaction and sometimes it is impossible to isolate a certain component to absorb the total amount of laser energy.

3. Research objectives

The present thesis is dedicated to shed further light on the role of sulfate ion radical in the transition metal catalyzed autoxidation of hydrated SO_2, more generally, autoxidation of S(IV). The catalytic effect of silver(I) ions in the presence of peroxodisulfate ($S_2O_8^{2-}$) ions is investigated. Traditional methods of aqueous solution kinetics are employed, as well as laser flash photolysis technique for the direct observation of $SO_4^{\bullet-}$. Computational simulations are carried out to study the potential effect of diffusion and spatial inhomogeneities during laser flash photolysis experiments.

4. Experimental methods

4.1. Materials

All chemicals used in this study were of analytical reagent grade and were purchased from commercial sources. Sodium sulfite stock solutions were prepared freshly from $Na_2S_2O_5$ (Reanal) every day. Whenever necessary, pyrosulfite solutions were deaerated by bubbling Ar (purity > 99.95%) for at least 15 min in order to increase the reproducibility of measurements under anaerobic conditions.

Potassium peroxodisulfate stock solutions were prepared from $K_2S_2O_8$ (Reanal). This solution was oxygenated during the O_2-dependent experiments. Silver(I) catalyst solutions were prepared by dissolving a weighed amount of $AgNO_3$ (Reanal) to a known final volume. Doubly deionized and ultrafiltered water from a Millipore Q system was used in the entire work. Most of the experiments were carried out at high and constant acid concentration (0.10 or 0.33 M sulfuric acid). Therefore, additional salt was not used to adjust the ionic strength.

4.2. Instrumentation and softwares

4.2.1. UV-vis spectrophotometric experiments related to S(IV) autoxidation

UV-vis spectra were recorded on a Perkin Elmer Lambda 2S or a Perkin Elmer Lambda 25 scanning spectrophotometer. Kinetic experiments were carried out in standard quartz cuvettes (optical path length = 1.000 cm). The overall sample volume was 3.00 cm^3 in each case. Constant temperature (25.0 ± 0.1 °C) was maintained with an external thermostat and circulating thermal bath.

Samples were prepared by the following method. Required aliquots of pyrosulfite, peroxodisulfate and sulfuric acid solutions were mixed with water and thermostated for 3-4 min. The process was started by adding the catalyst immediately prior to commencing the detection in the spectrophotometer.

Reaction rates were determined by linear fitting of data curves. One can calculate the actual rate from the slopes of absorbance versus time functions by using the molar absorption coefficient of sulfur(IV), known from independent experiments. From a mathematical point of view, the rate determination requires numerical differentiation. Under the usual conditions, the accuracy of reaction rates are ±10%, indicated by the error bars in Figure 5.3-Figure 5.7Figure 5.9. In the silver(I) catalysis study, another method was applied to compute the reaction rates (which were fairly constant within a single experiment) and compare them with the results of numerical derivation. The slopes of the sections preceding the break point were calculated (see

Figure 5.2) The absorbance change can be transferred into concentration change by dividing it with the (apparent) molar absorption coefficient valid at the pH of the reaction system. The main advantage of the latter method is that it avoids the possible problems arising from imperfect thermostating, which may occur at the beginning of experiments.

Reaction rates determined with the two different methods were in very good agreement, and we used the results of the method of initial rates in the final calculations.

4.2.2. Laser flash photolysis measurements

Laser flash photolysis (hereafter referred to as LFP) experiments have been carried out in an LKS.60 nanosecond transient absorption spectrometer, shown in Figure 4.1.

Figure 4.1. Applied Photophysics LKS.60 nanosecond laser flash photolysis instrument

The instrument is equipped with a Quantel Brilliant Nd:YAG laser along with its second, third, fourth and fifth harmonic generators (referred as SHG, THG, FoHG, FiHG). Nd:YAG (Neodymium doped yttrium aluminum garnet) is a common solid-state laser type, where the lasing medium is a $Y_3Al_5O_{12}$ crystal doped with 0.1-1% Nd^{3+}. The primary wavelength of an Nd:YAG laser light is 1064 nm, its harmonics emit at 532 (2nd), 355 (3rd), 266 (4th) and 213 nm (5th). Harmonics are generated by specific crystals that exhibit non-linear optical effects. Common non-linear crystals are KDP, DKDP, $LaTiO_3$, $BaTiO_3$ etc.

Table 4. Specification of the fourth harmonic of Quantel Brillant Nd:YAG laser

Wavelength	266 nm
Pulse length (full width at half maximum)	6 ns
Repetition rate	10 Hz
Energy per pulse (max.)	40 mJ
Beam diameter	6 mm
Q-switch	ON

In the present thesis, the fourth harmonic of the Nd:YAG laser was used to generate sulfate ion radicals and other transient species. Table 4 contains the characteristic features of the laser beam. Unfortunately, the fifth harmonic generator reduced the energy of the laser pulse too much and it could not be employed for any practical purposes in this study.

Q-switching is a frequent technique applied to increase laser power by shortening the laser pulse. Originally, the Q-factor (or quality factor) is a term of electronics, it describes the goodness of an RLC circuit. Q-switching is realized by a Pockels-cell in the LKS.60 instrument.

The analyzing light source was a 150 W ozone free xenon arc lamp (OSRAM 150W/CR OFR) and its light beam entered a 1.00 × 1.00 cm fluorescence quartz cuvette. We have implied cross-beam excitation, the probe beam and the laser beam were introduced into the sample in a perpendicular arrangement. The cuvette was placed in an adjustable sample holder, which was positioned horizontally so that the analyzing light beam hit close to the front face of the cuvette where laser beam entered. This is an important setting as the concentration of transient species generated by the laser excitation typically decreases rapidly with the distance from the front window (see also Section 5.3.7.).

A programmable f/3.4 grating monochromator with a symmetrical Czerny-Turner optical configuration was combined with a R928 photomultiplier for the transient signal detection at different wavelengths. Data points were collected by an Agilent Infiniium digital storage oscilloscope (model number DSO8064A, maximum sampling speed 4 GSa/s (0.25 ns between data points), bandwidth 600 MHz, output impedance 50 Ω).

The excitation of tris(bipyridine)ruthenium(II) chloride ($Ru(bpy)_3Cl_2$) by the third harmonic of the laser (355 nm) was used as a test reaction (Figure 4.2).[148]

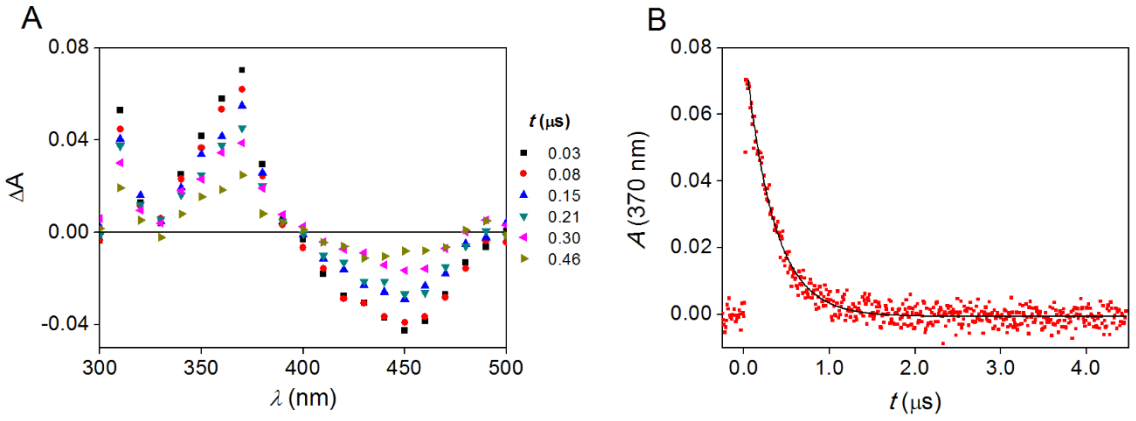

Figure 4.2. A) Transient absorption spectra of tris(bipyridine)ruthenium(II) chloride after 355 nm laser pulse. The signals were recorded at the indicated time points after the laser pulse. **B)** First order decay of triplet $Ru(bpy)_3^{2+}$. The solid line represents the non-linear least square fit to the observed data points. $[Ru(bpy)_3^{2+}]$ = 31 μM, λ_{ex} = 355 nm

4.3. Computation and data analysis

4.3.1. Software

Transient absorption kinetic curves were registered with the control software of the LFP instrument, Pro-Data LKS (version number 1.1.0.5) and visualized by Pro-Data Viewer (version number 4.2.5). Pro-Data Viewer has a built-in curve fitting application that was used in first order fitting. The required calculations were mostly implemented in Microsoft Excel 2010 and 2013, figures and charts were prepared by Origin 8.0.

4.3.2. Parameter fitting

The determination of kinetic parameters requires linear or non-linear least square fit of the recorded kinetic curves. Computer assisted fitting algorithms are more convenient and offer more exact parameter values than the different linearization techniques that were widely used in earlier literature. An outline of the equations used in this thesis for parameter fitting purposes with the interpretation of the individual parameters is given below.

Single exponential curves from pseudo-first order reactions were fit to eq. (12), integrated rate law of first order kinetics.

$$\mathrm{Abs} = a \cdot \exp(-k \cdot \mathrm{t}) + c \tag{12}$$

Here, a denotes the absorbance change associated with the process, k is the observed first order rate constant (k_{obs} in the figures and tables) and c is the final absorbance.

In the case of double exponential curves (Section 5.2.4), eq. (13) was used.

$$\mathrm{Abs} = a_1 \cdot \exp(-k_1 \cdot \mathrm{x}) + a_2 \cdot \exp(-k_2 \cdot \mathrm{x}) + c \tag{13}$$

Here, a_1 and a_2 mean the absorbance changes of the two steps, k_1 and k_2 are the observed rate constants (see Figure 5.17, assignment or rate constants is discussed there). It is worth noting that double exponential fitting is more sensitive to the initial estimates than the single exponential counterpart, as 5 parameters have to be optimized instead of 3.

Second order curves (for the recombination of sulfate ion radical or second order decay of halide molecule anions) were fitted by Micromath Scientist 2.01, based on eq. (14).

$$\mathrm{Abs} = a/(1 + b\,\mathrm{t}) \tag{14}$$

According to the integrated law of pure second order kinetics, (14) can be transformed into (15):

$$\mathrm{Abs_t} = \frac{\mathrm{Abs_0}}{1 + 2k\,\mathrm{t}\dfrac{\mathrm{Abs_0}}{\varepsilon l}} \tag{15}$$

This means that *a* is the initial absorbance of the curve, and the second order rate constant can be calculated from *b*, using the molar absorption coefficient of the absorbing species (16).

$$k = \frac{b\varepsilon l}{2\mathrm{Abs_0}} = \frac{b\varepsilon l}{2a} \tag{16}$$

4.3.3. Pseudo-first order data processing

The reactions of sulfate ion radical with a variety of reactants in Section 5.2 were studied under pseudo-first order conditions whenever possible. The detected kinetic data were processed according to the mathematical description of pseudo-first order kinetics (17).

$$k_{\mathrm{obs}} = k\,[\mathrm{reactant}] \tag{17}$$

Here k_{obs} is the observed pseudo-first order rate constant and *k* is the sought second order rate constant. k_{obs} = f([reactant]) functions were found to be linear and either went through the origin or had a non-zero vertical intercept. The intercept was accepted as significant if its value was higher than three times its standard deviation. In the case of a zero (insignificant) intercept, the obtained second order rate constant equals the slope of the respective function, according to (17). When a non-zero intercept occurs, then it is presumable that the studied reaction is not a bimolecular elementary step, but either it is a reversible reaction or some other by-reaction is operative. In fact, at [reactant] = 0, the reaction cannot by definition be pseudo-first order, only the second order recombination of sulfate ion radical takes place. Even though measured data points at [reactant] = 0 are not indicated in the figures, these types of control experiments were included in each series of concentration dependence studies. The lack of data points implies that, depending of the detection wavelength and the applied time scale, process (26) could not be observed or the curves were too noisy for an acceptable fit.

4.3.4. Solution of Partial Differential Equations

Calculations required for the solution of PDEs describing the two-dimensional diffusion in the sulfate ion radical–iodide system were carried out using MATLAB R2007a software. Actual concentrations in the volume elements were calculated by numerical integration using the fourth order Runge-Kutta method (RK4).[91,149] Further details of the numerical calculations are discussed in Section 5.3.

5. Results and discussion

5.1. Autoxidation of sulfur(IV) in the presence of silver(I) and peroxodisulfate ions

5.1.1. Preliminary observations

Sulfite ion and oxygen do not react in the absence of catalysts in acidic aqueous solutions, even at elevated temperatures. Hydrated sulfur dioxide, $H_2O{\cdot}SO_2$, is the most important form of sulfur(IV) in the pH range of the present autoxidation study (pK_a = 1.74 at 25.0 °C in 1.0 M $NaClO_4$). It has a UV absorption band centered around 276 nm (Figure 5.1).

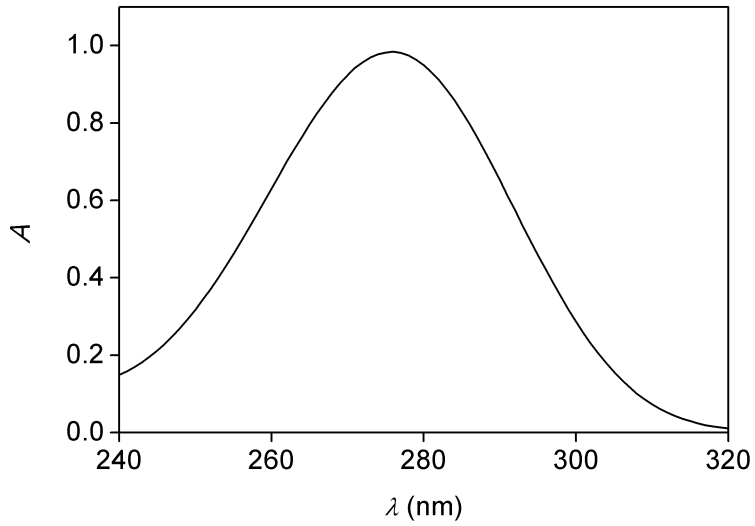

Figure 5.1. Spectrum of sulfur(IV) in aqueous sulfuric acid solution. [S(IV)] = 2.7 mM; [H_2SO_4] = 0.17 M; path length 1.000 cm; V = 3.00 cm^3; T = 25.0 °C.

Preliminary experiments have shown that a reaction between sulfur(IV) and peroxodisulfate ions does not occur in the absence of a catalyst. In the presence of silver(I), the shapes of recorded kinetic traces became quite unusual, they were basically straight lines with a sharp final break point (Figure 5.2). It is known from previous studies that the appearance of the break point typically refers to the total depletion of dissolved oxygen from the system.[46,79] The autoxidation process takes places in this phase. During the subsequent period of the reaction, peroxodisulfate ion plays the role of the oxidizing agent. The loss of sulfur(IV) is much slower in this region.

Even though S(IV) concentration is lower for trace a, trace b starts from higher initial absorbance in Figure 5.2. The reason is that silver(I) nitrate, which was added as a catalyst, also has some absorption at this wavelength.

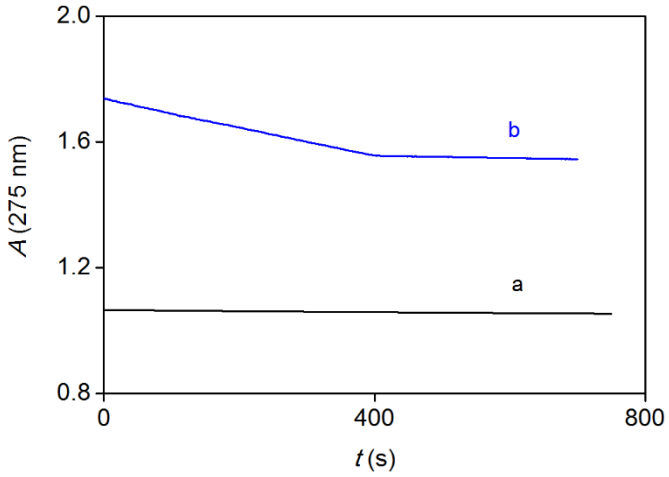

Figure 5.2. Typical kinetic traces measured during the autoxidation of sulfur(IV) in the absence and presence of catalyst. **a)** [S(IV)] = 3.0 mM; $[S_2O_8^{2-}] = 3.70 \cdot 10^{-2}$ M; $[H_2SO_4]$ = 0.103 M; T = 25.0 °C; **b)** [S(IV)] = 2.76 mM; $[S_2O_8^{2-}] = 3.33 \cdot 10^{-2}$ M; $[H_2SO_4]$ = 0.33 M; $[Ag^+]$ = 0.167 mM; T = 25.0 °C; optical path length = 1.000 cm, V = 3.00 cm^3.

5.1.2. Detailed kinetic studies

Comprehensive kinetic studies were performed in order to find out how the reactant and catalyst concentrations and pH influence the reaction rate. Peroxodisulfate ions were present in excess over sulfite ions and silver(I) was added in catalytic amounts.

Dependence of the reaction rate on the concentration of O_2

First, the effect of dissolved oxygen is presented. The amount of dissolved oxygen was varied by changing the time of the oxygenation of the $K_2S_2O_8$ stock solution. Actual oxygen concentrations were determined from the change of absorbance in the first section of the kinetic traces (preceding the break point) using the stoichiometric equation given in eq. (1).

The reaction turned out to be zeroth-order with respect to concentration of dissolved oxygen (Figure 5.3) within experimental error. This may seem quite a surprising observation in an autoxidation process, where oxygen acts as a reactant, but in fact it is not unexpected given the previous experience with the autoxidation of sulfur(IV).[77,79] This conclusion is also in agreement with the fact that the detected kinetic traces were zeroth-order as dissolved oxygen was the limiting reagent in each case.

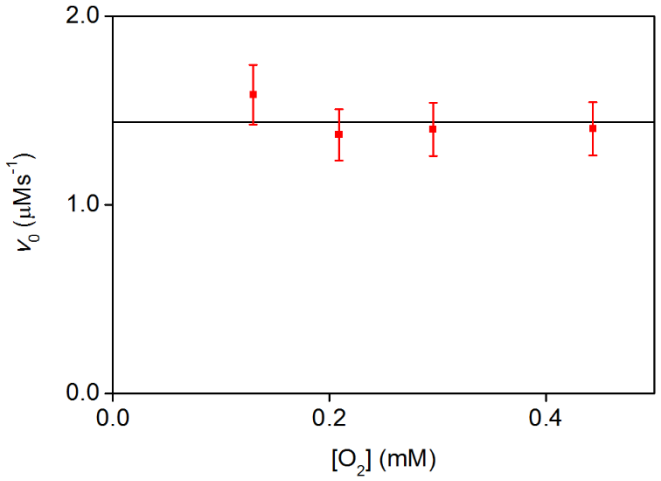

Figure 5.3. Reaction rates as a function of the dissolved oxygen concentration in the autoxidation of sulfur(IV). The solid line represents the best fit to the proposed mechanism shown in Scheme 1. [S(IV)] = 3.0 mM; [$S_2O_8^{2-}$] = $3.00 \cdot 10^{-2}$ M; [H_2SO_4] = 0.103 M; [Ag^+] = 0.260 mM; [O_2] = 0.130 mM; path length 1.000 cm; V = 3.00 cm^3; T = 25.0 ºC.

Dependence of the reaction rate on the concentration of S(IV)

The rate of reaction (1) as a function of sulfur(IV) concentration is plotted in Figure 5.4. As already mentioned, the major absorbing species in the system is hydrated sulfur dioxide ($H_2O \cdot SO_2$).

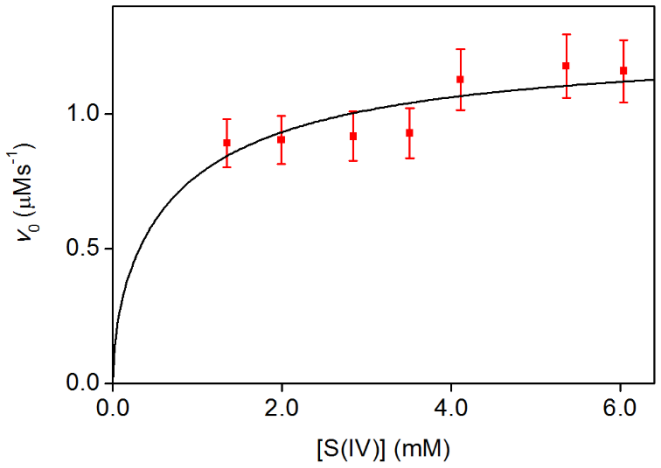

Figure 5.4. Reaction rates as a function of the sulfur(IV) concentration in the autoxidation of sulfur(IV). The solid line represents the best fit to the proposed mechanism shown in Scheme 1. [$S_2O_8^{2-}$] = 0.0301 M; [H_2SO_4] = 0.103 M; [Ag^+] = 0.167 mM; [O_2] = 0.130 mM; path length = 1.000 cm; V = 3.00 cm^3; T = 25.0 °C.

Dependence of the reaction rate on the concentration of silver(I)

The influence of the concentration of silver(I) ions on the rate is shown in Figure 5.5.

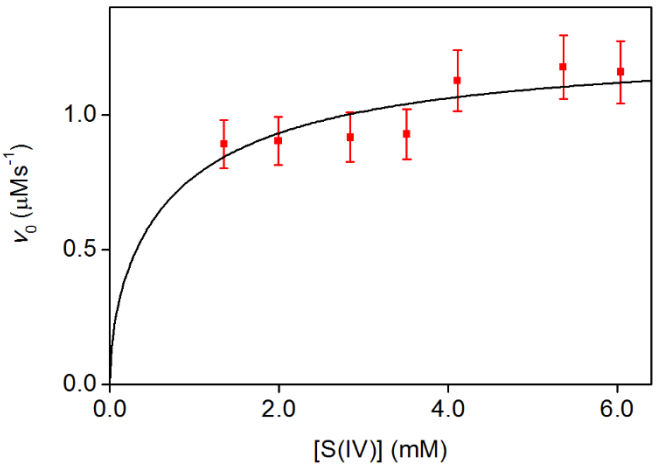

Figure 5.5. Reaction rates as a function of the silver(I) ion concentration in the autoxidation of sulfur(IV). The solid line represents the best fit to the proposed mechanism shown in Scheme 1. [S(IV)] = 3.0 mM; [$S_2O_8^{2-}$] = 0.0300 M; [H_2SO_4] = 0.103 M; [O_2] = 0.130 mM; path length 1.000 cm; V = 3.00 cm^3; T = 25.0 °C.

Similarly to the case of sulfur(IV), the dependence of the reaction rate on the catalyst concentration cannot be described by a simple equation. A quantitative explanation will be given later together with the proposed mechanism.

Dependence of the reaction rate on the concentration of peroxodisulfate ions

The concentration of peroxodisulfate ion also affects the reaction rate in a complex manner, Figure 5.6 shows the measured points and the fitted curve calculated from the proposed mechanism.

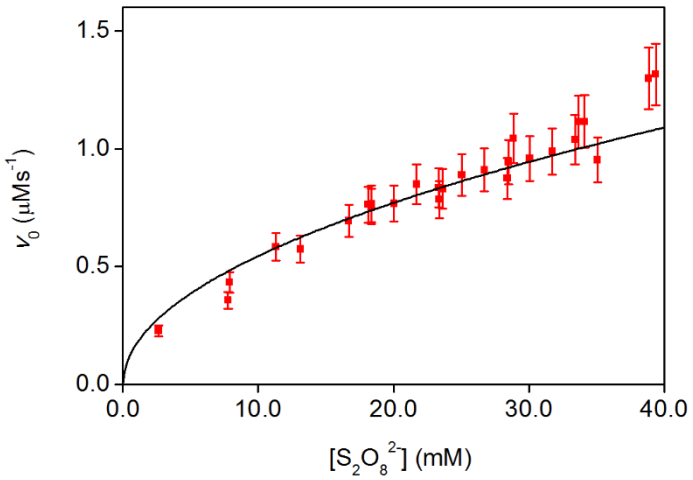

Figure 5.6. Reaction rates as a function of the peroxodisulfate ion concentration in the autoxidation of sulfur(IV). The solid line represents the best fit to the proposed mechanism shown in Scheme 1. [S(IV)] = 3.0 mM; [H_2SO_4] = 0.103 M; [Ag^+] = 0.167 mM; path length = 1.000 cm; [O_2] = 0.130 mM; V = 3.00 cm^3; T = 25.0 °C.

Dependence of the reaction rate on pH

Finally, the effect of pH on the rate of the zeroth order process is shown in Figure 5.7. The pH was calculated from the concentration of added sulfuric acid considering the fact that hydrogen sulfate ion is not a strong acid (pK_{a2} = 1.06 at 25 °C)

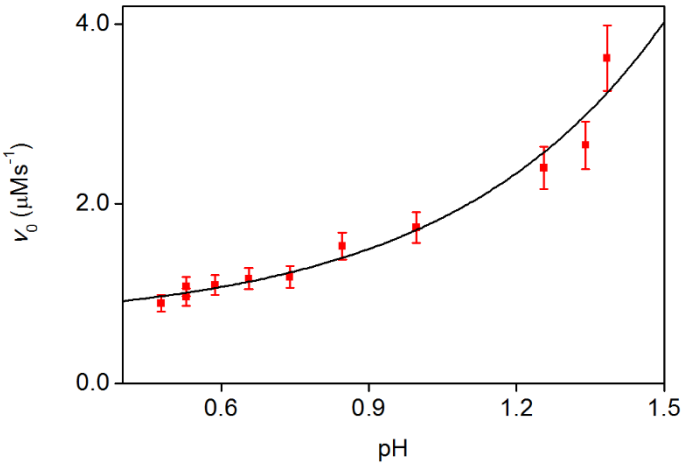

Figure 5.7. Reaction rates as a function of the pH in the autoxidation of sulfur(IV). [S(IV)] = 3.0 mM; [$S_2O_8^{2-}$] = 0.0284 M; [Ag^+] = 0.167 mM; [O_2] = 0.130 mM; path length = 1.000 cm; V = 3.00 cm^3; T = 25.0 °C.

5.1.3. Suggested mechanism

Our kinetic observations, in accordance with earlier results of investigations[77,79] about the autoxidation of S(IV), confirm that a chain reaction takes place in the studied system.

The initiation step is very likely to be the well-known reaction between silver(I) and peroxodisulfate ions (2), which produces two reactive chain carriers, silver(II) and sulfate ion radicals. Another initiation step will be mentioned later, as the reverse direction of a chain termination step.

$$Ag^{+} + S_2O_8^{2-} \xrightarrow{k_{18}} Ag^{2+} + SO_4^{\bullet-} + SO_4^{2-} \quad (18)$$

Among the propagation steps, the reaction of Ag(I) and $SO_4^{\bullet-}$ producing silver(II) and HSO_4^- certainly occurs (19).

$$Ag^{+} + SO_4^{\bullet-} \xrightarrow{k_{19}} Ag^{2+} + SO_4^{2-} \quad (19)$$

Previous studies revealed that the possible direct reaction between sulfate ion radical and sulfur(IV) does not play a role in the autoxidation process.[62,77,79] Therefore, it is reasonable to assume that silver(II) reacts with sulfur(IV) in the chain reaction. Ag(II) is a strong oxidizing species, which can easily be reduced by S(IV) in a one-electron step (20).

$$Ag^{2+} + S(IV) \xrightarrow{k_{20}} Ag^{+} + SO_3^{\bullet-} \quad (20)$$

It is also known from the literature that sulfite ion radical reacts very quickly with dissolved oxygen[124] and it is likely that the product of this reaction, peroxomonosulfate ion radical ($SO_5^{\bullet-}$), oxidizes sulfur(IV) (21, 22).

$$SO_3^{\bullet-} + O_2 \xrightarrow{k_{21}} SO_5^{\bullet-} \quad (21)$$

$$SO_5^{\bullet-} + S(IV) \xrightarrow{k_{22}} SO_4^{2-} + SO_4^{\bullet-} \quad (22)$$

At this point, one can see that steps (19 – 22) compose a chain in which one cycle leads to the formation of two sulfate ions by the reaction of one oxygen and two sulfur(IV).

With regard to chain termination, one can consider the disproportion of silver(II) into silver(I) and silver(III) which is also a previously published assumption.[43,45]

$$2Ag^{2+} \xrightarrow{k_{23}} Ag^{+} + Ag(III) \quad (23)$$

$$Ag^{+} + Ag(III) \xrightarrow{k_{24}} 2Ag^{2+} \quad (24)$$

Eqs. (23) and (24) describe a reversible process in which the reverse step acts as initiation, as it produces a chain carrier. This should be taken into account in the derivation of the rate law.

Silver(III) is a very reactive species and it react with sulfur(IV) in a two-electron process (25), where silver(I) is reproduced, ready to join the catalytic cycle again.

$$Ag(III) + S(IV) \xrightarrow{k_{25}} Ag^{+} + SO_4^{2-} \quad (25)$$

Silver(III) is supposed to occur as the AgO^{+} oxocation in aqueous solution, which means that reaction (25) possibly occurs as oxygen atom transfer.[45]

The recombination of sulfate ion radicals to peroxodisulfate ion (26) has always appeared in the chain mechanisms of the autoxidation processes of sulfur(IV) examined before.[77,79] For this reason, it seems appropriate to consider it in the scheme as a possible termination step.

$$2SO_4^{\bullet-} \xrightarrow{k_{26}} S_2O_8^{2-} \quad (26)$$

Scheme 1.

The suggested mechanism of the autoxidation of sulfur(IV) in the presence of silver(I) and peroxodisulfate ions.

$$Ag^{+} + S_2O_8^{2-} \xrightarrow{k_{18}} Ag^{2+} + SO_4^{\bullet-} + SO_4^{2-} \qquad v_1 = k_{18}[Ag^{+}][S_2O_8^{2-}] \quad (R1)$$

$$Ag^{+} + SO_4^{\bullet-} \xrightarrow{k_{19}} Ag^{2+} + SO_4^{2-} \qquad v_2 = k_{19}[Ag^{+}][SO_4^{\bullet-}] \quad (R2)$$

$$Ag^{2+} + S(IV) \xrightarrow{k_{20}^{obs}} Ag^{+} + SO_3^{\bullet-} \qquad v_3 = k_{20}^{obs}[Ag^{2+}][S(IV)] \quad (R3)$$

$$SO_3^{\bullet-} + O_2 \xrightarrow{k_{21}} SO_5^{\bullet-} \qquad v_4 = k_{21}[SO_3^{\bullet-}][O_2] \quad (R4)$$

$$SO_5^{\bullet-} + S(IV) \xrightarrow{k_{22}^{obs}} SO_4^{2-} + SO_4^{\bullet-} \qquad v_5 = k_{22}^{obs}[SO_3^{\bullet-}][S(IV)] \quad (R5)$$

$$2Ag^{2+} \xrightarrow{k_{23}} Ag^{+} + Ag(III) \qquad v_6 = k_{23}[Ag^{2+}]^2 \quad (R6)$$

$$Ag^{+} + Ag(III) \xrightarrow{k_{24}} 2Ag^{2+} \qquad v_7 = k_{24}[Ag^{+}][Ag(III)] \quad (R7)$$

$$Ag(III) + S(IV) \xrightarrow{k_{25}^{obs}} Ag^{+} + SO_4^{2-} \qquad v_8 = k_{25}^{obs}[Ag(III)][S(IV)] \quad (R8)$$

$$2SO_4^{\bullet-} \xrightarrow{k_{26}} S_2O_8^{2-} \qquad v_9 = k_{26}[SO_4^{\bullet-}]^2 \quad (R9)$$

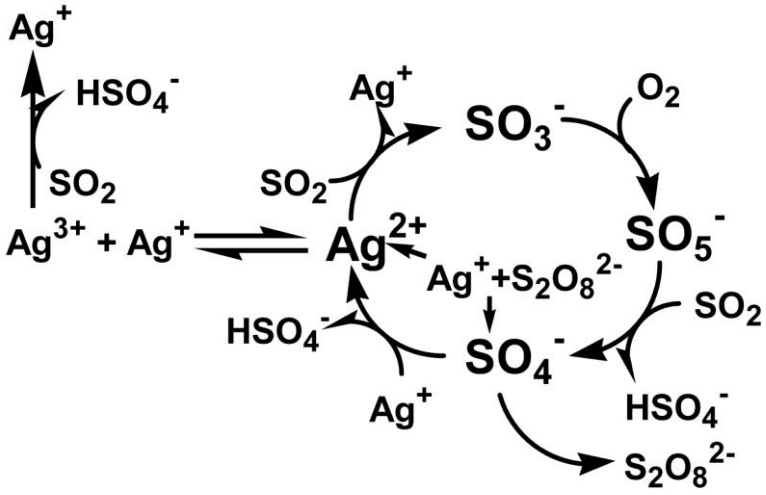

Figure 5.8. The suggested mechanism of the autoxidation of sulfur(IV) in the presence of silver(I) and peroxodisulfate ions.

5.1.4. Derivation of the rate law

The regular mathematical treatment of chain reactions is the long-chain approach.[91] Essentially, it is built on two main pillars:

- the steady-state approximation can be applied to every reactive intermediates (Ag(II), Ag(III), $SO_3^{\bullet-}$, $SO_4^{\bullet-}$, $SO_5^{\bullet-}$ in the present study)
- the rate of chain initiation or termination is lower than those of the propagation steps.

Two generally applied conclusions can be drawn from the assumptions above:

i. Each propagation step has the same rate as the rate of the net reaction.

ii. The rate of initiation and termination steps are equal. If more than one initiation or propagation steps occur, then equality refers to the sum of the rates of a certain type:

$$\sum_j v_{I,j} = \sum_k v_{T,k}$$

Here j is the number of initiation steps (I), k is the number of termination steps (T).

The rate of reaction (1) may be described by eq. (27).

$$v = -\frac{1}{2}\frac{\mathrm{d}[\mathrm{H_2O \cdot SO_2}]}{\mathrm{dt}} = -\frac{\mathrm{d}[\mathrm{O_2}]}{\mathrm{dt}} \qquad (27)$$

The rate is equal to the rate of any propagation steps, so it can be derived from eqs. (19)-(22). It is convenient to use eq. (20) for this purpose, in order to simplify subsequent calculations.

$$v = v_3 = k_{20}^{\text{obs}}[\text{Ag}^{2+}]_{\text{ss}}[\text{S(IV)}] \tag{28}$$

here subscript ss indicate steady-state concentrations

All reactions discussed are supposed to be second order, and these are elementary steps except for reactions (20), (22) and (25). In the latter cases, the deprotonation of $H_2O{\cdot}SO_2$ should be taken into account in the pH-range of the study. $H_2O{\cdot}SO_2$ and HSO_3^- forms are related by a fast pre-equilibrium. Consequently, the rate of step (20) is given in eq. (29)

$$v = [\text{Ag}^{2+}]_{\text{ss}}(k_{20}[\text{H}_2\text{O}{\cdot}\text{SO}_2] + k_{20}'[\text{HSO}_3^-]) \tag{29}$$

Considering the equilibrium of the two S(IV) forms, the formula takes the following form:

$$v = \frac{[\text{Ag}^{2+}]_{\text{ss}}[\text{S(IV)}]}{[\text{H}^+] + K_{\text{a}}}(k_{20}[\text{H}^+] + k_{20}'K_{\text{a}}) \tag{30}$$

Implying the long-chain assumption (ii), one can obtain eq. (31):

$$k_{18}[\text{Ag}^+][\text{S}_2\text{O}_8^{2-}] + k_{24}[\text{Ag}^+][\text{Ag(III)}]_{\text{ss}} = k_{23}[\text{Ag}^{2+}]_{\text{ss}}^2 + k_{26}[\text{SO}_4^{\bullet-}]_{\text{ss}}^2 \tag{31}$$

The steady-state concentration of silver(III) can be expressed from eq. (32) as follows:

$$[\text{Ag(III)}]_{\text{ss}}[\text{S(IV)}]\frac{k_{25}[\text{H}^+] + k_{25}'K_{\text{a}}}{[\text{H}^+] + K_{\text{a}}} + k_{24}[\text{Ag(III)}]_{\text{ss}}[\text{Ag}^+] = k_{23}[\text{Ag}^{2+}]_{\text{ss}}^2 \tag{32}$$

$$[\text{Ag(III)}]_{\text{ss}} = \frac{k_{23}[\text{Ag}^{2+}]_{\text{ss}}^2}{[\text{S(IV)}]\dfrac{k_{25}[\text{H}^+] + k_{25}'K_{\text{a}}}{[\text{H}^+] + K_{\text{a}}} + k_{24}[\text{Ag}^+]} \tag{33}$$

The steady-state concentration of sulfate ion radicals can be given from the fact that the rates of propagation steps are equal ($v_2 = v_3$):

$$k_{19}[\text{SO}_4^{\bullet-}]_{\text{ss}}[\text{Ag}^+] = [\text{Ag}^{2+}]_{\text{ss}}[\text{S(IV)}]\frac{k_{20}[\text{H}^+] + k_{20}'K_{\text{a}}}{[\text{H}^+] + K_{\text{a}}} \tag{34}$$

$$[\text{SO}_4^{\bullet-}]_{\text{ss}} = \frac{[\text{Ag}^{2+}]_{\text{ss}}[\text{S(IV)}]}{[\text{Ag}^+]} \cdot \frac{k_{20}[\text{H}^+] + k_{20}'K_{\text{a}}}{k_{19}([\text{H}^+] + K_{\text{a}})} \tag{35}$$

Substituting the steady-state concentrations in eqs. (33) and (35) into eq. (31) yields:

$$k_{18}[\mathrm{Ag^+}][\mathrm{S_2O_8^{2-}}] + k_{24}[\mathrm{Ag^+}]\frac{k_{23}[\mathrm{Ag^{2+}}]_{ss}^{\ 2}}{[\mathrm{S(IV)}]\dfrac{k_{25}[\mathrm{H^+}] + k_{25}'K_a}{[\mathrm{H^+}] + K_a} + k_{24}[\mathrm{Ag^+}]} =$$

$$= k_{23}[\mathrm{Ag^{2+}}]_{ss}^{\ 2} + k_{26}\frac{[\mathrm{Ag^{2+}}]_{ss}^{\ 2}[\mathrm{S(IV)}]^2}{[\mathrm{Ag^+}]^2}\cdot\left(\frac{k_{20}[\mathrm{H^+}] + k_{20}'K_a}{k_{19}([\mathrm{H^+}] + K_a)}\right)^2 \tag{36}$$

From eq. (36), the steady-state concentration of silver(II) can be expressed:

$$[\mathrm{Ag^{2+}}]_{ss}^2 = \frac{\dfrac{k_{18}}{k_{23}}[\mathrm{Ag^+}][\mathrm{S_2O_8^{2-}}]}{1 + \dfrac{k_{26}}{k_{23}}\dfrac{[\mathrm{S(IV)}]^2}{[\mathrm{Ag^+}]^2}\cdot\left(\dfrac{k_{20}[\mathrm{H^+}] + k_{20}'K_a}{k_{19}([\mathrm{H^+}] + K_a)}\right)^2 - \dfrac{k_{24}[\mathrm{Ag^+}]}{[\mathrm{S(IV)}]\dfrac{k_{25}[\mathrm{H^+}] + k_{25}'K_a}{[\mathrm{H^+}] + K_a} + k_{24}[\mathrm{Ag^+}]}} \tag{37}$$

The combination of eqs. (30) and (37) leads to the final rate law:

$$v = \frac{[\mathrm{S(IV)}](k_{20}[\mathrm{H^+}] + k_{20}'K_a)}{[\mathrm{H^+}] + K_a}\times$$

$$\times\sqrt{\frac{\dfrac{k_{18}}{k_{23}}[\mathrm{Ag^+}][\mathrm{S_2O_8^{2-}}]}{1 + \dfrac{k_{26}}{k_{23}}\dfrac{[\mathrm{S(IV)}]^2}{[\mathrm{Ag^+}]^2}\cdot\left(\dfrac{k_{20}[\mathrm{H^+}] + k_{20}'K_a}{k_{19}([\mathrm{H^+}] + K_a)}\right)^2 - \dfrac{k_{24}[\mathrm{Ag^+}]}{[\mathrm{S(IV)}]\dfrac{k_{25}[\mathrm{H^+}] + k_{25}'K_a}{[\mathrm{H^+}] + K_a} + k_{24}[\mathrm{Ag^+}]}}} \tag{38}$$

The suggested model fits the observed kinetic data very well. Solid lines in Figure 5.3-Figure 5.6 represent the best fit to the proposed mechanism. Figure 5.9 shows the correlation between all reaction rates measured at one given pH ($[H_2SO_4]$ = 0.103 M). The horizontal axis contains the measured rates, while data on the vertical axis are the rates calculated with the parameters from the best fit. The correlation plot also confirms that the model provides excellent quantitative interpretation of the kinetic results.

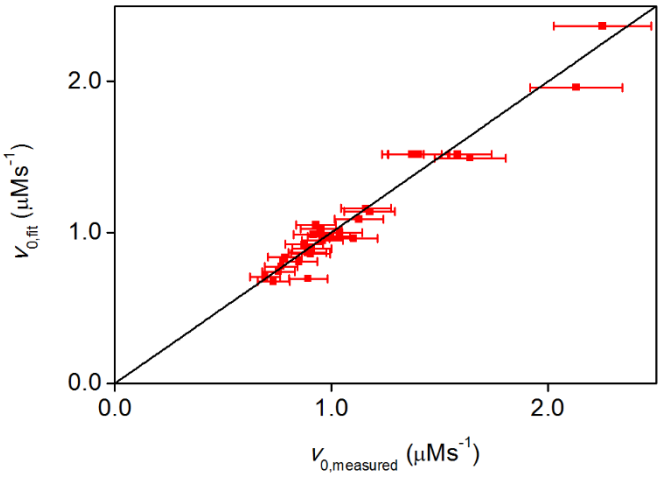

Figure 5.9. Correlation between measured and calculated rates.

5.2. Laser flash photolysis studies on the reactions of sulfate ion radical

5.2.1. Generation and recombination of the sulfate ion radical ($SO_4^{\bullet-}$)

Previously published generation methods and characterization of the sulfate ion radical, $SO_4^{\bullet-}$, are extensively discussed in Section 2.3. In our experiments, $SO_4^{\bullet-}$ was generated by the photolysis of an aqueous solution of $K_2S_2O_8$ (3). The radicals are the product of the homolytic scission of the peroxy bond in $S_2O_8^{2-}$ ion.

$$S_2O_8^{2-} \xrightarrow{h\nu} SO_4^{\bullet-} \tag{39}$$

Whenever required for the calculations, $\varepsilon(SO_4^{\bullet-})_{450\ nm}$ = 1600 $dm^3\ mol^{-1}\ cm^{-1}$ was used, based on the studies of McElroy.[118]

Following the photolysis of a 0.0967 M $K_2S_2O_8$ solution at 266 nm, kinetic traces similar to the one in Figure 5.10 were detected. The recorded kinetic traces in the absence of any other reactants were fitted with second order curves, and they all gave a very good fit. Therefore, it is reasonable to assume that the recombination of sulfate ion radicals into the precursor peroxodisulfate ions takes place under these conditions (40), which is the same process as the last chain termination step in Scheme 1. (R9).

$$2SO_4^{\bullet-} \xrightarrow{k_{40}} S_2O_8^{2-} \tag{40}$$

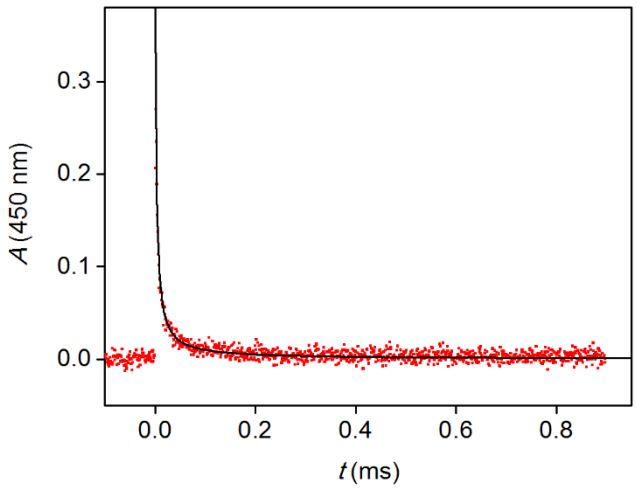

Figure 5.10. Transient absorption signal of the sulfate ion radical. [$K_2S_2O_8$] = 0.0967 M, T = 25 °C, V = 3.00 cm^3. The solid line represents the fitted second order curve ($k = 3.91 \times 10^8\ M^{-1}\ s^{-1}$).

The second order rate constant of the reaction, denoted here by k_{40}, was determined from the fitted parameters considering the molar absorption coefficient mentioned above. The value of the calculated second order rate constant was $(4.1 \pm 0.2) \times 10^8\ M^{-1}s^{-1}$.

The recombination process occurs on the millisecond timescale, which requires special treatment, as the basic settings of the instrument are configured for nanosecond measurements. In order to measure on longer timescales, the impedance of the oscilloscope has to be increased from 50 Ω into the kΩ range, up to 1 MΩ, by the installation of a variable resistance box between the signal cable from the photomultiplier tube and proper oscilloscope channel. Furthermore, at longer timescales, the Xe arc lamp has to be operated in continuous mode instead of pulsed mode, otherwise the lamp flashes would be too short for the detection of the transient species.

Theoretically, the LKS.60 instrument with its actual equipment is able to follow chemical reactions on the timescales between 1 ns to a few seconds with the convenient instrument settings and data evaluation methods implied.

In order to reveal a possible pH-dependence of the rate constant, k_{40} was measured over the acidic range. Figure 5.11 shows that the rate constant of the recombination process is independent of pH in the implied range.

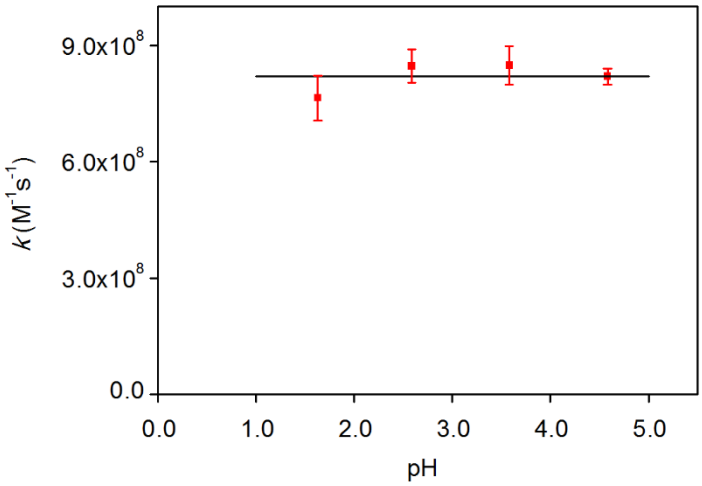

Figure 5.11. The effect of pH on the recombination rate of sulfate ion radicals. $[K_2S_2O_8]$ = 0.0967 M, T = 25 °C, V = 3.00 cm^3.

5.2.2. Reaction of sulfate ion radical and silver(I)-ion

In the subsequent stage of our kinetic investigation, the main focus was the role of sulfate ion radical in the autoxidation process of sulfur(IV). One can see from Scheme 1 that $SO_4^{\bullet-}$ is a chain carrier intermediate, it is produced in the initial step (2) and in a propagation step by the reduction of peroxomonosulfate ion radical.

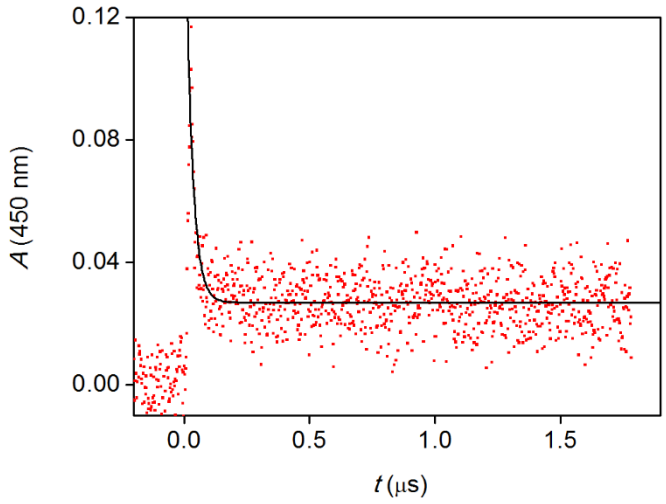

Figure 5.12. Absorption at 450 nm following the photolysis of $K_2S_2O_8$ (0.100 M) solution, containing $AgNO_3$ (6.12 mM). The solid line represents the fitted single exponential curve (k_{obs} = 3.8 × 10^7 s^{-1}).

The reaction between sulfate ion radical and silver(I) ion is of high importance in chain propagation, because it is the process through which the catalyst enters the cycle. Therefore, we intended to determine the rate constant of reaction (19) by means of laser flash photolysis.

An aqueous solution of $AgNO_3$ was photolyzed at 266 nm as a blank experiment in order to measure its contribution to the overall absorption in the reaction. It was found that silver nitrate does not show any transient absorption at 450 nm, thus the absorption can be attributed solely to sulfate ion radical. Figure 5.12 shows a representative transient absorption curve.

The reaction takes place on the nanosecond timescale, and can be fitted with a single exponential curve, thus referring to a first order process. Concentrations of the reactant were set in a way that pseudo-first order conditions would be fulfilled to Ag^+ ions over sulfate ion radicals.

A surprising observation was made following the photolysis of $K_2S_2O_8$–$AgNO_3$ aqueous solution. After a few laser shots (3-10 depending on the concentration ratio), dark grey cloudy precipitation was seen in the cuvette, first at the spot of laser excitation. Ag_2O formation was excluded upon the facts that the color of the precipitate is different from brownish Ag_2O, it does not dissolve in sulfuric acid and it appears even at very low pH. The dark grey precipitation is thus assumed to be elementary silver, the source of which is unknown so far. It was thought to be produced in the photodecomposition of $AgNO_3$, but in the absence of $K_2S_2O_8$, the precipitation did not occur.

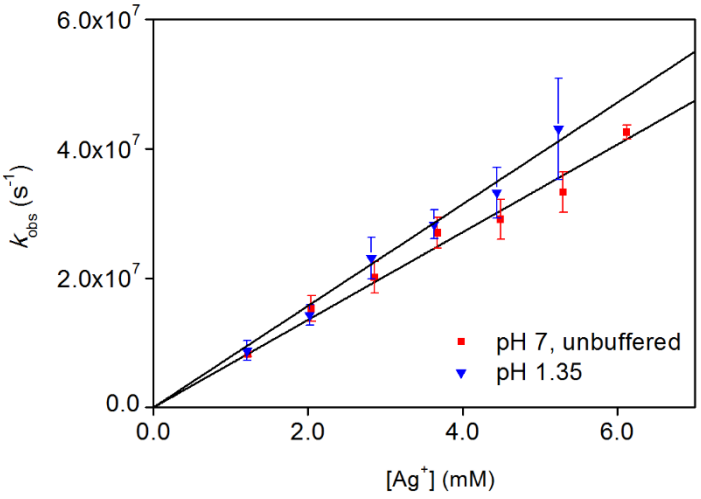

Figure 5.13. Pseudo-first order rate constant of the reaction between sulfate ion radical and silver(I) ion as a function of silver(I) ion concentration without pH adjustment (■) and in strongly acidic medium (▼). $[K_2S_2O_8]$ = 0.100 M, $[H_2SO_4]$ = 0.0270 M (▼), T = 25 °C, V = 3.00 cm^3. Error bars represent the standard deviation of parallel measurements at a given concentration.

$AgNO_3$ was replaced by $NaNO_3$ in order to examine the possible impact of the reaction between nitrate ion and $SO_4^{\bullet-}$, but only the recombination reaction (40) was observed.

The dependence of the pseudo-first rate constant (k_{obs}) on the initial concentration of $AgNO_3$ was investigated at constant peroxodisulfate concentration without pH adjustment and in strongly acidic medium (Figure 5.13).

The slope of the fitted line is equivalent to the second order rate constant of reaction (19), the value is (6.9 ± 0.4)× 10^9 M^{-1} s^{-1}. The average of the k_{obs}/[Ag+] values yields (6.8 ± 0.8) × 10^9 M^{-1} s^{-1}, in very good agreement with the slope of the line. Since mechanistic investigations described in Section 5.1.2 were carried out at low pH, similar measurements were performed in strongly acidic medium, the obtained rate constant at pH = 1.35 is (7.7 ± 0.5) × 10^9 M^{-1} s^{-1}.

5.2.3. Reaction of sulfate ion radical and cerium(III) ion

Cerium(III) has been shown to play an important catalytic role in the photoinitiated autoxidation of S(IV).[77] The oxidation of Ce(III) ion by sulfate ion radical is a chain carrier step according to Figure 2.3. Similarly to silver(I), we intended to measure the second order rate constant of reaction (41):

$$Ce^{3+} + SO_4^{\bullet-} = Ce^{4+} + SO_4^{2-} \qquad (41)$$

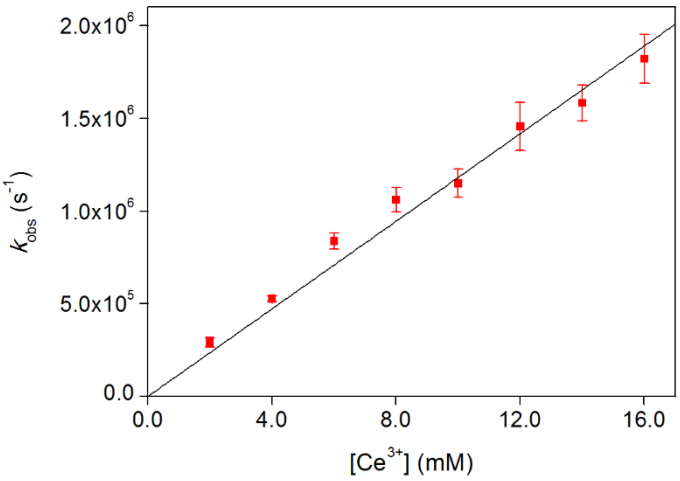

Figure 5.14. Pseudo-first order rate constant of the reaction between sulfate ion radical and cerium(III) ion as a function of cerium(III) ion concentration in strongly acidic medium. $[K_2S_2O_8]$ = 0.100 M, $[H_2SO_4]$ = 0.0090 M, T = 25 °C, V = 3.00 cm^3.

Pseudo-first order conditions were applied, using cerium sulfate in high excess. A high concentration of sulfuric acid was applied in order to avoid the hydrolysis of cerium(III). The measured second order rate constant at pH 1.78 is $(1.18 \pm 0.03) \times 10^8$ M^{-1} s^{-1}.

5.2.4. Reaction of sulfate ion radical and iodide ion

Taking into account the versatile photochemistry or halide ions and the fact that iodide ion efficiently catalyzes the photoinitiated autoxidation of S(IV),[79] we examined the reaction between the sulfate ion radical and iodide ion by means of laser flash photolysis. Similarly to the previous systems, sulfate ion radical was generated by the photolysis of potassium peroxodisulfate solution (3). Peroxodisulfate ion is able to oxidize iodide ion in a thermal reaction, even a commonly applied physical chemistry laboratory practice task is built on this reaction.[150] Because of this fact, we had to set the initial reactant concentrations very carefully, in order to maintain pseudo-first order conditions whilst keeping the thermal reaction negligible. Reaction 42 is a chain carrier in the reaction scheme presented in Figure 2.2.

$$I^- + SO_4^{\bullet -} = I + SO_4^{2-} \quad (42)$$

$$I^- + I \rightleftharpoons I_2^- \quad (43)$$

The assumption is that the sulfate ion radical oxidizes iodide ion in a one-electron process, where sulfate ions and iodine atoms are produced. The oxidation of iodide ion by sulfate ion radical is a useful alternative to the direct photolysis of iodide ions for the generation of iodine atoms.

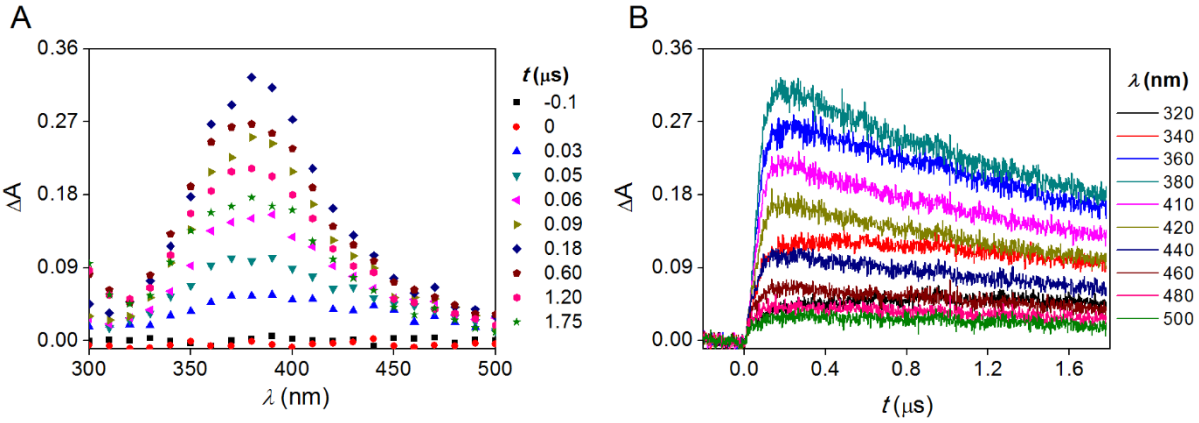

Figure 5.15. Time resolved transient absorption spectra of iodine molecule anion. [$K_2S_2O_8$] = 0.100 M, [KI] = 5.01 mM, T = 25 °C, V = 3.00 cm^3. Spectra were recorded at the indicated time points after the laser pulse. Negative time on panel A (-0.1 μs) refers to the pre-pulse section of the curves (panel B, t < 0).

Iodine atom and iodide ion form iodine molecule anion in an equilibrium process (43). This species is known to absorb strongly at 380 nm.[98,151-153] Our measurements confirmed that this is an appropriate wavelength for the kinetic study of the system. Figure 5.15 shows time resolved transient absorption spectra of iodine molecule anion.

Figure 5.16 is a representative example of the recorded kinetic curves. Two individual curves are merged in the chart, curve **a** represents the observed behavior on the shorter time scale (0-1 μs) whereas **b** is an example curve from the longer time scale (0-0.1 ms).

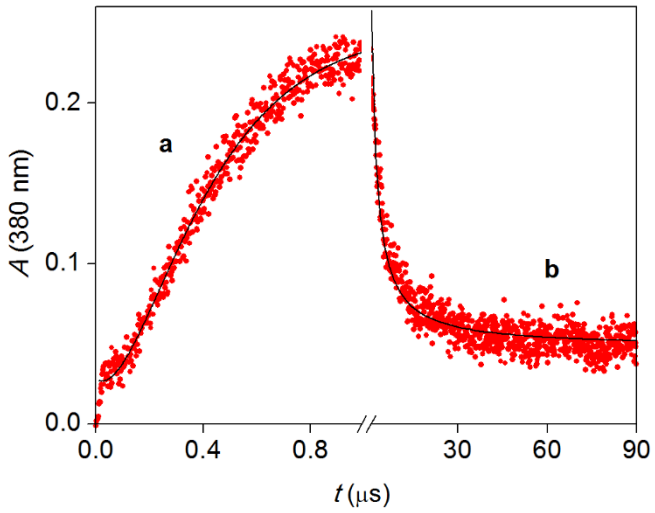

Figure 5.16. Representative kinetic curves of the reaction of sulfate ion radical and iodide ion. Circles: experimental points; solid line: **a)** double exponential **b)** second order fit. [$K_2S_2O_8$] = 0.100 M, [KI] = 0.503 mM**,** V = 3.00 cm^3, T = 25 °C.

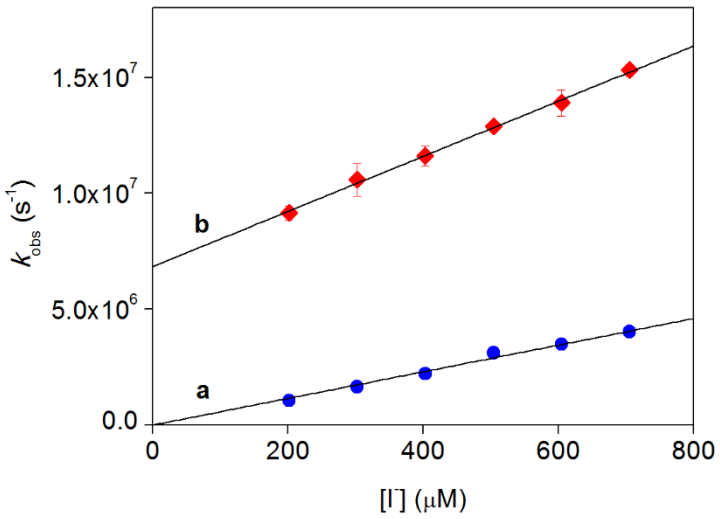

Figure 5.17. Observed pseudo-first order rate constants in the reaction of sulfate ion radical and iodide ions on the short time scale. $[K_2S_2O_8]$ = 0.100 M, V = 3.00 cm^3, T = 25 °C.

On the shorter time scale, double exponential curves fitted nicely to the recorded kinetic curves. The observed pseudo-first order rate constants obtained from the double exponential fit of the kinetic curves similar to the one in Figure 5.16 **a** showed linear dependence on the concentration of iodide ions (Figure 5.17). This fact confirms that pseudo-first order conditions were fulfilled in the applied experimental settings.

The integrated rate equation of double exponential kinetics is symmetrical with respect to the two rate constants.[91] Therefore, it is not always obvious to assign the obtained values to the corresponding reaction steps. Line **b** in Figure 5.17 has a non-zero vertical intercept, which suggests that the higher rate constant values correspond to reaction (43) and the lower ones (line **a**) belong to eq. (42). This statement is affirmed by the fact that reaction (42) is an irreversible second order step with iodide ion in high excess, thus the observed rate constant as a function of I^- concentration is expected to be linear going through the origin. Thus, the first step of the scheme is found to be the slower one, which is a little counterintuitive based on the shape of the detected curves (Figure 5.16 **a**), but is a kinetically well understood situation. The equilibrium constant of reaction (43) can be calculated as a ratio of the forward and backward rate constant, i.e. the slope and intercept of line **b** in Figure 5.17. The obtained rate constants are: k_{42} = (5.7 ± 0.1) × 10^9 M^{-1} s^{-1}, k_{43} = (1.2 ± 0.1) × 10^{10} M^{-1} s^{-1}, k_{-43} = (6.8 ± 0.3) × 10^6 s^{-1}. Thus, K_{43} = k_{43}/k_{-43} = (1.7 ± 0.2) × 10^3 M^{-1}.

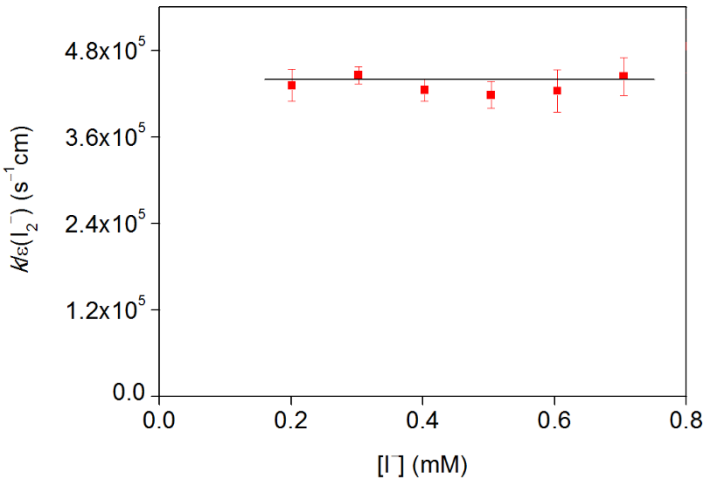

Figure 5.18. Ratio of second order rate constant and molar absorption coefficient of the decomposition of iodine molecule anion. [$K_2S_2O_8$] = 0.100 M, V = 3.00 cm^3, T = 25 °C.

On the longer time scale, second order fit was carried out, in accordance with the second order decomposition of I_2^- (44).[151,154]

$$2\ I_2^- \xrightarrow{k_{44}} I^- + I_3^- \qquad (44)$$

The rate constant of the decay was found to be independent of the iodide ion concentration (Figure 5.18), suggesting that (44) is an irreversible step. This is somehow trivial, it would be very unlikely for two stable species such as iodide and triiodide ion to combine spontaneously into a transient, short lived species such as iodine molecule anion.

Second order fitting differs from the pseudo-first order case in the need of actual concentration of the monitored species. For such short lived entities as the halide molecule anions, it is not evident to estimate their actual concentrations in the solutions. Therefore, we could only provide the value of $k/\varepsilon(X_2^-)$, where k is the second order rate constant of the decay and X = I, Cl, Br and ε is the molar absorption coefficient of the species. In the case of iodide ion, $k_{44} = (4.4 \pm 0.3) \times 10^5$ s^{-1} cm $\times\ \varepsilon(I_2^-)$.

5.2.5. Reaction of sulfate ion radical with chloride ion

The reaction of sulfate ion radical with chloride ion was studied next. Chlorine molecule anion is produced in reactions (45) and (46):

$$Cl^- + SO_4^{\bullet -} = Cl + SO_4^{2-} \qquad (45)$$

$$Cl^- + Cl \rightleftharpoons Cl_2^- \qquad (46)$$

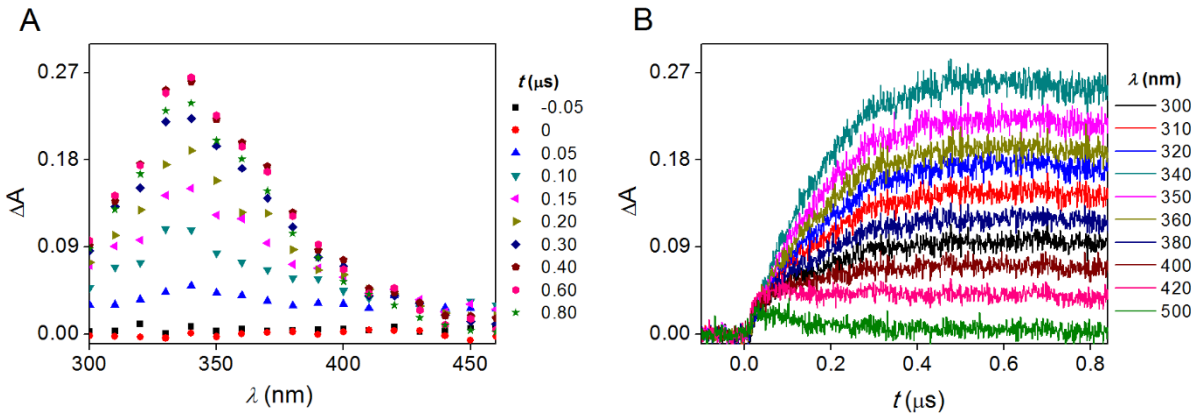

Figure 5.19. Time resolved transient absorption spectra of the chlorine molecule anion. [$K_2S_2O_8$] = 0.100 M, [NaCl] = 0.030 M, V = 3.00 cm^3, T = 25 °C, pH = 7 (unbuffered). Spectra were recorded at the indicated time points after the laser pulse. Negative time on panel A (-0.1 μs) refers to the pre-pulse section of the curves (panel B, t < 0).

Chlorine molecule anion strongly absorbs at λ = 340 nm,[118,155,156] the transient absorption spectra are shown in Figure 5.19. Kinetic data were collected at this wavelength.

Similarly to the case of iodide ion, the reaction was followed on shorter and longer time scales, under pseudo-first order conditions. Double exponential behavior on the shorter time scale, similar to the case of iodide ion (Figure 5.16 **a**), was not detected with chloride and bromide ions probably because the corresponding halide atom + ion equilibria (46 and 48) are established too quickly to be distinguishable on the time scale of the process.

On the shorter time scale, the second order rate constant was found to be (6.7 ± 0.2) × 10^8 M^{-1} s^{-1} in unbuffered aqueous solution and (7.5 ± 0.1) × 10^8 M^{-1} s^{-1} at pH 2.03 (Figure 5.20).

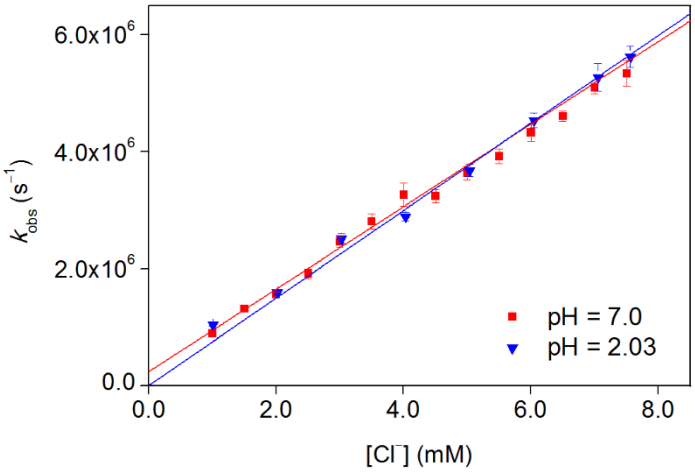

Figure 5.20. Pseudo-first order rate constants as a function of chloride ion concentration in the reaction of sulfate ion radical and chloride ion. [$K_2S_2O_8$] = 0.100 M, (■) unbuffered, (▼) [H_2SO_4] = 0.0049 M, T = 25 °C, V = 3.00 cm^3.

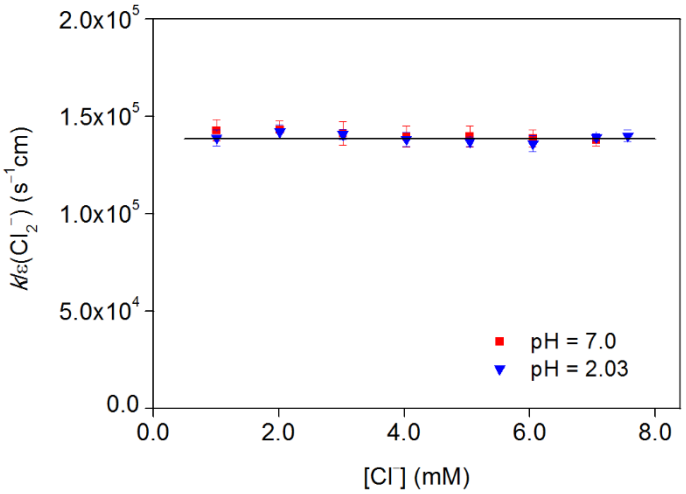

Figure 5.21. Ratio of second order rate constant of the decomposition and the molar absorption coefficient of chlorine molecule anion. $[K_2S_2O_8]$ = 0.100 M, (■) $[H_2SO_4]$ = 0 M, (▼) $[H_2SO_4]$ = 0.0049 M, T = 25 °C, V = 3.00 cm^3.

On the longer time scale, the second order decomposition of chlorine molecule anion was detected (see Figure 5.21). The second order rate constant of the decay of Cl_2^- is (1.4 ± 0.04) × 10^5 s^{-1} cm × $\varepsilon(Cl_2^-)$ at either pH = 2.03 or in unbuffered aqueous solution.

5.2.6. Reaction of sulfate ion radical with bromide ion

In the reaction of sulfate ion radical with bromide ion, bromide molecule anion is produced in reactions (47) and (48). Kinetic data were collected at 360 nm (see spectra in Figure 5.22).[157]

$$Br^- + SO_4^{\bullet-} = Br + SO_4^{2-} \quad (47)$$

$$Br^- + Br \rightleftharpoons Br_2^- \quad (48)$$

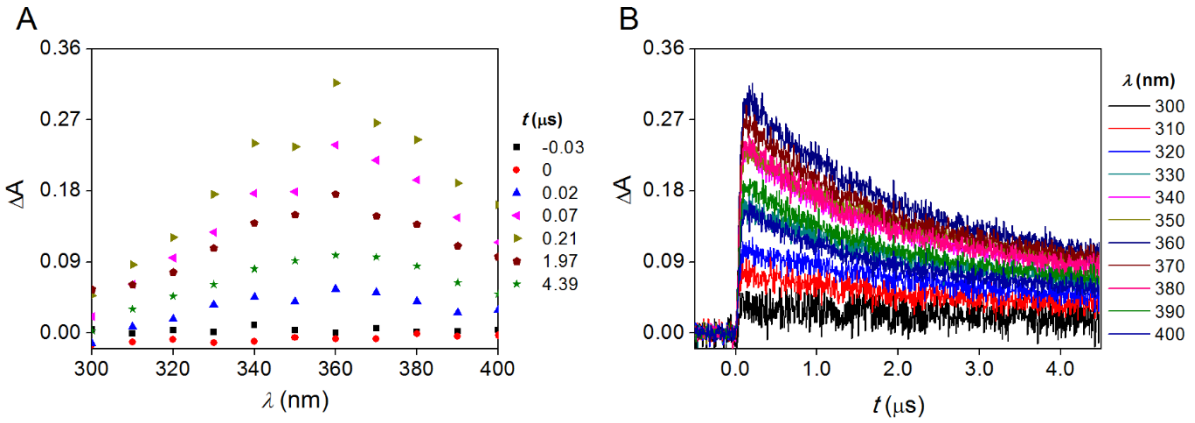

Figure 5.22. Time resolved transient absorption spectra of the bromine molecule anion. $[K_2S_2O_8]$ = 0.100 M, [KBr] = 0.010 M, V = 3.00 cm^3, T = 25 °C, pH = 7 (unbuffered). Spectra were recorded at the indicated time points after the laser pulse. Negative time on panel A (-0.1 μs) refers to the pre-pulse section of the curves (panel B, t < 0).

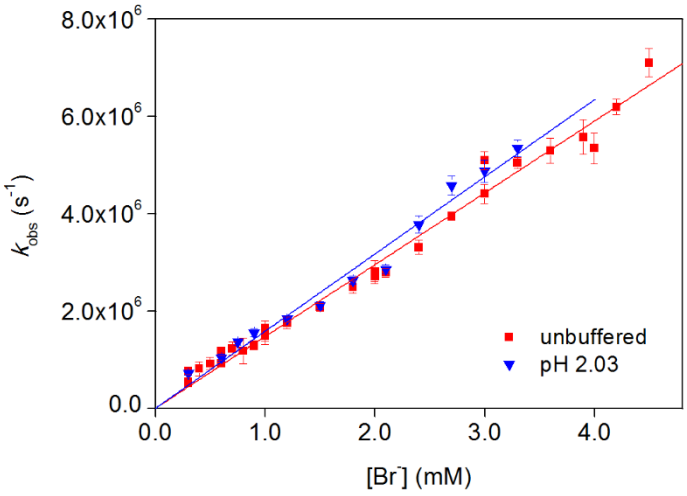

Figure 5.23. Pseudo-first order rate constants as a function of bromide ion concentration in the reaction of sulfate ion radical and bromide ion. $[K_2S_2O_8]$ = 0.100 M, (■) $[H_2SO_4]$ = 0 M, (▼) $[H_2SO_4]$ = 0.0049 M, T = 25 °C, V = 3.00 cm^3.

The reaction was followed on shorter and longer timescales, under pseudo-first order conditions. The second order rate constant was found to be (1.51 ± 0.02) × 10^9 M^{-1} s^{-1} in unbuffered aqueous solution and (1.59 ± 0.03) × 10^9 M^{-1} s^{-1} at pH 2.03 (Figure 5.23).

On the longer time scale, the second order decomposition of bromine molecule anion was detected, which was found to be independent from the bromide ion concentration (see Figure 5.24). The second order rate constant of the decay of Br_2^- is (1.8 ± 0.1) × 10^5 s^{-1} cm × $\varepsilon(Br_2^-)$ in unbuffered aqueous solution and at pH = 2.03.

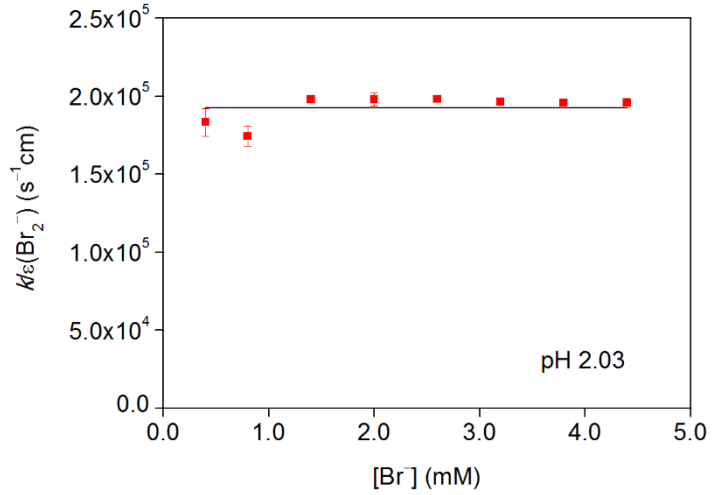

Figure 5.24. Ratio of second order rate constant and molar absorption coefficient of the decomposition of bromine molecule anion. $[K_2S_2O_8]$ = 0.100 M, $[H_2SO_4]$ = 0.0049 M, V = 3.00 cm^3, T = 25 °C.

5.2.7. Reaction of sulfate ion radical with tryptophan

The kinetics and mechanism of the oxidation of tryptophan (Trp) and its derivatives by peroxomonosulfate ions have been recently studied in our laboratory.[158] Since tryptophan is an aromatic amino acid with numerous potential oxidation sites (Figure 5.25), the detailed characterization of its oxidation reactions is a rather challenging task that needs to be approached by a combination of experimental techniques.

The laser flash photolysis method provides an efficient tool to study the one electron oxidation reactions of Trp that involve short lived reactive intermediates. The one electron oxidation of aromatic amino acids such as tryptophan and tyrosine plays an important role in the formation of protein radicals,[159-163] thus participating in electron transport and redox regulation.

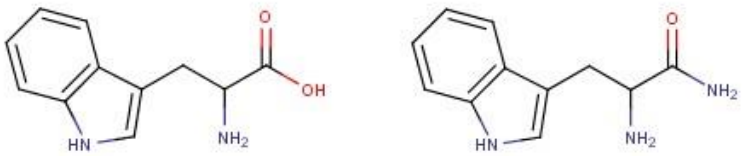

Figure 5.25. Structure of L-tryptophan and L-tryptophanamide.

The photolysis of tryptophan at 266 nm on a microsecond time scale led to kinetic curves containing a positive and a negative peak (see representative curve in Figure 5.26). The positive peak could be assigned to the transient absorption of the intermediate product of the photolysis of Trp, whereas the negative peak presumably corresponds to the laser induced fluorescence of Trp. Negative peaks are completely interpretable in the context of flash photolysis curves, since the measured value is in fact the difference between the absorbance of the ground state species and the excited species. Figure 5.26A shows that the intensity of the negative peak exceeds that of the positive one. The ratio of these values (in favor of the absorption peak) could be optimized by the alteration of the wavelength of the analyzing beam (Figure 5.26B).

The emission-to-absorption ratio was found to be optimal at 580 nm, further kinetic experiments were carried out at this wavelength. The 580 nm peak in the transient spectrum of excited tryptophan was previously assigned to be the photoionization product of Trp, a radical cation ($Trp^{\bullet+}$).[164]

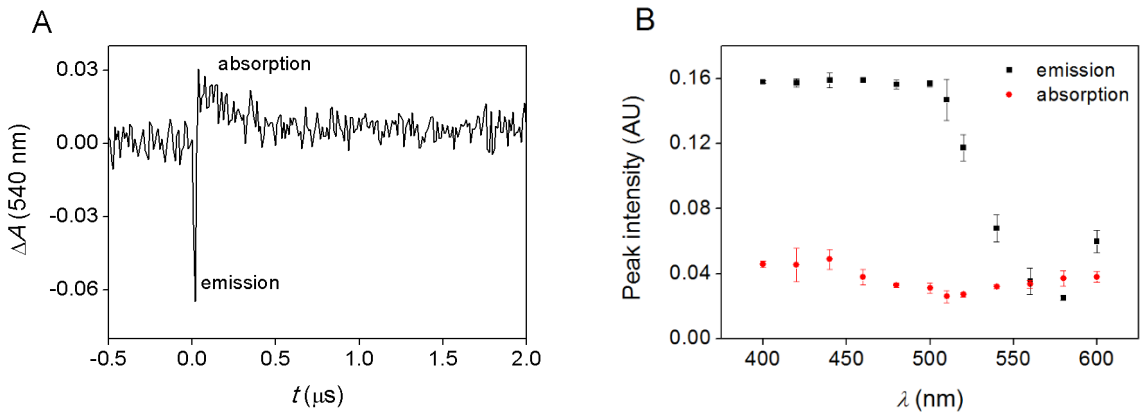

Figure 5.26. A) Representative kinetic curve of the 266 nm photolysis of aqueous solution of tryptophan. **B)** Intensity of light absorption and emission in the 266 nm photolysis of aqueous solution of tryptophan, based on kinetic curves as in panel A. The peak intensity corresponds to the absolute value of the maxima of the positive and negative peaks, in absorbance units. Conditions for both panels: [Trp] = 0.5 mM, unbuffered, V = 3.00 cm^3, T = 25 °C, l = 1.000 cm. The plots represent A) the average B) the average and standard deviation of 5 parallel measurements, where fresh sample was applied for each laser shot.

Figure 5.27 shows the linear dependence of the observed pseudo-first order rate constants on the concentration of tryptophan. 580 nm was not suitable to follow the reaction at pH 7.21 due to poor signal to noise ratio. 520 nm was found to be optimal with regards to emission to absorption ratio. 520 nm is the reported absorption maximum of TrpN• radical.[162,165-167]

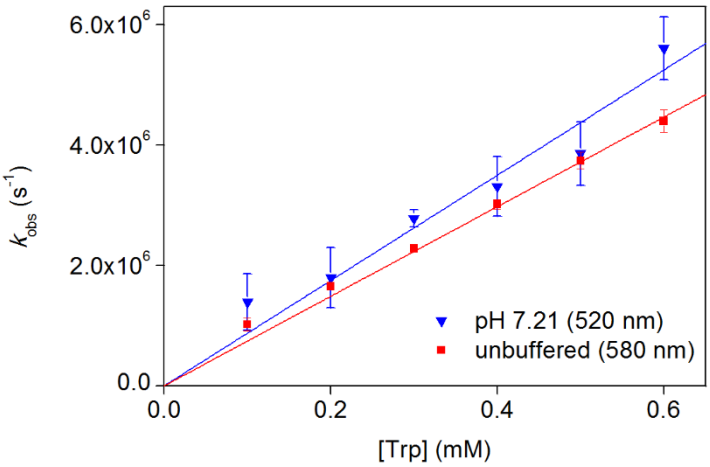

Figure 5.27. Pseudo-first order rate constants in the reaction of sulfate ion radical and tryptophan. The data points and error bars represent the average and standard deviation of 5 parallel measurements, where fresh sample was applied for each laser shot. The measured second order rate constants were (7.4 ± 0.1) × 10^9 M^{-1} s^{-1} in unbuffered solution and (8.7 ± 0.4) × 10^9 M^{-1} s^{-1} close to physiological pH (7.21). [$K_2S_2O_8$] = 0.100 M, unbuffered (■), pH = 7.21 (20 mM phosphate buffer, ▼), V = 3.00 cm^3, T = 25 °C, l = 1.000 cm.

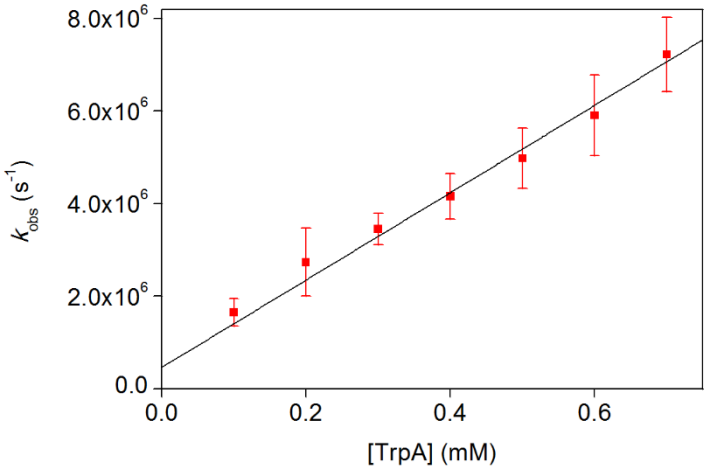

Figure 5.28. Pseudo-first order rate constants in the reaction of sulfate ion radical and L-tryptophanamide. The data points and error bars represent the average and standard deviation of 5 parallel measurements, where a fresh sample was applied for each laser shot. The solid line represents the linear least square fit to the measured points. The slope of the line is $(8.8 \pm 0.2) \times 10^9$ M^{-1} s^{-1} and the intercept is $(0.8 \pm 0.2) \times 10^6$ s^{-1}. $[K_2S_2O_8]$ = 0.100 M, pH = 7.21 (phosphate buffer), V = 3.00 cm^3, T = 25°C, l = 1.000 cm, λ = 520 nm.

L-Tryptophanamide (TrpA) was tested in experiments similar to those with Trp, the aqueous solution of TrpA and $K_2S_2O_8$ was photolyzed at 266 nm and the absorbance was followed at 520 nm. The observed rate constant depends linearly on the concentration of TrpA, with a positive intercept on the vertical axis (Figure 5.28).

Effect of dissolved oxygen concentration in the reaction of sulfate ion radical and tryptophan

We altered the concentration of oxygen in the sulfate ion radical–tryptophan radical system in order to reveal any potential influence of dissolved oxygen on the observed rate constants. When argon or nitrogen was vigorously bubbled into the reagent solutions for 15-20 minutes before the excitation, it had no observable effect on the photolysis of tryptophan solution. On the other hand, upon the application of a laser shot on the de-aerated samples, a previously unobserved yellow product appeared in the solutions. The characterization of the nature of this product would require detailed spectroscopic and kinetic studies.

From a kinetic point of view, the increase or decrease of oxygen concentration in the solutions caused only slight differences in the measured rate constants. The measured second order rate constants were $(9.4 \pm 0.5) \times 10^9$ M^{-1} s^{-1} in air saturated solution and $(9.0 \pm 0.3) \times 10^9$ M^{-1} s^{-1} in de-aerated samples. Data points obtained upon oxygenation of the solutions still show linear dependence, although the function has a positive intercept on the vertical axis.

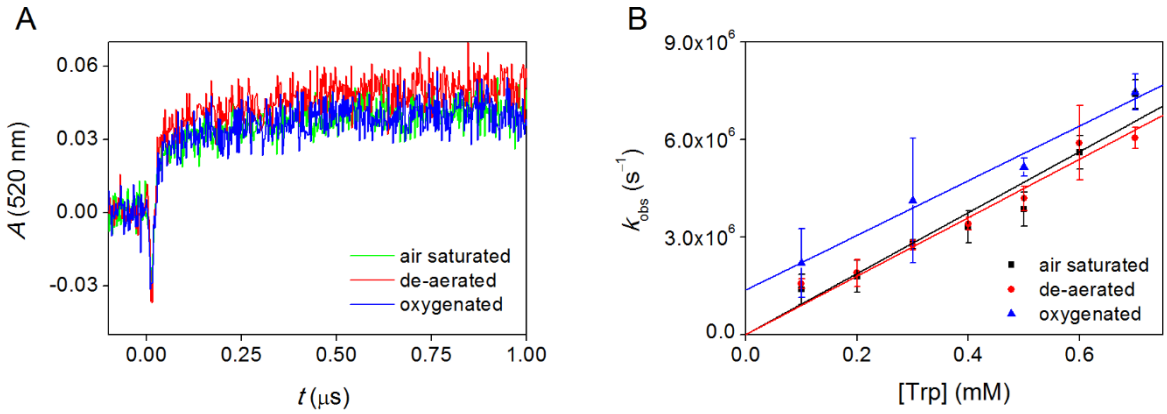

Figure 5.29. A) Representative kinetic curves in the reaction of sulfate ion radical with L-tryptophan with different oxygen concentrations. Oxygen was removed by vigorously bubbling argon in the reagent solutions for 20 min, whereas oxygenation was achieved by introducing extra oxygen in the samples from a gas bottle for 15-20 min. **B)** Pseudo-first order rate constants in the reaction of sulfate ion radical with L-tryptophan from kinetic curves as shown in A). The data points and error bars represent the average and standard deviation of 5 parallel measurements, where fresh sample was applied for each laser shot. The solid line represents the linear least square fit to the measured points. The slope of the blue line is $(8.4 \pm 0.8) \times 10^9$ M^{-1} s^{-1} and the intercept is $(1.4 \pm 0.4) \times 10^6$ s^{-1}. $[K_2S_2O_8] = 0.100$ M, pH = 7.21 (phosphate buffer), $V = 3.00$ cm^3, $T = 25$ °C, $l = 1.000$ cm, $\lambda = 520$ nm.

Figure 5.29A shows three representative kinetic curves recorded at 520 nm in air saturated, de-aerated and oxygenated solutions, respectively. Figure 5.29B shows the observed pseudo-first order rate constants as a function of the applied tryptophan concentration with different oxygen saturation in the samples. The measured second order rate constants were $(9.4 \pm 0.5) \times 10^9$ M^{-1} s^{-1} in air saturated solution and $(9.0 \pm 0.3) \times 10^9$ M^{-1} s^{-1} in de-aerated samples. Data points obtained upon oxygenation of the solutions still show linear dependence, although the function has a positive intercept on the vertical axis.

Alternative generation of tryptophanyl radical

The literature claims that tryptophanyl radical can be generated by the oxidation of aqueous tryptophan by bromine molecule anion (Br_2^-).[165,168] The experimental constraint is that we were not able to detect Br_2^- directly upon the photolysis of bromide solution, but only by the oxidation of bromide with sulfate ion radical (see Figure 5.23). It is still feasible to oxidize Trp by bromine molecule anion in the presence of $K_2S_2O_8$. However, one should take the oxidation of Trp by sulfate ion radical into account as well according to the above mentioned rates. Therefore, in the $SO_4^{\bullet-}$–Trp–bromide system, we should consider eq. (47) as well. The introduction of Trp increases the observed rate constant of the reaction in such a mixture (Figure 5.30). The reaction was followed at 360 nm, the absorption maximum of bromine molecule anion, on a microsecond time scale. The decay curves did not fit nicely to a single exponential curve. A second order fit was much better curves in agreement with the second order decay of Br_2^-.

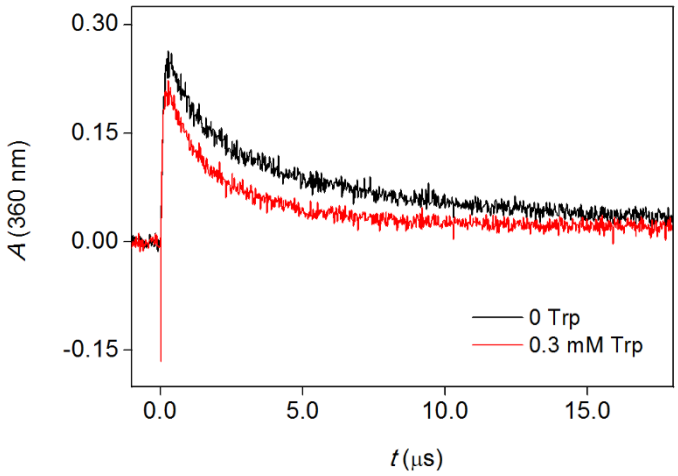

Figure 5.30. Second order decay of bromine molecule anion in the absence and presence of L-tryptophan. [$K_2S_2O_8$] = 0.100 M, unbuffered solution, V = 3.00 cm^3, T = 25 °C, l = 1.000 cm. The introduction of 0.3 mM Trp led to a 3-fold increase in the observed rate constant.

5.2.8. Reaction of sulfate ion radical with tyrosine

Similarly to the study carried out with tryptophan, another aromatic amino acid, tyrosine (Tyr) was also reacted with sulfate ion radical, in order to measure the second order rate constant of reaction (49).

$$Tyr + SO_4^{\bullet -} \rightarrow Tyr^{\bullet} + SO_4^{2-} \qquad (49)$$

The reaction was followed at 450 nm, because in the applied concentration range, the concentration of Tyr radical that is generated is insufficient to produce decent absorption signal. Under pseudo-first order conditions, the observed rate constants showed linear dependence on the concentration of tyrosine, as indicated in Figure 5.31. The data points measured in acidic solutions fit very well to linear functions going through the origin. The obtained second order rate constants were $(6.1 \pm 0.1) \times 10^9$ M^{-1} s^{-1} in acidic medium (black line – the pH is not constant in this case, concentration of added sulfuric acid is increasing) and $(5.1 \pm 0.1) \times 10^9$ M^{-1} s^{-1} at pH 2.72. Close to neutral pH, the dependence remains linear, although the linear function has a small positive intercept.

The second order recombination of the tyrosyl radical leads to the formation of dityrosine, which is known to have an emission peak at 405 nm and forms the basis of several fluorescent assays in the biochemical laboratory practice.[169,170]

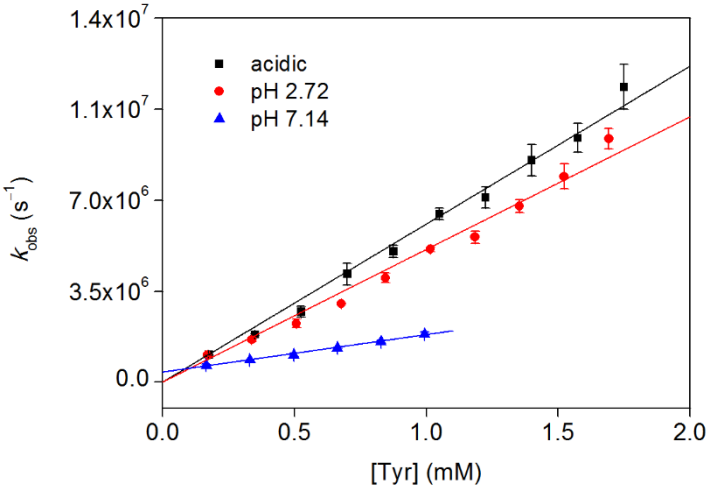

Figure 5.31. Observed rate constants in the reaction of sulfate ion radical and tyrosine as a function of tyrosine concentrations at different pH values. $[K_2S_2O_8]$ = 0.100 M, ■: changing pH ($[H_2SO_4]$ from 1.5 to 15 mM), ●: pH = 2.72 (measured); ▲: pH = 7.14 (0.1 M phosphate buffer), V = 3.00 cm^3, T = 25 °C, λ = 450 nm. Solid lines represent the linear fit to the measured data points. The blue line has a slope of $(1.4 \pm 0.1) \times 10^9$ M^{-1} s^{-1} and an intercept of $(0.4 \pm 0.3) \times 10^6$ s^{-1}.

5.2.9. Reaction of sulfate ion radical with S(IV)

In the next phase of our studies, we intended to examine the reaction of sulfate ion radical with sulfuroxy anions ($S_xO_y^{z-}$), preferably with the ones containing sulfur in the oxidation state of +4. During the autoxidation cycles of S(IV) (see Figure 5.8), $SO_3^{\bullet-}$ and $SO_5^{\bullet-}$ are produced as chain carriers along with the sulfate ion radical. We sought independent methods to study the reactions of these species. We postulated the existence of reaction (50):

$$SO_4^{\bullet-} + SO_3^{2-} = SO_4^{2-} + SO_3^{\bullet-} \quad (50)$$

To check this possible process, we reacted sulfate ion radical with sulfite solutions. The technique was similar to the one applied previously: sulfate ion radical was generated by the photolysis of potassium persulfate.

Sulfur(IV) has an absorption peak at 275 nm (see Figure 5.1) in acidic medium. Therefore, $K_2S_2O_8$ has to be in high excess in order to absorb the majority of light from the incident (laser) pulse. In our systems, $K_2S_2O_8$ is usually present in 0.1 M concentration in the samples, whereas the reactant species are applied in the millimolar concentration range, $K_2S_2O_8$ is in 10-100-fold excess. On the other hand, the reactant species has to be in excess over the generated sulfate ion radical, because pseudo-first order approach is applied in the data processing. The pseudo-first order conditions are favorable in free radical reactions because the actual concentrations of the transient species are not required. The third requirement is that the reactant has to be applied in an appropriate amount in order to reach decent signal-to-noise ratio in the observed kinetic curves. Sometimes other factors are to be considered as well, such as the solubility of the compound, possible light sensitivity, thermal reaction with $K_2S_2O_8$, etc. Because of the above mentioned factors, the optimal concentration range should be the subject of careful consideration.

Sodium pyrosulfite or metabisulfite ($Na_2S_2O_5$) was used as a source of sulfite ions, similarly to the autoxidation studies of S(IV) presented in the Section 5.1. The effect of pH along with dissolved oxygen concentration was examined on the rate constant of (50) and the reaction was followed at 450 nm. Significant difference was observed when the medium was changed from neutral to strongly acidic (Figure 5.32).

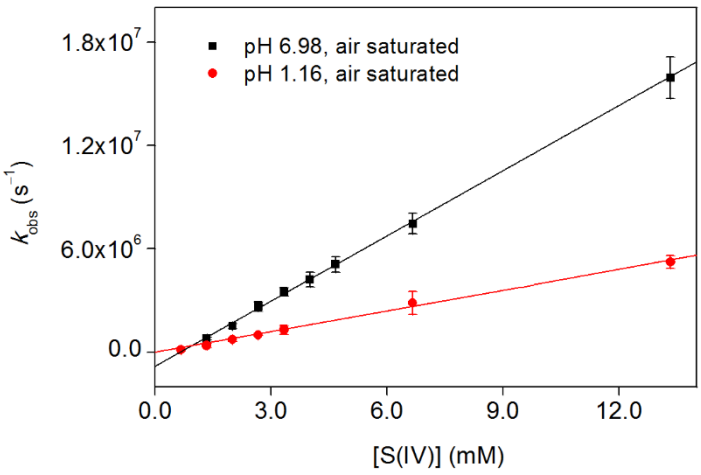

Figure 5.32. Pseudo-first order rate constants as a function of S(IV) concentration in the reaction of sulfate ion radical and S(IV). [$K_2S_2O_8$] = 0.100 M, pH = 6.98 (0.1 M phosphate buffer, ■) or 1.16 (0.045 M H_2SO_4, ●), V = 3.00 cm^3, T = 25 °C, λ = 450 nm. The solid lines represent the linear fit to the measured data points. The black line has a slope of $(1.3 \pm 0.01) \times 10^9$ $M^{-1}s^{-1}$ and its intercept with the vertical axis is at $(-0.8 \pm 0.1) \times 10^6$ s^{-1}, whereas the slope of the red line, thus the respecting second order rate constant is $(0.4 \pm 0.01) \times 10^9$ $M^{-1}s^{-1}$.

The negative intercept at neutral pH shown in Figure 5.32 implies that the dissolved oxygen present in the samples might oxidize a portion of the S(IV), thus the indicated values are overestimations of the actual concentrations that participate in reaction (50). Therefore, the effect of dissolved oxygen was tested by bubbling argon in the solutions and repeating the experiments with de-aerated samples, in neutral and acidic medium as well (Figure 5.33 and Figure 5.34). The negative intercept becomes insignificant when argon is introduced, confirming the contribution of dissolved oxygen to the oxidation process.

Figure 5.34 would also suggest that the concentration of dissolved oxygen actually has an influence on the rate constant under acidic conditions, if only the red and the blue data series were taken into account (since the pH values are very close). However, considering the black points as well, measured in air saturated solutions such as the red one, the more probable explanation is that the rate constant is highly sensitive to pH, and dissolved oxygen has little effect compared to the acidity of the medium. The pH dependence can be observed in de-aerated samples, too (Figure 5.35).

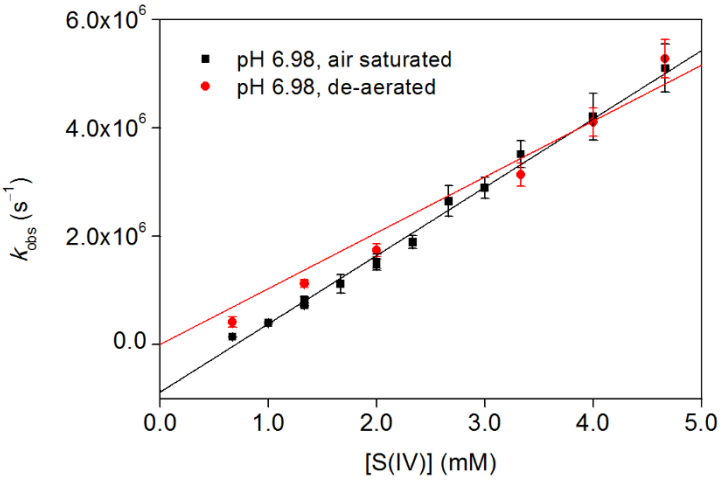

Figure 5.33. Pseudo-first order rate constants of the reaction of sulfate ion radical and S(IV) as a function of S(IV) concentration at different dissolved oxygen concentrations. [$K_2S_2O_8$] = 0.100 M, pH = 6.98 (0.1 M phosphate buffer), V = 3.00 cm^3, T = 25 °C, λ = 450 nm. For de-aeration, argon was vigorously bubbled into the reactant solutions prior to measurements for 15 min (●). The black line has a slope of (1.3 ± 0.03) × 10^9 M^{-1}s^{-1} and its intercept with the vertical axis is at (–0.9 ± 0.1) × 10^6 s^{-1}, whereas the slope of the red line, thus the respecting second order rate constant is (1.0 ± 0.04) × 10^9 M^{-1}s^{-1}.

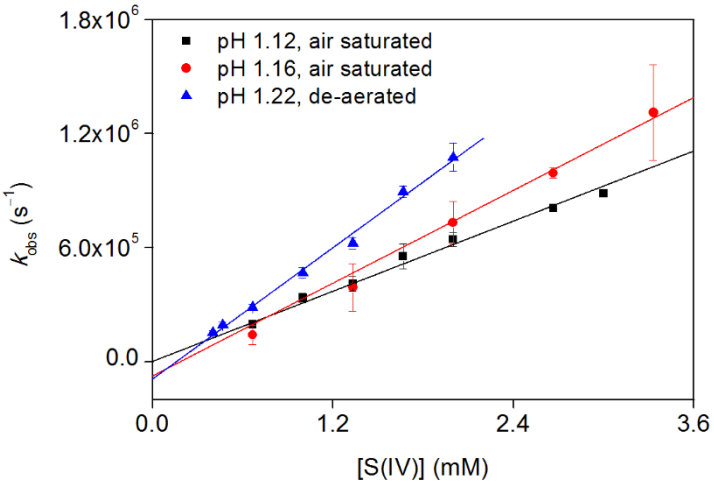

Figure 5.34. Pseudo-first order rate constants of the reaction of sulfate ion radical and S(IV) as a function of S(IV) concentration at different oxygen concentrations. [$K_2S_2O_8$] = 0.100 M, pH = 1.12 (■, 0.050 M H_2SO_4); 1.16 (●, 0.045 M H_2SO_4); 1.22 (▲, 0.038 M H_2SO_4), V = 3.00 cm^3, T = 25 °C, λ = 450 nm. For de-aeration purpose, argon was vigorously bubbled into the reactant solutions prior to measurements for 15 min (▲). The slope of black line is (3.1 ± 0.1) × 10^8 M^{-1}s^{-1}. The red line has a slope of (4.4 ± 0.1) × 10^8 M^{-1}s^{-1} and its intercept with the vertical axis is at (–1.7 ± 0.2) × 10^5 s^{-1}. The respective values for the blue line are (5.8 ± 0.2) × 10^8 M^{-1}s^{-1} and (–0.9 ± 0.2) × 10^5 s^{-1}.

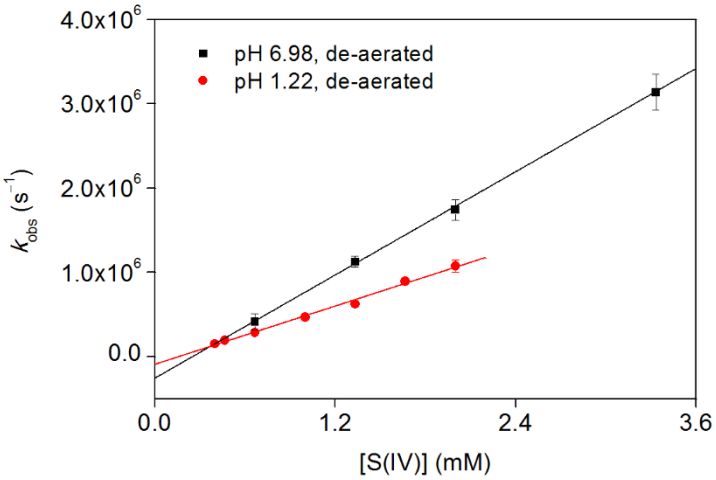

Figure 5.35. Pseudo-first order rate constants as a function of S(IV) concentration in the reaction of sulfate ion radical and S(IV) in de-aerated samples. [$K_2S_2O_8$] = 0.100 M, pH = 6.98 (0.1 M phosphate buffer, ■) or 1.22 (0.038 M H_2SO_4, ●), V = 3.00 cm^3, T = 25 °C, λ = 450 nm. The solid lines represent the linear fit to the measured data points. The slope of the black line is (1.0 ± 0.06) × 10^6 M^{-1} s^{-1}, the intercept is (-0.3 ± 0.03) × 10^6 s^{-1}. The respective values for the red line are (0.6 ± 0.02) × 10^6 M^{-1} s^{-1} and (-0.1 ± 0.02) × 10^6 s^{-1}.

Now, if we disregard the effect of dissolved oxygen and compare each measured data series with a focused view on pH dependence, Table 5 is obtained, which shows that the deprotonated form of pyrosulfite ions react much faster with sulfate ion radical than the protonated form.

Table 5. pH dependence of the rate constant of the reaction of sulfate ion radical and S(IV). The average and standard deviation of three values is indicated at pH 6.98.

pH	Slope (M^{-1} s^{-1})
1.12	(3.1 ± 0.1) × 10^8
1.16	(4.4 ± 0.1) × 10^8
1.22	(5.8 ± 0.2) × 10^8
6.98	(1.2 ± 0.1) × 10^9

5.2.10. Reactions of sulfate ion radical with hydrogen carbonate ions

The reaction of $SO_4^{\bullet-}$ with hydrogen carbonate ion was followed at 600 nm, absorption maximum of the product carbonate radical.[100,107-111] As expected, the rate constant is very sensitive to pH, due to hydrogen carbonate / carbonate (radical) protonation equilibria (Figure 5.36).

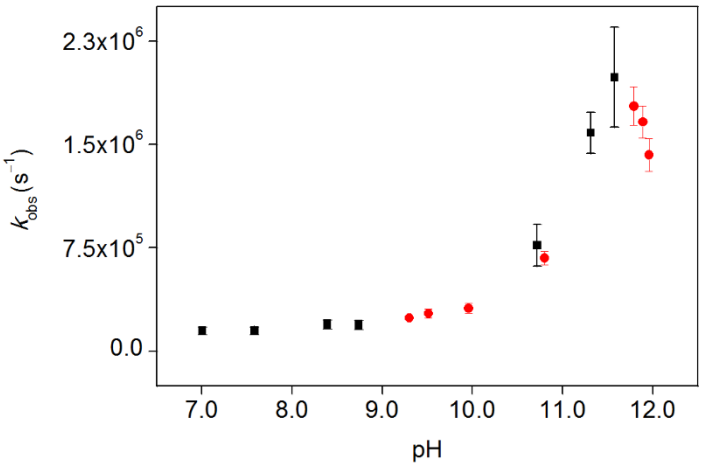

Figure 5.36. Observed rate constant of the reaction of sulfate ion radical and hydrogen carbonate ions as a function of pH. $[K_2S_2O_8]$ = 0.111 M, $[NaHCO_3]$ = 7.4 mM, V = 2.70 cm^3, T = 25 °C, λ = 600 nm. The black and red data points were measured on subsequent days.

The rate constant increases above pH 8.46, its dependence on the hydrogen carbonate concentration was measured at this value and is shown in Figure 5.37.

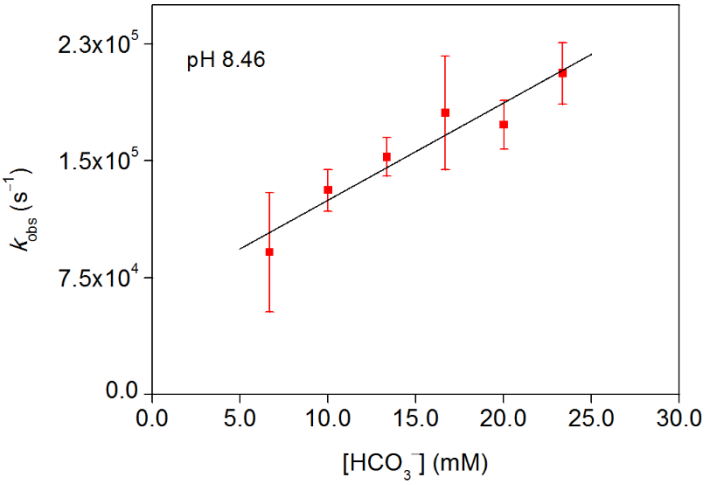

Figure 5.37. Observed rate constants in the reaction of sulfate ion radical with hydrogen carbonate ions as a function of HCO_3^- concentrations. The solid line represents the linear least square fit to the data point, with a slope of (6.2 ± 0.9) × 10^3 M^{-1} s^{-1} and an intercept of (6.2 ± 1.5) × 10^4 s^{-1}. $[K_2S_2O_8]$ = 0.111 M, V = 3.00 cm^3, T = 25 °C, λ = 600 nm.

5.2.11. Summary of rate constants of the sulfate ion radical

This subsection is dedicated to summarizing the collected kinetic data regarding the reactivity of the sulfate ion radical. For the sake of clarity, the rate constants are tabulated by reactant groups. The second group (Table 6B) is a union of two subgroups, catalysts and halide ions. This choice is motivated by the fact that iodide ion is an intersection and thus a direct link between the two subgroups.

The observed pseudo-first order rate constants showed linear dependence on the concentration of the reactants in the presented cases. The slope and intercept is given for each linear function, together with their standard deviations. In case of a zero (insignificant) intercept the slope of the respective function equals the obtained second order rate constant (see Section 4.3.3 for data analysis principles). The rate constant of the self-reaction of sulfate ion radical was determined from second order fit.

Table 6. Measured rate constants for the reaction of sulfate ion radical by reactant groups

A) Second order recombination

	Second order rate constant (M^{-1} s^{-1})		**Conditions**
Reactant	**This work**	**Ref.**	
$SO_4^{\bullet-}$	$(4.1 \pm 0.2) \times 10^8$	27,29,99,102,103,105,113,118,135,156,171	pH independent over the pH range 1.63-4.58 $\varepsilon = 1600\ M^{-1}\ cm^{-1}$

B) Catalysts of S(IV) autoxidation and halide ions

Reactant	**Slope (M^{-1} s^{-1})**	**Intercept (s^{-1})**	**Ref.**	**Conditions**
Ag^+	$(6.9 \pm 0.4) \times 10^9$	—	99,172	unbuffered
	$(7.7 \pm 0.5) \times 10^9$	—		pH 1.35
Ce(III)	$(1.18 \pm 0.03) \times 10^8$	—	101,173,174	pH 1.78
I^-	$(5.7 \pm 0.1) \times 10^9$	—		unbuffered
Cl^-	$(6.7 \pm 0.2) \times 10^8$	$(3.0 \pm 0.7) \times 10^5$	27,29,99,113,118, 155,156,171,175	unbuffered
	$(7.5 \pm 0.1) \times 10^8$	—		pH 2.03
Br^-	$(1.51 \pm 0.02) \times 10^9$	—	157,176	unbuffered
	$(1.59 \pm 0.03) \times 10^9$	—		pH 2.03

C) Other rate constants from the reactions of $SO_4^{\bullet-}$ with halide ions

	Rate constant	
Reaction	**This work**	**Ref.**
$I + I^- \rightarrow I_2^-$	$(1.2 \pm 0.1) \times 10^{10}$ M^{-1} s^{-1}	151,153,177
$I_2^- \rightarrow I + I^-$	$(6.8 \pm 0.3) \times 10^6$ s^{-1}	

	Second order rate constant (M^{-1} s^{-1})		Conditions
Reaction	**This work**	**Ref.**	
I_2^- decay	$(4.4 \pm 0.3) \times 10^5$ s^{-1} cm $\times \varepsilon(I_2^-)$	154	pH independent
Cl_2^- decay	$(1.40 \pm 0.02) \times 10^5$ s^{-1} cm $\times \varepsilon(Cl_2^-)$	154	
Br_2^- decay	$(1.8 \pm 0.1) \times 10^5$ s^{-1} cm $\times \varepsilon(Br_2^-)$	154,178	

D) Biomolecules

Reactant	**Slope (M^{-1} s^{-1})**	**Intercept (s^{-1})**	**Ref.**	**Conditions**
Trp	$(7.4 \pm 0.1) \times 10^9$	—	100,107-112,179,180	unbuffered
	$(9.4 \pm 0.5) \times 10^9$	—		pH = 7.21
	$(9.0 \pm 0.3) \times 10^9$	—		pH = 7.21, de-aerated
	$(8.4 \pm 0.8) \times 10^9$	$(1.4 \pm 0.4) \times 10^6$		pH = 7.21, oxygenated
Tyr	$(6.1 \pm 0.1) \times 10^9$	—		acidic, pH not constant
	$(5.1 \pm 0.1) \times 10^9$	—		pH = 2.72
	$(1.4 \pm 0.1) \times 10^6$	$(0.4 \pm 0.3) \times 10^6$		pH = 7.14
TrpA	$(8.8 \pm 0.2) \times 10^9$	$(0.8 \pm 0.2) \times 10^6$		pH = 7.21

E) Conjugate bases of weak inorganic acids

Reactant	**Slope (M^{-1} s^{-1})**	**Intercept (s^{-1})**	**Ref.**	**Conditions**
S(IV)	$(1.3 \pm 0.01) \times 10^9$	$(-0.8 \pm 0.1) \times 10^6$	40,181	pH = 6.98
S(IV)	$(4.0 \pm 0.1) \times 10^8$	—		pH = 1.16
S(IV)	$(3.1 \pm 0.1) \times 10^8$	—		pH = 1.12
S(IV)	$(1.03 \pm 0.04) \times 10^9$	—		pH = 6.98, de-aerated
S(IV)	$(5.8 \pm 0.2) \times 10^8$	$(-0.9 \pm 0.2) \times 10^5$		pH = 1.22, de-aerated
HCO_3^-	$(6.2 \pm 0.9) \times 10^3$	$(6.2 \pm 1.5) \times 10^4$	100,107-112,179,180	pH = 8.46

5.3. Modelling spatial inhomogeneities in laser flash photolysis experiments

5.3.1. Motivation and objectives

In the previous sections, the reactions of sulfate ion radical between transition metal ions, a few biomolecules and several small inorganic anions have been presented. Throughout the investigation of these systems, the assumption of pseudo-first order behavior was applied in the experimental setup and the data analysis. It is generally accepted that in a reaction of two components, one reactant should be present in at least 10-fold excess over the reaction partner so that its concentration stay constant during the reaction and the observed kinetic behavior will be determined by the order of reaction of the other reactant. When the high excess requirement is not fulfilled, the handling of the time course becomes trickier. Processing of mixed second order kinetics is already challenging and requires the knowledge of the initial and actual concentration of the reactants at every time points. As shown in Section 5.2, pseudo-first order conditions were met for the majority of the studied reactions, apart from a few exceptions, k_{obs} = f([reactant]) functions were linear, going through the origin.

Discussions in the present section will focus on the reaction between sulfate ion radical and iodide ion, presented in Section 5.2.4. This reaction system is of particular interest, because unlike the other two halide ions, the oxidation of iodide ions by sulfate ion radical can be separated into two distinct phases, the formation of iodine atom is distinguishable (see Figure 5.17. and discussion below). Figure 5.17 illustrates that reaction 42 shows pseudo-first order behavior even in the 0.2-0.8 mM range of iodide ion concentration. In order to make an assumption of the concentration of the sulfate ion radical in the samples, one should consider a few extra factors listed below:

i. Sulfate ion radical is generated from peroxodisulfate ions (see eq. (3)) *locally* along the path of the laser beam
ii. The diameter of the laser beam is around 5 mm (the instrument specifications give 6 mm, but our measurements showed that 5 mm is much closer to reality). On the other hand, the width of the cuvette (its path length in the direction of detection) is 1.000 cm, therefore the initial concentration of $SO_4^{\bullet-}$ is inevitably inhomogeneous
iii. $SO_4^{\bullet-}$ is a highly reactive, short lived intermediate species, its concentration immediately drops by a second order self-reaction as well as by the reaction with the given reactant, there is no time to reach homogeneous spatial distribution
iv. Although Beer's law stands for transient as well as for stable species, the measured absorbance is not as direct indicator of the actual concentration, because the molar

absorption coefficients are more difficult to determine, which leads to a high level of uncertainty in the ε values[106] (see Section 2.3).

Still, we can make a rough estimation of $[SO_4^{\bullet-}]_0$, where $t = 0$ represents the time point of the laser excitation (note that the excitation also pulse has a non-zero length in time, ~20 ns but for our purposes it can be handled as a point). A second order fit of the recombination curves gives an idea of the initial concentration, using $\varepsilon = 1600\ M^{-1}\ cm^{-1}$ published by McElroy[118] and $l = 0.5$ cm as an optical path length. Fitting of pure second order recombination curves of sulfate ion radical gave a value of 2×10^{-4} M, which is comparable to the applied concentration of iodide ion. This fact raised some questions: why are the detected curves exponential and why does the dependence on the concentration of iodide ion give a reasonably good straight line?

Returning to the above mentioned considerations (i-iv), the concentration of $SO_4^{\bullet-}$ is a local value, it applies for the location of the detection that is limited to a fractional volume in the cuvette. The total volume is 3.00 cm^3, so if the *average* concentration of $SO_4^{\bullet-}$ is calculated over the total volume, a much lower value is obtained. Additionally, while $SO_4^{\bullet-}$ goes through a rapid decay, iodide ion can be permanently replenished by diffusion from outside of the reaction space, thus maintaining the high excess of iodide over sulfate ion radical. In the following paragraphs, an attempt will be made to analyze the effect of diffusion in the sulfate ion radical–iodide ion system and to explore the effect of spatial inhomogeneity on the observed rate constants.

5.3.2. Reaction-diffusion equation using cylindrical coordinates

A general reaction-diffusion (hereinafter referred to as: RD) equation has a closed form shown in (51):

$$\frac{\partial \mathbf{c}}{\partial t} = \mathbf{D}\Delta\mathbf{c} + \mathbf{R}(\mathbf{c}) \tag{51}$$

Here, **c** is the vector of concentrations, **D** is the matrix of the diffusion coefficients, Δ is the Laplace operator or Laplacian and **R** is a complex operator embedding all of the ongoing reactions in the system. **D**Δ**c** is called the *diffusion term*, **R**(**c**) forms the *reaction term*.

Inspired by the seminal work of Alan Turing on morphogenesis (shape formation in biological systems),[182] reaction-diffusion systems stand in the main focus of research on chemical and biological pattern formation[183-185] as well as other nonlinear dynamic phenomena such as oscillation, chaos or self-organizing systems.[186,187]

Eq. (51) is a second order, semilinear, parabolic partial differential equation (PDE) system, in which each chemical entities is represented by a time-dependent variable.[149,188] The solution of eq. (51) is a vector of $c(t)$ functions, where each concentration is explicitly expressed as a function of time.

The Laplacian (Δ) is a differential operator with a scalar value that gives the divergence of the gradient of a real valued function. For an $f(x,y,z)$ function in the three-dimensional Euclidean space,

$$\Delta f = \nabla^2 f = \frac{\partial^2}{\partial x^2} + \frac{\partial^2}{\partial y^2} + \frac{\partial^2}{\partial z^2} \tag{52}$$

where ∇ is the gradient of f,

$$\nabla = \left(\frac{\partial}{\partial \mathrm{x}}, \frac{\partial}{\partial \mathrm{y}}, \frac{\partial}{\partial \mathrm{z}} \right) \tag{53}$$

Eq. (52) describes the Laplacian in Cartesian coordinates, but it is favorable for our purposes to transform the problem into a cylindrical coordinate system, since the reaction space is a circular cylinder (see Section 5.3.4). Figure 5.38 shows the transformation from Cartesian to cylindrical coordinates, and eq. (54) is the form of Laplacian in the new coordinate system.

$$\Delta = \frac{\partial^2}{\partial x^2} + \frac{1}{r}\frac{\partial}{\partial r} + \frac{\partial^2}{\partial r^2} + \frac{1}{r^2}\frac{\partial^2}{\partial \phi^2} \tag{54}$$

The angular (fourth) term in eq. (54) can be neglected in our model because of the cylindrical symmetry. Thus, applying eq. (54) in eq. (51) yields:

$$\frac{\partial \mathbf{c}}{\partial \mathrm{t}} = \mathbf{D}\left(\frac{\partial^2 \mathbf{c}}{\partial x^2} + \frac{1}{r}\frac{\partial \mathbf{c}}{\partial r} + \frac{\partial^2 \mathbf{c}}{\partial r^2} \right) + \mathbf{R}(\mathbf{c}) \tag{55}$$

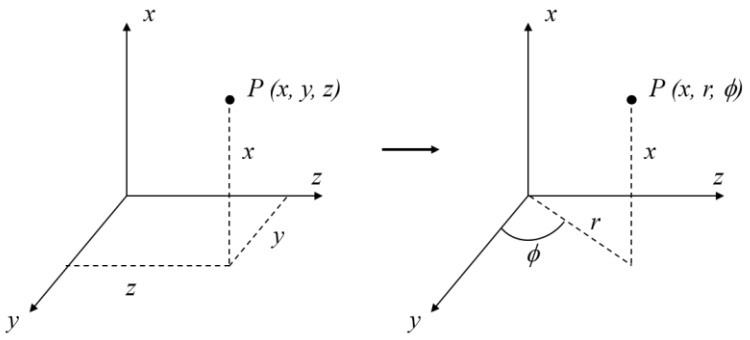

Figure 5.38. Transformation from Cartesian to cylindrical coordinates. $x = x$, $y = r \cdot \cos(\phi)$ and $z = r \cdot \sin(\phi)$.

In the present case, two concentration functions are to be calculated, $c_{SO_4^{\bullet-}}(x,r,t)$ and $c_{I^-}(x,r,t)$, the objective is to gather an insight of the spatial distribution of the reactants at each particular time point.

5.3.3. Approximation of the partial derivatives

Infinitesimal quantities cannot be handled computationally, partial derivatives involved in eq. (55) need to be approximated. Traditionally, derivatives are approximated by *finite differences*, that is, the slope of the tangent at a certain point on the graph is close to the slope of a secant lying on two nearby graph points (Figure 5.39).[189,190]

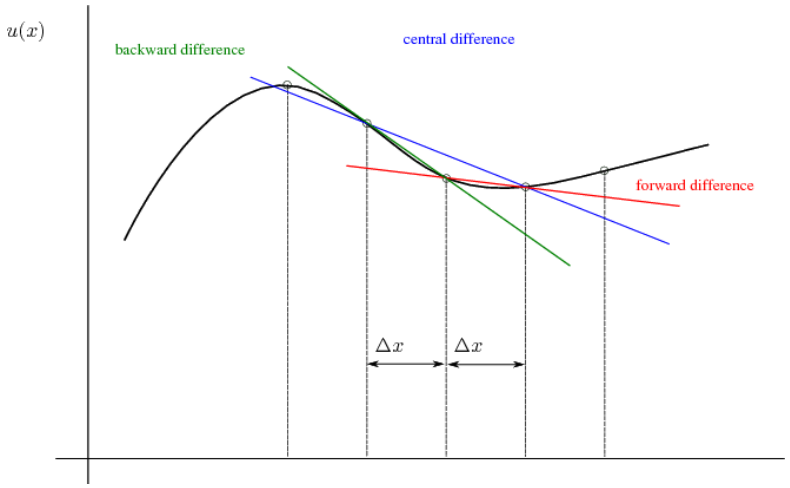

Figure 5.39. Geometric interpretation of the finite differences approximation.

Given with formulae:

$$u'(x_i) \approx \frac{u(x_i + \Delta x) - u(x_i)}{\Delta x} \approx \frac{u(x_i) - u(x_i - \Delta x)}{\Delta x} \approx \frac{u(x_i + \Delta x) - u(x_i - \Delta x)}{2\Delta x} \qquad (56)$$

The left side is the derivative of the $u(x)$ function at point x_i, Δx is a small arbitrary distance on the x axis and the terms are called forward, backward and central differences, respectively (it is easy to see that the central difference is the average of the forward and the backward ones). It is very common in numerical problems (e.g. integration of functions or searching for roots of polynomials) that an appropriate grid (also called mesh) is defined on the domain of the function, values of the function are known at the grid points and further values are calculated using these previously known values. Equidistant grids (where Δx is constant) are useful and practical for many cases, but the grid points have to be chosen cautiously at other times to minimize the error of the approximation (the difference between the real and the calculated

values). Using such a method, complicated differential and integral issues can be discretized and rendered computationally solvable.

Higher order derivatives can be similarly estimated by finite differences, e.g. second order central difference is given in eq. (57):

$$u''(x_i) \approx \frac{u(x_i + \Delta x) - 2u(x_i) + u(x_i - \Delta x)}{\Delta x^2} \tag{57}$$

It is convenient to rewrite eqs. (56) and (57) into a closed form using matrix multiplication. Assuming an equidistant one-dimensional grid with an interval length of h, the central difference in eq. (56) takes the following form:

$$u'(x_i) \approx \frac{1}{2h}\begin{pmatrix}1 & 0 & -1\end{pmatrix}\begin{pmatrix}u_{xi+1}\\ u_{xi}\\ u_{xi-1}\end{pmatrix} \tag{58}$$

Here, u_{xi} denotes the value of u at grid point x_i, and $x_{i+1} = x_i + h$, $x_{i-1} = x_i - h$.

The second order difference can be similarly represented with matrix multiplication, by

$$u''(x_i) \approx \frac{1}{h}\begin{pmatrix}1 & -2 & 1\end{pmatrix}\begin{pmatrix}u_{xi+1}\\ u_{xi}\\ u_{xi-1}\end{pmatrix} \tag{59}$$

Eqs. (58) and (59) are easily applicable to multivariate functions. Our model requires a two dimensional grid to resolve the x and r extents of the reaction space. According to eq. (55), $\frac{\partial^2 c}{\partial x^2}$, $\frac{\partial c}{\partial r}$ and $\frac{\partial^2 c}{\partial r^2}$ need to be approximated. Applying eqs. (56) and (57) in eq. (55) gives:

$$\left(\frac{\partial^2 c}{\partial x^2} + \frac{1}{r}\frac{\partial c}{\partial r} + \frac{\partial^2 c}{\partial r^2}\right)_{i,j} \approx \frac{c(x_{i+1},r_j) - 2c(x_i,r_j) + c(x_{i-1},r_j)}{\Delta x^2} + \frac{1}{r}\frac{c(x_i,r_{j+1}) - c(x_i,r_{j-1})}{\Delta r} + \tag{60}$$

$$+ \frac{c(x_i,r_{j+1}) - 2c(x_i,r_j) + c(x_i,r_{j-1})}{\Delta r^2}$$

Here i and j are the indices of the grid representing x and r, axes and c can either be $c(SO_4^{\bullet -})$ or $c(I^-)$. The sum of eqs. (61)-(63) yields eq. (60) if eqs. (58) and (59) are used in a two-dimensional arrangement.

$$\left(\frac{\partial^2 c}{\partial x^2}\right)_{i,j} \approx {}_{i\rightarrow}\begin{pmatrix} & & \overset{j}{\downarrow} & & \\ -2 & 1 & 0 & \cdots & 0 \\ 1 & \ddots & & & \vdots \\ \vdots & 1 & -2 & 1 & \vdots \\ \vdots & & & \ddots & 1 \\ 0 & \cdots & 0 & 1 & -2 \end{pmatrix} \times \begin{pmatrix} & \vdots & \\ & c(x_{i-1},r_j) & \\ \cdots & c(x_i,r_j) & \cdots \\ & c(x_{i+1},r_j) & \\ & \vdots & \end{pmatrix} \times \frac{1}{\Delta x^2} \tag{61}$$

$$\frac{1}{r}\left(\frac{\partial c}{\partial r}\right)_{i,j} \approx \begin{pmatrix} & \vdots & & & \\ \cdots & c(x_i,r_{j-1}) & c(x_i,r_j) & c(x_i,r_{j+1}) & \cdots \\ & \vdots & & & \end{pmatrix} \times {}_{i\rightarrow}\begin{pmatrix} 0 & -1 & \overset{j}{\downarrow} & \cdots & 0 \\ 1 & \ddots & -1 & & \vdots \\ \vdots & & 0 & & \vdots \\ \vdots & & 1 & \ddots & -1 \\ 0 & \cdots & \cdots & 1 & 0 \end{pmatrix} \times \frac{1}{\Delta r} \times \frac{1}{r} \tag{62}$$

$$\left(\frac{\partial^2 c}{\partial r^2}\right)_{i,j} \approx \begin{pmatrix} & \vdots & & & \\ \cdots & c(x_i,r_{j-1}) & c(x_i,r_j) & c(x_i,r_{j+1}) & \cdots \\ & \vdots & & & \end{pmatrix} \times {}_{i\rightarrow}\begin{pmatrix} -2 & 1 & \overset{j}{\downarrow} & \cdots & 0 \\ 1 & \ddots & 1 & & \vdots \\ \vdots & & -2 & & \vdots \\ \vdots & & 1 & \ddots & 1 \\ 0 & \cdots & \cdots & 1 & -2 \end{pmatrix} \times \frac{1}{\Delta r^2} \tag{63}$$

The limitation of this method (i.e. the production of the differences by matrix multiplication using coefficient matrices) arises from the $r = 0$ case (eq. (62) contains r in the denominator), which is one of the boundary conditions for solving eq. (55). Physically, $r = 0$ is at the central axis of the cylinder, no diffusion occurs along this axis as a consequence of the cylindrical symmetry. This condition cannot be handled in the frame of the formulation above, an alternative treatment of the diffusion term is given in the following sections.

5.3.4. Model of the reaction space

Our description of the reaction space is a modified version of a model provided by Cassidy and Long (see Section 2.4).[141] These authors published a two-dimensional model for measuring pseudo-first order rate constants in laser flash photolysis experiments in collinear arrangement, where the laser beam and the analyzing beam are parallel to each other. In our calculations, we assumed crossed or perpendicular arrangement in accordance based on the experimental setup. Figure 5.40 shows the geometric model applied to represent the physical reaction space.

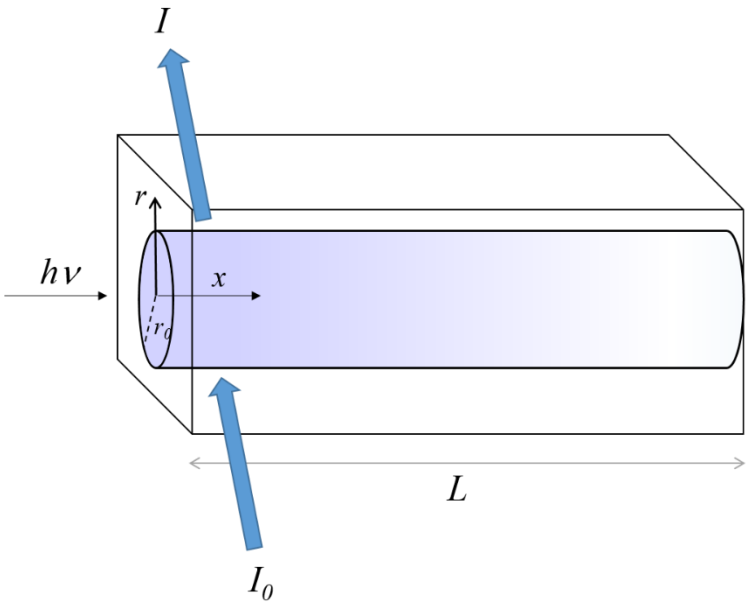

Figure 5.40. Model geometry for modelling the role of diffusion in laser flash photolysis experiments. See explanation of the labels in the text below.

The arrow labelled '*hν*' represents the laser beam and the blue arrow is the analyzing beam that is used to follow the concentration of the transient species. Adapting the common notations of Beer's law, I_0 is the intensity of the entering light beam and I is the intensity of the leaving beam. x and r are the labels of the spatial axes, L is the path length of the cuvette in the direction of the laser beam. The cross section of the laser beam is considered to be circular with r_0 radius, and the origin is fixed to the center of this circle at the entering point of the laser. The shading refers to the decreasing concentration of the transient species along the laser beam.

Sulfate ion radical is generated by the laser pulse along the x axis, radially from the origin within r_0, thus forming a cylinder-shaped volume. An external radius is defined (r_{ex}, Figure 5.41) around this object, diffusion of both sulfate ion radical and iodide ions is allowed from this outer shell to the internal cylinder and vice versa.

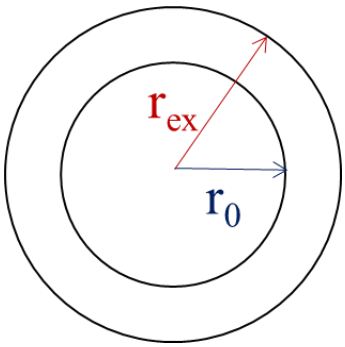

Figure 5.41. Cross section of the reaction space, approximated by the unity of an inner (r_0) and outer (r_{ex}) cylinder.

5.3.5. Discrete random walk model of diffusion

According to Section 5.3.4., the reaction of sulfate ion radical and iodide ion takes place in a cylindrical space, surrounded by an external tube which is accessible for the diffusive motion of the particles. In order to calculate the spatial distribution of each reactant, the reaction space (including the outer shell) is divided into small volume units that are shaped like cylinder rings (Figure 5.42.).

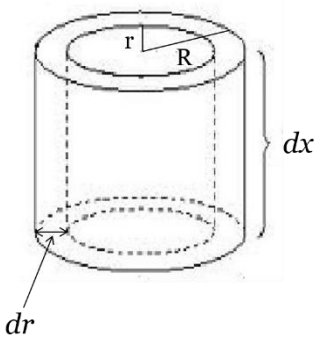

Figure 5.42. Shape of the volume units.

This kind of resolution into elementary volumes or cells replaces the interpretation in 5.3.3, where a two dimensional grid was introduced on the *x* and *r* axes. This model is conceptually different, in a sense that instead of approximating each partial derivatives in eq. (55) individually, diffusion in each volume unit is treated as a matter exchange with the neighboring cells.

The number of particles in a certain cell in a given time interval changes via two ways: species can arrive from the nearby cells and others can leave the unit to enter those adjacent cells. Therefore, the change of concentration in the cell will be the resultant of the outflow and the inflow via diffusion. It is important to note that only the diffusion term is considered at this point, the reaction term is introduced at a later stage.

An arbitrary volume unit is in juxtaposition with four other ones, two in axial, two in radial directions. In the *x* direction, they form a shape like a longer tube, whereas in the radial dimension, the smaller ones are embedded into the bigger ones.

The nearby volume units have common ‘walls’, through which diffusion takes place. In accordance with Fick’s 1st law, the flow rate of the components between two chosen units is proportional to the common surface and the concentration gradient.[56] Reactants are only allowed to move until they reach the borders of the reaction space ($0 \le r \le r_{ex}$ and $0 \le x \le L$), there is no flux of matter on the boundaries.

Let's take a cylinder ring with an inner radius of *r*, an outer radius of *r* + *dr* and a height of *dx*. For the sake of simplicity, we can assume that *dr* = *dx* = 1.

The surface of such an object consists of four parts (see Table 7), two circle rings or annulus of equal area, an outer side and an inner side, both of which have the shape of a curved rectangular.

Table 7. Surface area of the parts of a cylinder ring with a grid size of *dr* = *dx* =1

outer radius = *r*	Surface area	Fraction of the total area
Upper annulus	$r^2\pi-(r-1)^2\pi=(2r-1)\pi$	$\frac{2r-1}{8r-4}=\frac{1}{4}$
Lower annulus	$r^2\pi-(r-1)^2\pi=(2r-1)\pi$	$\frac{2r-1}{8r-4}=\frac{1}{4}$
Outer surface	$2r\pi$	$\frac{2r}{8r-4}$
Inner surface	$2(r-1)\pi$	$\frac{2r-2}{8r-4}$
Total	$(8r-4)\pi$	1

Clearly, the inner surface of this unit is the outer surface of the one inside it and reversely, its outer surface is equal to the inner surface of the next one with increased radius.

The volume of the described object is:

$$V = r^2\pi - (r-1)^2\pi = (2r-1)\pi \tag{64}$$

The volumes of its neighboring cells are $(2r-1)\pi$ (upper and lower; $x\pm1$, r), $(2r+1)\pi$ (outside; x,r+1) and $(2r-3)\pi$ (inside; x, r–1).

As stated before, the diffusion term can be decomposed into outflow and inflow from and into each particularly volume unit. The outflow term is quite straightforward to demonstrate. It is assumed that all particles leave the cell, at each surface part according to its ratio to the total surface (Table 7, column 3). In a general volume unit, where the actual concentration is $c(x,r)$, the scheme of the diffusion is shown in Figure 5.43.

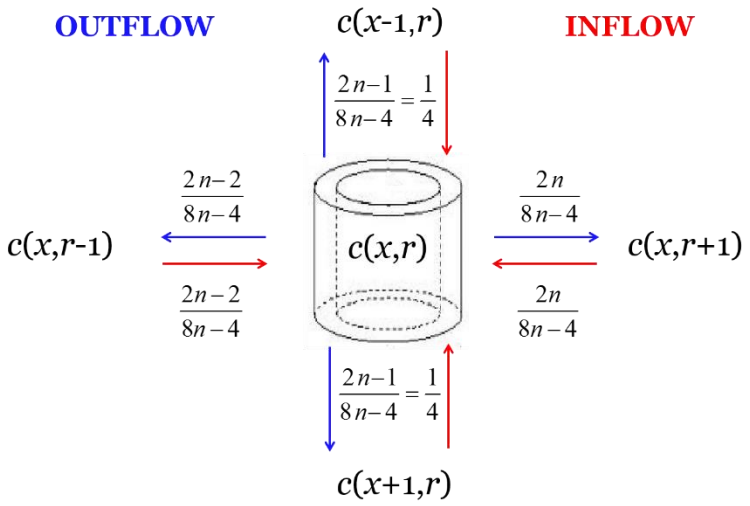

Figure 5.43. Exchange of matter in a volume unit of general position. The unit shown has an inner radius of $r - 1$ and an outer radius of r, having an index of n in the radial direction ($r = 0$ is the first one, where $n = 1$). The ratios given in the figure have to be multiplied by the diffusion coefficient. Blue arrows represent the outflow from the cell, right arrows correspond to the inflow from the neighboring units.

Figure 5.43 refers to a cell in general position, i.e. it is located inside the reaction space, it does not reach any of the boundaries ($r \neq 0$; $r \neq r_{ex}$; $x \neq 0$; $x \neq$ L). When the cell has one or two border surfaces, then it is assumed that the fraction of the particles corresponding to that surface area do not leave the cell.

The inflow part is further divided into the inflow from the x and r neighbors. In the x direction, cells have the same volume (since r is constant). Therefore, the number of residing particles has the same ratio as their concentrations. Eq. (65) gives the x inflow into the $c(x,r)$ unit.

$$\frac{1}{4}c(x-1,r)+\frac{1}{4}c(x+1,r)=\begin{pmatrix}\frac{1}{4} & 0 & \frac{1}{4}\end{pmatrix}\begin{pmatrix}c_{x-1,r}\\ c_{x,r}\\ c_{x+1,r}\end{pmatrix} \tag{65}$$

In the case of the radial inflow, not only the common surface, but the ratio of the volumes is considered in the following multiplication:

$$\text{radial inflow} = c(x,r+1)\frac{A_{in,n+1}}{A_{tot,n+1}}\frac{V_{n+1}}{V_n}+c(x,r-1)\frac{A_{out,n-1}}{A_{tot,n-1}}\frac{V_{n-1}}{V_n} \tag{66}$$

Substituting the known volumes and surfaces into eq. (66) gives:

$$c(x,r+1)\frac{2n}{8n+4}\frac{2n+1}{2n-1}+c(x,r-1)\frac{2n-2}{8n-12}\frac{2n-3}{2n-1} \tag{67}$$

Upon simplification, the following equation is obtained:

$$c(x,r+1)\frac{2n}{8n-4}+c(x,r-1)\frac{2n-2}{8n-4}=\begin{pmatrix}c_{x,r-1} & c_{x,r} & c_{x,r+1}\end{pmatrix}\begin{pmatrix}v(r)\\0\\u(r)\end{pmatrix} \tag{68}$$

Here $v(r)$ and $u(r)$ are the coefficients describing the inflow from the inner and the outer cells, respectively.

Separate matrices were defined for coefficients containing the x inflow (DX), the r inflow (DR) and the outflow as well (DE). Using these matrices, the right hand side of eq. (55), still without the reaction term, can be reconstituted as eq. (69)

$$\mathrm{D}\cdot(\mathrm{DX}\times\mathbf{c}+\mathbf{c}\times\mathrm{DR}+\mathrm{DE}.\times\mathbf{c}) \tag{69}$$

Here, $\cdot$ is the regular multiplication sign, $\times$ is the matrix multiplication and $.\times$ is the element-wise multiplication of matrices. Matrix multiplication is sensitive to the order of the factors, and the matrix dimensions have to match for a valid operation.

5.3.6. Numerical integration

According to the Newton-Leibniz formula, one of the fundamental theorems of calculus, the definite integral of an $u(x)$ univariate function between x_i and x_{i+1} point is given as

$$u(x_{i+1})=u(x_i)+\int_{x_i}^{x_{i+1}}u'(s)ds \tag{70}$$

Eq. (70) is in the background in the numerical solutions of kinetic differential equations, where the independent variable is time and the dependent variables are concentrations. Our previous efforts were targeted to give a reasonable approximation of the right hand side of (55), i.e. the derivative of concentrations with respect to time. The next step is to define how to obtain the $\mathbf{c}(t+h)$ concentrations in the possession of the $\mathbf{c}(t)$ values.

Definite integration is another operation that computers cannot handle directly (although symbolic softwares such as Mathematica contain numerous primitive functions). A plethora of algorithms exist for numerical integration, the approximation of definite integrals between two time points (or whatever is the independent variable).[191]

The most widely used algorithm in chemical kinetics is the fourth-order Runge-Kutta method (RK4),[91] because it is relatively easy to code and it has high accuracy, given that time step length (h) is chosen correctly. Adaptive time stepping is practical in most cases, where the step size gradually changes as the iteration proceeds.

In the light of the points above, our calculations were built up by the following stages:

- Estimation of the initial spatial distribution of the concentrations of $SO_4^{\bullet-}$ and I^- ($c(x,r)_0$)
- Composition of the inflow and outflow matrices for the diffusion term (approximation of derivatives)
- Numerical integration by the RK4 algorithm
- Testing the diffusion matrices
- Introduction of the second order reaction between the two reactants
- Numerical integration (RK4)
- Processing; potential effect of diffusion is tested

5.3.7. Initial concentrations

From a chemical point of view, the studied system is a second order reaction between sulfate ion radical and iodide ion, only reaction (42) is taken into account. $SO_4^{\bullet-}$ is generated by the laser beam (from $K_2S_2O_8$), iodide ion in homogeneous spatial distribution is already in the cuvette.

Eqs. (71)-(73) give the spatial concentration distribution of the reactants at $t = 0$.

$$c_{A0} = \frac{N_{hv}}{A_{ex}} \cdot \varepsilon(S_2O_8^{2-}) \cdot \Phi \cdot c(S_2O_8^{2-}) \tag{71}$$

$$c_A = \begin{cases} c_{A0} \cdot 10^{-Abs_{1\,cm} \cdot \frac{x}{1\,mm}} & 0 \le r \le r_0 \\ 0 & r_0 < r \le r_{ex} \end{cases} \tag{72}$$

$$c_B = c_{B0} \tag{73}$$

The meaning of the variables and parameters in eqs. (71)-(73) is listed below (all given and used in SI units to avoid any ambiguities in the calculations).

- A and B denote the two reactants, $SO_4^{\bullet-}$ and I^-, respectively
- c_A and c_B are the variables that represent the actual concentration of the reactants (number of particles in a given volume unit).
- $\frac{N_{hv}}{A_{ex}}$: number of photons per excited area (which is a circle with r_0 radius)
- Energy/pulse = 40 mJ

- $\varepsilon(S_2O_8^{2-})$: molar absorption coefficient of persulfate ions at the excitation wavelength (λ_{ex} = 266 nm; ε(266 nm) = 1.047 m^2 mol^{-1})
- Φ: quantum efficiency of the homolytic scission of the peroxy bond in peroxodisulfate ion (eq. 3)
- $c(S_2O_8^{2-})$ = 0.15 M
- $Abs_{1\ cm}$ = 1.5 (absorption of the $K_2S_2O_8$ solution over a 1.000 cm path length)
- x is the axial distance measured from the front face of the cuvette

Eq. (72) corresponds to Beer's law in a sense that the measured absorption is linearly proportional to the optical path length. It shows that the initial concentration of the sulfate ion radical will be maximal at the front face of the cuvette (where the laser beam is introduced).

The axially decreasing concentration of the transient species is also an important experimental issue, the analyzing beam is commonly adjusted to measure very close to the front window. Yet, with a low absorbing species such as the sulfate ion radical, one often has to work with *Abs* values in the 0.04-0.1 range.

c_{B0} will be equal within the entire volume of the reaction space, as stated in eq. (73).

For the sake of simplicity, the laser beam is supposed to have uniform energy distribution, this fact is used for the calculation of photon flux ($N_{h\nu}/A_{ex}$).

5.3.8. Effect of diffusion

Starting with the c_{A0} and c_{B0} initial matrices, numerical integration was carried out with the RK4 method in order to test if our algorithm fulfills some chemically grounded conditions.

i. The first requirement was that the law of mass conservation had to be met, the total number of particles had to remain constant throughout the calculation
ii. Since the driving force of diffusion is the concentration gradient, the diffusive motion has to proceed until uniform spatial distribution is reached in the reaction space
iii. The distribution of iodide ions should not change since they are evenly distributed at the initial time point

The time step size was chosen in a way that the highest concentration would not change more than 2% in an integration step. All three criteria were satisfied, which confirmed the validity or our model. Following this test, we could proceed to examine the effect of diffusion when the second order reaction of the two components took place.

5.3.9. Introducing the reaction term

Although the reaction between sulfate ion radical and iodide ion is a multistep system, as shown in eqs. (42)-(43), only eq. (42) is taken into account in the present RD system, the direct reaction between $SO_4^{\bullet-}$ and I^-. The measured second order rate constant of the reaction (42), $k_{42} = (5.7 \pm 0.1) \times 10^9\ M^{-1}\ s^{-1} = (5.7 \pm 0.1) \times 10^6\ m^3\ mol^{-1}\ s^{-1}$ (SI base units), is given as an input parameter. This is the slope of the line **a** in Figure 5.17. Together with the included reaction term and substituting (69), eq. (55) takes the following form:

$$\frac{\partial \mathbf{c}}{\partial t} = D \cdot (DX \times c + c \times DR + DE. \times c) - k \cdot c_A . \times c_B \qquad (74)$$

In the new algorithm, we defined a maximum step number to limit the calculation time and a modified stop condition was given. The loop was finished once the total number of $SO_4^{\bullet-}$ decreased to 1% of the initial value. The law of mass conservation was no longer valid, the sulfate ion radical gradually disappeared as it was reduced by I^-.

It was observed that the species did not reach the walls, they only started to move towards the borders of the reaction space, before the ongoing reaction consumed them rapidly.

5.3.10. Calculation of absorbance

Examination of the probe beam of the laser flash photolysis instrument showed that the beam has a circular shape with a 3 mm diameter (*w*) and the edge of the detection circle is 1 mm (*s*) away from the front face of the cuvette (Figure 5.44). This is by no mean negligible compared to the 6 mm diameter of the laser beam and the entire path length of the excitation. Consequently, the effective optical path (*l*(*r*)), which is the length the detection beam travels through the sample, is shorter than the diameter of the reaction space.

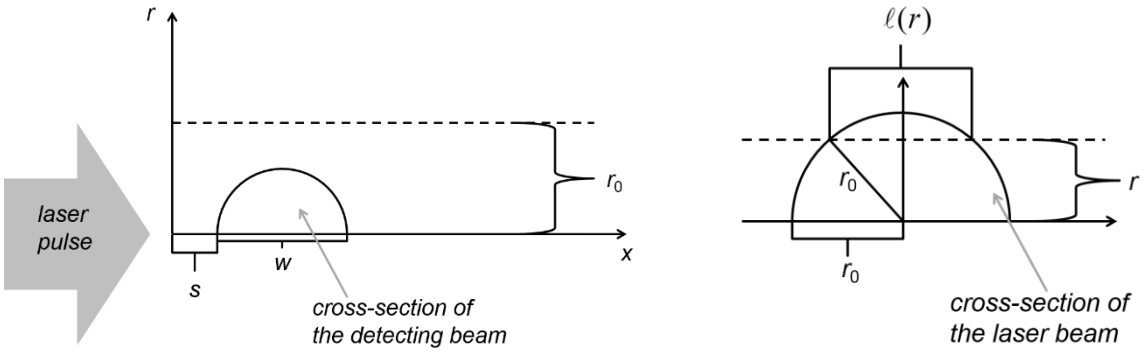

Figure 5.44. Schematic geometric depiction of the absorbance detection in laser flash photolysis experiments.

Therefore, the absorbance values had to be evaluated numerically at each time point. Again, it was assumed that the detection light beam is homogeneous, i.e. the intensity per unit area does not depend on the spatial coordinated within the cross section of the beam.

A rather long but also highly routine mathematical derivation showed for this particular geometry, the detected absorbance can be calculated by the following integral:

$$A_{\text{detected}} = -\log_{10} \frac{8}{w^2 \pi} \int_0^{w/2} \left[\int_{s+w/2-\sqrt{w^2/4-r^2}}^{s+w/2+\sqrt{w^2/4-r^2}} e^{-\varepsilon_A 2 \int_0^{\sqrt{r_0^2-r^2}} c_A\left(x,\sqrt{r^2+\rho^2}\right) d\rho} dx \right] dr \tag{75}$$

This value of the integral was calculated numerically at each time point of the simulations.

5.3.11. Obtained second order rate constant

The simulated data were processed as follows.

- Absorbance was calculated as described above and plotted against time
- The obtained plot was fitted with a single exponential curve (pseudo-first order plot)
- The initial concentration of iodide ion was altered and the fitted k_{obs} parameters were plotted against the applied I^- concentration

Observations:

- The simulated curves fitted nicely to single exponential curves from 1:2.5 = $[SO_4^{\bullet -}]_0$: $[I^-]_0$ ratio
- Below this limit, mixed second order fit was required
- The obtained k_{obs} values showed linear dependence on the excess iodide ion concentrations (Figure 5.45)
- The slope of the linear fit to this function provided a second order rate constant of 5.65 $\times$ 10^9 M^{-1} s^{-1}, which is in very good agreement with the k value given as the input parameter.

Figure 5.45 shows that diffusion did not have a significant effect on the time scale of the reaction. The rate constants nicely agree in the millimolar range of iodide ion concentrations.

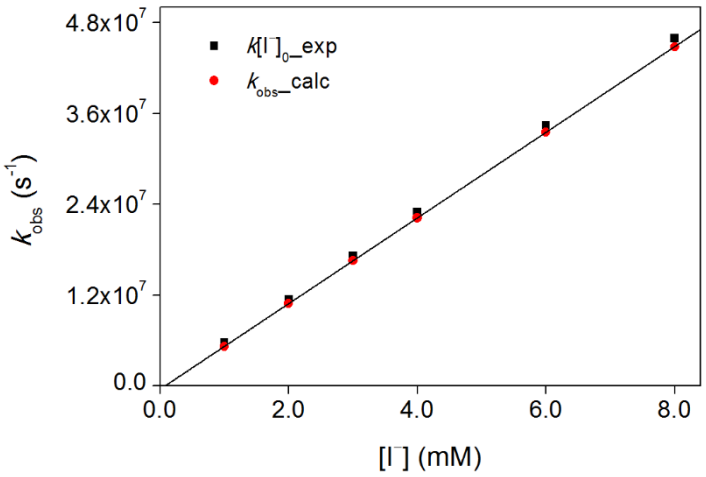

Figure 5.45. Simulated pseudo-first order rate constants as a function of initial iodide ion concentrations (c_{B0}). Linear dependence was obtained with a slope of 5.65×10^6 (values are given in mM in horizontal axis), which agrees very well with an experimental rate constant of $(5.7 \pm 0.1) \times 10^9$ M^{-1} s^{-1}, showing that diffusion does not interfere significantly in such a rapid reaction within the reaction time.

6. Summary

This thesis is a sequel and completion of previous studies from our research group, focusing on the kinetics and mechanisms of photoinitiated autoxidation of S(IV). Earlier works revealed the catalytic role of iron(II), iodide ions and cerium(III) ions in the autoxidation mechanisms and introduced the application of diode array spectrophotometer to drive and detect the reaction.[55,77-79]

Free radical mediated chain mechanisms govern the autoxidation systems, in which sulfite, sulfate and peroxomonosulfate ion radicals ($SO_3^{\bullet-}$, $SO_4^{\bullet-}$ and $SO_5^{\bullet-}$) are the common chain carriers. Sulfate ion radical seems to be of main importance in the catalysis for two reasons. The reaction of $SO_4^{\bullet-}$ with the catalyst is essential for chain propagation and its second order recombination into peroxodisulfate ion usually provides the only significant route of chain termination.

In order to gain full understanding of autoxidation mechanisms, we set our sights on the investigation of all possible subsystems. The redox reaction of S(IV) with the $S_2O_8^{2-}$ ions (product of chain termination) is expected to produce sulfate ion radical via synproprotionation. However, previous kinetic studies showed that this particular reaction is undetectably slow in acidic medium in the absence of catalysts. Oxidation reactions of peroxodisulfate ion are generally slow, despite the high respective redox potential. Silver(I) ion is a well-known catalysts for such reactions, because it initiates the disproportionation of $S_2O_8^{2-}$ into sulfate ion and sulfate ion radical, with the formation of Ag(II), a highly oxidizing species.[43-45] Therefore, we aimed to catalyze the synproportionation by the addition of silver nitrate. Preliminary results showed that the autoxidation of S(IV) was successfully initiated in this way. Photoinitiation was not necessary in this case, the application of diode array spectophotometers was therefore avoided to prevent photochemical side reactions. This thesis presents and discusses detailed kinetic studies of the silver(I) catalyzed autoxidation in the presence of peroxodisulfate as a co-catalyst as well as mechanistic conclusions drawn from such experiments. A reaction scheme of 9 steps is suggested (Scheme 1) and a fairly complicated but well established rate law is derived in eq. (38) to interpret the observed kinetic data.

The second order reaction of sulfate ion radical with silver(I) ion (R2 in Scheme 1) is a putative chain propagation step of the proposed scheme of the Ag^+ catalyzed autoxidation. During the derivation of the rate law, the long chain assumption was applied, which postulates that propagation steps are faster than the initiation and the termination steps (otherwise the chain would not be viable) and the rates of all propagation steps are equal. Independent confirmation

of the rapid nature of the reaction of silver(I) and sulfate ion radical became available by the application of the laser flash photolysis technique. A newly acquired Applied Photophysics laser flash photolysis (LFP) instrument of nanosecond time resolution allowed us to study the reactions of the sulfate ion radical in a direct manner. $SO_4^{\bullet-}$ was generated by the photolysis of $K_2S_2O_8$ by a 266 nm pulse and followed by its absorption at 450 nm. The second order rate constant of its reaction with silver(I) ion was determined under pseudo-first order conditions, the measured value is $(7.7 \pm 0.5) \times 10^9$ M^{-1} s^{-1} in strongly acidic medium. This value approaches the diffusion controlled limit, affirming the role of reaction (19) in chain propagation.

Similarly to the case of silver(I), the second order reactions of sulfate ion radical with previously recognized catalysts of the autoxidation of S(IV) were studied. Rate constants for Ce(III) and iodide ions were determined, as well as further rate constants with halide ions, a few biomolecules and S(IV).

In the sulfate ion radical–iodide ion system, interesting kinetic behavior was observed. The recorded kinetic curves fitted to double exponential kinetics, and both fitted parameters showed linear dependence on the concentration of iodide ion. One of the two dependence functions went through the origin. Therefore, the respective rate constant was assigned to reaction (42). The other line had a significant intercept with the vertical axis, it was thus concluded to belong to the reversible reaction of iodide ion and iodine atom, producing iodide molecule anion (I_2^-). This was suggested as a novel method for generation iodine atoms and the equilibrium constant of (43) was determined.

Pseudo-first order behavior was observed in the sulfate ion radical–iodide ion system, even though the prerequisite for pseudo-first order kinetics, the high excess of iodide ions, was not reached *locally* at the site of observation. The potential replenishment of iodide ions by diffusion from outside the reaction space was examined by a numerical model. The reaction space was divided into unit volumes and an outer radius was defined inside which diffusion of particles was allowed. The random walk model of diffusion was applied to simplify the solution of the operative partial differential equation (PDE) system. Using a chemically conceivable parameter set, it was shown that for a rate constant in the 10^9 M^{-1} s^{-1} order of magnitude, diffusion does not influence the determination of the rate constant within the time frame of the reaction.

7. Összefoglalás

Ez az értekezés közvetlen folytatása és kiegészítése a kutatócsoportunkban korábban lezajlott vizsgálatoknak a kén(IV) autooxidációjának kinetikájával és mechanizmusával kapcsolatosan. Ezek a korábbi munkák feltárták a Ce(III) és I^- ionok katalitikus szerepét valamint a Fe(II) ionok lehetséges részvételét a fotoiniciált autooxidációs mechanizmusban. A kísérletek során diódasoros spektrofotométert alkalmaztak a reakciók indítására és követésére egyaránt.[54,75-77]

Az autooxidációs folyamatok mechanizmusa gyökös láncreakció, amelyben szulfit-, szulfát- és peroxomonoszulfát-iongyökök (rendre $SO_3^{\bullet-}$, $SO_4^{\bullet-}$ és $SO_5^{\bullet-}$) a közös láncvivők. Az eredmények azt mutatják, hogy a szulfátiongyök ($SO_4^{\bullet-}$) kiemelt szerepet tölt be a katalízisben, kétféle okból. A szulfátiongyök reakciója a katalizátorral fontos láncvivő lépés valamint a peroxodiszulfát ionokat termelő másodrendű rekombinációja többnyire az egyetlen jelentős lánclezáró lépés.

Az autooxidáció mechanizmusának mélyebb megértése érdekében célul tűztük ki a mechanizmust felépítő részrendszerek független vizsgálatát. Egy ilyen részrendszer a S(IV) reakciója a lánczáró lépésben képződő peroxodiszulfát-ionnal, amely vélhetően szinproporciós folyamatban szulfátiongyököt termel. Korábbi eredmények alapján az említett reakció savas közegben, katalizátor távollétében rendkívül lassú. Az $S_2O_8^{2-}$ ionok redoxireakciói kinetikai gátlás miatt többnyire igen lassúak a nagy redoxipotenciál ellenére is. Az ezüstionok a peroxodiszulfát ion oxidációs reakcióinak jól ismert katalizátorai, mivel az iniciáló lépés termékei a szulfátion mellett igen reaktív részecskék, Ag(II) és szulfátiongyök.[43-45] Vizsgálataink során ezért ezüst-nitrátot adtunk a S(IV)–oxigén–peroxodiszulfát reakcióelegyekhez, erősen savas közegben. Előkísérletek alapján a S(IV) autooxidációja ily módon hatékonyan iniciálható. A fotokémiai mellékreakció kizárása érdekében a diódasoros spektrofotométer alkalmazását kísérleteink során kizártuk, normál spektrofotométer segítségével követtük a reakciót.

Ez a dolgozat részletesen ismerteti a S(IV) ezüst ionok által katalizált autooxidációjának kinetikai vizsgálatát, peroxodiszulfát-ion, mint ko-katalizátor jelenlétében. A kísérletekből levont mechanisztikus következtetések ugyancsak a dolgozat tárgyát képezik. Kilenc lépésből álló mechanizmust javasoltunk (Scheme 1), valamint egy némileg összetett, ugyanakkor kinetikailag megalapozott sebességi egyenletet vezettünk le (38) a kinetikai adatok értelmezésére.

A szulfátiongyök és az ezüstionok közötti másodrendű reakció (Scheme 1; R2) az ezüstionok által katalizált autooxidáció általunk javasolt mechanizmusának egyik láncvivő lépése. A sebességi egyenlet levezetése során a hosszú láncot feltételező megközelítést alkalmaztuk, amely feltételezi, hogy a láncvivő lépések sebessége nagyobb, mint a láncindító és a lánclezáró lépéseké (mivel másképp a láncreakció nem tudna lezajlani), illetve azt is, hogy a láncvivő lépések sebessége megegyezik. Annak igazolását, hogy a szulfátiongyök ($SO_4^{\bullet-}$) és az Ag^+ ionok között igen gyors reakció játszódik le, lézeres villanófény-fotolízis módszer alkalmazása tette lehetővé. A tanszékünkön nemrégiben megvásárolt Applied Photophysics nanoszekundum időfelbontású villanófény-fotolízis készülék segítségével közvetlenül tudtuk tanulmányozni a szulfátiongyök reakcióinak kinetikáját. Az $SO_4^{\bullet-}$ gyököket $K_2S_2O_8$ oldat fotolízisével állítottuk elő 266 nm hullámhosszúságú lézerimpulzus segítségével. A reakciókat 450 nm-en, a szulfátiongyök elnyelési maximumán követtük. Az ezüstionnal való reakciót pszeudo-elsőrendű körülmények között vizsgáltuk, és a másodrendű sebességi állandó mért értéke $(7.7 \pm 0.5) \times 10^9\ M^{-1}s^{-1}$ volt, erősen savas körülmények között. Ez az érték megközelíti a diffúzió kontrollált reakciók sebességi állandójának maximális értékét, megerősítve a (19) reakció láncvivő lépésként való részvételét a mechanizmusban.

Az ezüstionokhoz hasonlóan tanulmányoztuk a szulfátiongyök másodrendű reakcióit az autooxidáció korábban megismert katalizátoraival is. Meghatároztuk a másodrendű sebességi állandók értékeit Ce(III) ionokkal és I^- ionokkal, valamint egyéb halogenidionokkal, néhány biomolekulával és S(IV) tartalmú részecskékkel.

A szulfátiongyök–jodidion rendszerben érdekes kinetikai viselkedést figyelhettünk meg. A reakciót 340 nm-en, a jód molekulaion (I_2^-) elnyelési maximumán követtük és a felvett kinetikai görbéket két exponenciális görbe összegével illesztettük. Mindkét illesztett sebességi állandó típusú paraméter lineáris függést mutatott a jodidionok koncentrációjától. Az egyik lineáris függvény átment az origón, így ezt az állandót hozzárendeltük a (42) reakcióhoz. A másik függvénynek jelentős függőleges tengelymetszete volt, így ebből a függvényből meghatároztuk a (43) reakció oda- és visszairányú sebességi állandóját, valamint a folyamatot jellemző egyensúlyi állandót. Ezzel új módszert találtunk a jódatomok előállítására.

A szulfátiongyök–jodidion rendszerben pszeudo-elsőrendű viselkedést tapasztaltunk, noha ennek feltétele, a jodidionok nagy feleslege *lokálisan* nem teljesül a reakcióelegyben, mivel a szulfátiongyök egy kis térfogatrészben képződik a lézersugár haladási iránya által meghatározott módon. Matematikai modellt vezettünk be annak vizsgálatára, hogy van-e mód

a jodidionok diffúzió általi pótlására a reakciótéren kívüli térrészből és ezáltal a pszeudo-elsőrendű kinetikához szükséges koncentrációarány visszaállítására.

A henger alakú reakcióteret kis térfogatelemekre bontottuk és meghatároztunk egy külső sugarat, amelyen belülről megengedett a részecskék diffúziója a reakciótérbe és onnan kifelé. A diffúzió véletlen bolyongás modelljét alkalmaztuk a rendszert leíró parciális differenciál egyenletrendszer megoldásának egyszerűsítésére. Egy kémiailag reális paraméterkészlet használatával azt találtuk, hogy 10^9 M^{-1} s^{-1} nagyságrendű másodrendű sebességi állandó esetén a diffúzió nem befolyásolja a pszeudo-elsőrendű sebességi állandó meghatározását, a reakció időskáláján nincs meghatározó szerepe.

8. References

1. Greenwood, N. N.; Earnshaw, A. *Chemistry of the Elements, 2nd ed.*; Butterworth-Heinemann: Oxford, U.K., **1997**.

2. *Wikipedia - Goldschmidt classification*; https://en.wikipedia.org/wiki/Goldschmidt_classification; accessed: 29 Dec 2015

3. Goldschmidt, V. M., *J. Chem. Soc.* **1937**, 655-673.

4. *The Internet Classics Archive - The Odyssey by Homer*; http://classics.mit.edu/Homer/odyssey.12.xii.html; accessed: 8 Dec 2015

5. Lente, G., *Egyetemi Meteorológiai Füzetek* **2014**, *25*, 57-62.

6. Michie, C. A.; Langslow, D. R., *Br. Med. J.* **1988**, *297*, 1697-1699.

7. Editorial, *Nat. Chem.* **2009**, *1*, 333.

8. *Six Common Air Pollutants*; http://www3.epa.gov/airquality/urbanair/; accessed: 30 Dec 2015

9. Bannenberg, G.; Atzori, L.; Xue, J.; Auberson, S.; Kimland, M.; Ryrfeldt, A.; Lundberg, J. M.; Moldeus, P., *Respiration; international review of thoracic diseases* **1994**, *61*, 130-137.

10. Sunyer, J.; Atkinson, R.; Ballester, F.; Le Tertre, A.; Ayres, J. G.; Forastiere, F.; Forsberg, B.; Vonk, J. M.; Bisanti, L.; Anderson, R. H.; Schwartz, J.; Katsouyanni, K.; study, A., *Occup. Environ. Med.* **2003**, *60*, e2.

11. Day, J. J.; Yang, Z.; Chen, W.; Pacheco, A.; Xian, M., *ACS Chem. Biol.* **2016**.

12. Huie, R. E.; Neta, P., *Atmos. Environ.* **1987**, *21*, 1743-1747.

13. Graedel, T. E.; Crutzen, P. J., *Sci. Am.* **1989**, 58-68.

14. Schwartz, S. E., *Science* **1989**, *243*, 753-763.

15. Rose, J., *Environ. Sci. Technol.* **1993**, *27*, 2627.

16. Lynch, J. A.; Bowersox, V. C.; Grimm, J. W., *Environ. Sci. Technol.* **2000**, *34*, 940-949.

17. Penkett, S. A.; Jones, B.; Brice, K.; Eggleton, A. E., *Atmos. Environ.* **2007**, *41*, 154-168.

18. Hewitt, C. N.; Jackson, A. V. *Atmospheric science for environmental scientists*; John Wiley & Sons, **2009**.

19. Sandström, M.; Jalilehvand, F.; Persson, I.; Gelius, U.; Frank, P.; Hall-Roth, I., *Nature* **2002**, *415*, 893-897.

20. Charlson, R. J.; Valero, F. P. J.; Seinfeld, J. H., *Science* **2005**, *308*, 806-807.

21. Crutzen, P. J., *Clim. Change* **2006**, *77*, 211-220.

22. Pierce, J. R.; Weisenstein, D. K.; Heckendorn, P.; Peter, T.; Keith, D. W., *Geophys. Res. Lett.* **2010**, *37*.

23. Herrmann, H., *Phys. Chem. Chem. Phys.* **2007**, *9*, 3935-3964.

24. Antoniou, M. G.; Armah, A.; Dionysiou, D. D., *Applied Catalysis B: Environmental* **2010**, *96*, 290-298.

25. Gligorovski, S.; Strekowski, R.; Barbati, S.; Vione, D., *Chem. Rev.* **2015**, *115*, 13051-13092.

26. Herrmann, H.; Reese, A.; Zelhrer, R., *J. Mol. Struct.* **1995**, *348*, 183-186.

27. Herrmann, H., *Chem. Rev.* **2003**, *103*, 4691-4716.

28. Grgić, I.; Podkrajšek, B.; Barzaghi, P.; Herrmann, H., *Atmos. Environ.* **2007**, *41*, 9187-9194.

29. Herrmann, H.; Hoffmann, D.; Schaefer, T.; Bräuer, P.; Tilgner, A., *ChemPhysChem* **2010**, *11*, 3796-3822.

30. Deng, Y.; Ezyske, C. M., *Water Res.* **2011**, *45*, 6189-6194.

31. He, X.; Armah, A.; O'Shea, K. E.; Dionysiou, D. D., *Water Res.* **2014**, *63*, 168-178.

32. Lutze, H. V.; Bircher, S.; Rapp, I.; Kerlin, N.; Bakkour, R.; Geisler, M.; von Sonntag, C.; Schmidt, T. C., *Environ. Sci. Technol.* **2015**, *49*, 1673-1680.

33. Lutze, H. V.; Kerlin, N.; Schmidt, T. C., *Water Res.* **2015**, *72*, 349-360.

34. Wu, Y.; Bianco, A.; Brigante, M.; Dong, W.; De Sainte-Claire, P.; Hanna, K.; Mailhot, G., *Environ. Sci. Technol.* **2015**.

35. Zhou, D.; Zhang, H.; Chen, L., *J. Chem. Technol. Biotechnol.* **2015**, *90*, 775-779.

36. Vellanki, B. P.; Batchelor, B.; Abdel-Wahab, A., *Environ. Eng. Sci.* **2013**, *30*, 264-271.

37. Gau, B. C.; Chen, H.; Zhang, Y.; Gross, M. L., *Anal. Chem.* **2010**, *82*, 7821-7827.

38. *Handbook of Chemistry and Physics*; 93rd ed.; Haynes, W. M.; CRC Press, 2012-2013.

39. Das, T. N.; Huie, R. E.; Neta, P., *J. Phys. Chem. A* **1999**, *103*, 3581-3588.

40. Brandt, C.; van Eldik, R., *Chem. Rev.* **1995**, *95*, 119-190.

41. Bellér, G.; Bátki, G.; Lente, G.; Fábián, I., *J. Coord. Chem.* **2010**, *63*, 2586-2597.

42. Bellér, G.; Lente, G.; Fábián, I., *Inorg. Chem.* **2010**, *49*, 3968-3970.

43. House, D. A., *Chem. Rev.* **1962**, *62*, 185-203.

44. Kalb, A. J.; Allen, T. L., *J. Am. Chem. Soc.* **1964**, *86*, 5107-5112.

45. Kimura, M.; Kawajiri, T.; Tanida, M., *J. Chem. Soc., Dalton Trans.* **1980**, 726-730.

46. Lente, G.; Fábián, I., *Inorg. Chem.* **2004**, *43*, 4019-4025.

47. Takano, B., *Science* **1987**, *235*, 1633-1635.

48. Oh, S. R.; Kim, J. K.; Lee, M. J.; Choi, K., *Environ. Toxicol.* **2008**, *23*, 211-217.

49. Creutz, C.; Sutin, N., *Proc. Natl. Acad. Sci. U. S. A.* **1973**, *70*, 1701-1703.

50. Lambeth, D. O.; Palmer, G., *J. Biol. Chem.* **1973**, *248*, 6095-6103.

51. *ChemEngineering*; https://chemengineering.wikispaces.com/Claus+process; accessed: 4 Sep 2015

52. Nagy, P.; Winterbourn, C. C. In *Advances in Molecular Toxicology*; Elsevier: Netherlands, 2010; Vol. 4, p 183-222.

53. van Woerden, H. F., *Chem. Rev.* **1963**, *63*, 557-571.

54. Connick, R. E.; Tam, T. M.; Von Deuster, E., *Inorg. Chem.* **1982**, *21*, 103-107.

55. Kerezsi, I., *Fotokémiai jelenségek a szulfition redoxireakcióiban*, PhD Thesis, University of Debrecen, Debrecen, Hungary, **2006.** and references therein

56. Atkins, P. W. *Physical Chemistry*; 6th ed.; Oxford University Press: Oxford, U.K., **1998**.

57. Barcza, L.; Buvári, A. *A minőségi kémiai analízis alapjai*; Medicina Kiadó: Budapest, Hungary, **1997**.

58. Kraft, J.; van Eldik, R., *J. Chem. Soc., Chem. Comm.* **1989**, 790-792.

59. Kraft, J.; van Eldik, R., *Inorg. Chem.* **1989**, *28*, 2306-2312.

60. Kraft, J.; van Eldik, R., *Inorg. Chem.* **1989**, *28*, 2297-2305.

61. Kraft, J.; van Eldik, R., *Atmos. Environ.* **1989**, *23*, 2709-2713.

62. Brandt, C.; Fábián, I.; van Eldik, R., *Inorg. Chem.* **1994**, *33*, 687-701.

63. Brandt, C.; van Eldik, R., *Transit. Metal Chem.* **1998**, *23*, 667-675.

64. Fábián, I.; Csordás, V., *Adv. Inorg. Chem.* **2003**, *54*, 395-461.

65. Berglund, J.; Elding, L. I., *Atmos. Environ.* **1995**, *29*, 1379-1391.

66. Berglund, J.; Elding, L. I., *Inorg. Chem.* **1995**, *34*, 513-519.

67. Brandt, C.; Elding, L. I., *Atmos. Environ.* **1998**, *32*, 797-800.

68. Fronaeus, S.; Berglund, J.; Elding, L. I., *Inorg. Chem.* **1998**, *37*, 4939-4944.

69. Alexander, B.; Park, R. J.; Jacob, D. J.; Gong, S., *J. Geophys. Res.: Atmos.* **2009**, *114*, D02309.

70. Alipazaga, M. V.; Moreno, R. G.; Linares, E.; Medeiros, M. H.; Coichev, N., *Dalton Trans.* **2008**, 5636-5644.

71. Moreno, R. G.; Alipazaga, M. V.; Medeiros, M. H.; Coichev, N., *Dalton Trans.* **2005**, 1101-1107.

72. Anast, J. M.; Margerum, D. W., *Inorg. Chem.* **1981**, *20*, 2319-2326.

73. Lepentsiotis, V.; Domagala, J.; Grgic, I.; van Eldik, R.; Muller, J. G.; Burrows, C. J., *Inorg. Chem.* **1999**, *38*, 3500-3505.

74. Muller, J. G.; Hickerson, R. P.; Perez, R. J.; Burrows, C. J., *J. Am. Chem. Soc.* **1997**, *119*, 1501-1506.

75. Wietzerbin, K.; Muller, J. G.; Jameton, R. A.; Pratviel, G.; Bernadou, J.; Meunier, B.; Burrows, C. J., *Inorg. Chem.* **1999**, *38*, 4123-4127.

76. von Sonntag, C. *Free-radical-induced DNA damage and its repair*; Springer, **2006**.

77. Kerezsi, I.; Lente, G.; Fábián, I., *J. Am. Chem. Soc.* **2005**, *127*, 4785-4793.

78. Kerezsi, I.; Lente, G.; Fábián, I., *Dalton Trans* **2006**, 955-960.

79. Kerezsi, I.; Lente, G.; Fábián, I., *Inorg. Chem.* **2007**, *46*, 4230-4238.

80. Bäckström, H. L., *J. Am. Chem. Soc.* **1927**, *49*, 1460-1472.

81. Bäckström, H. L., *Trans. Faraday Soc.* **1928**, *24*, 601-605.

82. Alyea, H. N.; Bäckström, H. L., *J. Am. Chem. Soc.* **1929**, *51*, 90-109.

83. Hayon, E.; Treinin, A.; Wilf, J., *J. Am. Chem. Soc.* **1972**, *94*, 47-57.

84. Huie, R. E. In *Fossil Fuels Utilization - Environmental concerns*; ACS: ACS Symposium Series, 1986; Vol. 319, p 284-292.

85. Buxton, G.; McGowan, S.; Salmon, G.; Williams, J.; Wood, N., *Atmos. Environ.* **1996**, *30*, 2483-2493.

86. Bensasson, R.; Land, E.; Truscott, T. *Flash photolysis and pulse radiolysis: contributions to the chemistry of biology and medicine*; Elsevier, **2013**.

87. *The Nobel Prize in Chemistry 1967. Nobelprize.org. Nobel Media AB 2014.*; http://www.nobelprize.org/nobel_prizes/chemistry/laureates/1967/; accessed: 5 Sep 2015

88. *The Photochemistry Portal*; https://photochemistry.wordpress.com/2009/09/21/origins-of-flash-photolysis-george-porter/; accessed: 6 Dec 2015

89. Norrish, R. G. W.; Porter, G., *Nature* **1949**, *164*, 658.

90. Strehlow, H. *Rapid reactions in solution*; VCH Weinheim, **1992**.

91. Espenson, J. H. *Chemical kinetics and reaction mechanisms, 2nd Ed.*; McGraw-Hill: New York, **1995**.

92. Pilling, M. J.; Seakins, P. W. *Reaction Kinetics*; Oxford University Press: Oxford, U.K., **1995**.

93. Horváth, A. *Szervetlen fotokémia*; Veszprémi Egyetemi Kiadó: Veszprém, Hungary, **1998**.

94. Turro, N. J.; Ramamurthy, V.; Scaiano, J. C. *Principles of molecular photochemistry: an introduction*; University science books, **2009**.

95. Bakac, A. *Physical Inorganic Chemistry: Principles, Methods, and Models*; John Wiley & Sons, **2010**.

96. Kroó, N.; Csillag, L. *A lézerek titkai*; Móra Ferenc Könyvkiadó: Budapest, Hungary, **1987**.

97. *The Nobel Prize in Chemistry 1999. Nobelprize.org. Nobel Media AB 2014.*; http://www.nobelprize.org/nobel_prizes/chemistry/laureates/1999/; accessed: 5 Sep 2015

98. Hug, G. L., *(U.S.), N. B. S., Natl. Stand. Ref. Data Ser. (U. S., Natl. Bur. Stand.)*, NSRDS-NBS 69 1981.

99. Neta, P.; Huie, R. E.; Ross, A. B., *J. Phys. Chem. Ref. Data* **1988**, *17*, 1027-1284.

100. Dogliotti, L.; Hayon, E., *J. Phys. Chem.* **1967**, *71*, 2511-2516.

101. Dogliotti, L.; Hayon, E., *J. Phys. Chem.* **1967**, *71*, 3802-3808.

102. Lesigne, B.; Ferradini, C.; Pucheault, J., *J. Phys. Chem.* **1973**, *77*, 2156-2158.

103. Tang, Y.; Thorn, R. P.; Mauldin, R. L.; Wine, P. H., *J. Photochem. Photobiol., A* **1988**, *44*, 243-258.

104. Huie, R. E.; Clifton, C. L.; Altstein, N., *Radiat. Phys. Chem.* **1989**, *33*, 361-370.

105. McElroy, W. J.; Waygood, S. J., *J. Chem. Soc., Faraday Trans.* **1990**, *86*, 2557-2564.

106. Bonneau, R.; Carmichael, I.; Hug, G. L., *Pure Appl. Chem.* **1991**, *63*, 290-299.

107. Adams, G. E.; Boag, J. W.; Michael, B. D., *Proc. Roy. Soc. (London) A* **1965**, *289*, 321-341.

108. Adams, G. E.; Boag, J. W.; Michael, B. D., *Trans. Faraday Soc.* **1965**, *61*, 1674-1680.

109. Adams, G. E.; Boag, J. W.; Michael, B. D., *Trans. Faraday Soc.* **1965**, *61*, 1417-1424.

110. Hayon, E.; McGarvey, J. J., *J. Phys. Chem.* **1967**, *71*, 1472-1477.

111. Weeks, J. L.; Rabani, J., *J. Phys. Chem.* **1966**, *70*, 2100-2106.

112. Eriksen, T. E.; Lind, J.; Merenyi, G., *Radiat. Phys. Chem.* **1985**, *26*, 197-199.

113. Huie, R. E.; Clifton, C. L., *J. Phys. Chem.* **1990**, *94*, 8561-8567.

114. Roebke, W.; Renz, M.; Henglein, A., *Int. J. Radiat. Phys. Chem.* **1969**, *1*, 39-44.

115. Sharma, B. *Nuclear and radiation chemistry*; Krishna Prakashan Media, **1995**.

116. Jiang, P.-Y.; Nagaishi, R.; Yotsuyanagi, T.; Katsumura, Y.; Ishigure, K., *J. Chem. Soc., Faraday Trans.* **1994**, *90*, 93-95.

117. Loeffler, M.; Hudson, R.; Moore, M.; Carlson, R., *Icarus* **2011**, *215*, 370-380.

118. McElroy, W. J., *J. Phys. Chem.* **1990**, *94*, 2435-2441.

119. Dogliotti, L.; Hayon, E., *Nature* **1968**, *218*, 949-950.

120. Dogliotti, L.; Hayon, E., *J. Phys. Chem.* **1968**, *72*, 1800-1807.

121. Sadat-Shafai, T.; Pucheault, J.; Ferradini, C., *Radiat. Phys. Chem.* **1981**, *17*, 283-288.

122. Feng, C.; Tollin, G.; Enemark, J. H., *Biochim. Biophys. Acta* **2007**, *1774*, 527-539.

123. Kiss, T.; Gajda, T.; Gyurcsik, B. *Bevezetés a bioszervetlen kémiába*; Nemzeti Tankönyvkiadó, **2007**.

124. Neta, P.; Huie, R. E., *Environ. Health Perspect.* **1985**, *64*, 209.

125. Erben-Russ, M.; Bors, W.; Winter, R.; Saran, M., *Radiat. Phys. Chem.* **1986**, *27*, 419-424.

126. Erben-Russ, M.; Michel, C.; Bors, W.; Saran, M., *Free Radical Res.* **1987**, *2*, 285-288.

127. Erben-Russ, M.; Michel, C.; Bors, W.; Saran, M., *Radiat. Environ. Biophys.* **1987**, *26*, 289-294.

128. Mottley, C.; Mason, R. P.; Chignell, C. F.; Sivarajah, K.; Eling, T. E., *J. Biol. Chem.* **1982**, *257*, 5050-5055.

129. Mottley, C.; Trice, T. B.; Mason, R., *Mol. Pharmacol.* **1982**, *22*, 732-737.

130. Mottley, C.; Mason, R. P., *Arch. Biochem. Biophys.* **1988**, *267*, 681-689.

131. Ranguelova, K.; Mason, R. P., *Free Radic. Biol. Med.* **2009**, *47*, 128-134.

132. Ranguelova, K.; Chatterjee, S.; Ehrenshaft, M.; Ramirez, D. C.; Summers, F. A.; Kadiiska, M. B.; Mason, R. P., *J. Biol. Chem.* **2010**, *285*, 24195-24205.

133. Ranguelova, K.; Rice, A. B.; Lardinois, O. M.; Triquigneaux, M.; Steinckwich, N.; Deterding, L. J.; Garantziotis, S.; Mason, R. P., *Free Radic. Biol. Med.* **2013**, *60*, 98-106.

134. Ozawa, T.; Hanaki, A., *Biochem. Biophys. Res. Commun.* **1987**, *142*, 410-416.

135. Waygood, S. J.; McElroy, W. J., *J. Chem. Soc., Faraday Trans.* **1992**, *88*, 1525-1530.

136. Deister, U.; Warneck, P., *J. Phys. Chem.* **1990**, *94*, 2191-2198.

137. Fischer, M.; Warneck, P., *J. Phys. Chem.* **1996**, *100*, 15111-15117.

138. Das, T. N., *J. Phys. Chem. A* **2001**, *105*, 9142-9155.

139. Boag, J., *Trans. Faraday Soc.* **1968**, *64*, 677-685.

140. Bazin, M.; Ebbesen, T. W., *Photochem. Photobiol.* **1983**, *37*, 675-678.

141. Cassidy, J. F.; Long, C., *J. Photochem. Photobiol., A* **1990**, *54*, 1-10.

142. Bonneau, R.; Wirz, J.; Zuberbuhler, A., *Pure Appl. Chem.* **1997**, *69*, 979-992.

143. Goez, M.; Fehse, D.; Brautzsch, M., *J. Photochem. Photobiol., A* **2013**, *262*, 1-6.

144. Lin, C.-T.; Rorabacher, D., *J. Phys. Chem.* **1974**, *78*, 305-308.

145. Meagher, N. E.; Rorabacher, D. B., *J. Phys. Chem.* **1994**, *98*, 12590-12593.

146. Dunn, B. C.; Meagher, N. E.; Rorabacher, D. B., *J. Phys. Chem.* **1996**, *100*, 16925-16933.

147. Marcus, R. A.; Sutin, N., *Biochim. Biophys. Acta, Rev. Bioenerg.* **1985**, *811*, 265-322.

148. Müller, P.; Brettel, K., *Photochem. Photobiol. Sci.* **2012**, *11*, 632-636.

149. Bajcsay, P. *Matematika III. - Komplex függvények, Differenciálegyenletek*; Műegyetemi Kiadó: Budapest, Hungary, **1996**.

150. Ősz, K.; Bényei, A. *Fizikai kémia laboratóriumi gyakorlat II*; Debreceni Egyetemi Kiadó: Debrecen, Hungary, **2008**.

151. Grossweiner, L. I.; Matheson, M. S., *J. Phys. Chem.* **1957**, *61*, 1089-1095.

152. Thomas, J. K., *J. Phys. Chem.* **1967**, *71*, 1919-1925.

153. Baxendale, J. H.; Bevan, P.; Stott, D. A., *Trans. Faraday Soc.* **1968**, *64*, 2389-2397.

154. Langmuir, M. E.; Hayon, E., *J. Phys. Chem.* **1967**, *71*, 3808-3814.

155. George, C.; Chovelon, J.-M., *Chemosphere* **2002**, *47*, 385-393.

156. Yu, X.-Y.; Bao, Z.-C.; Barker, J. R., *J. Phys. Chem. A* **2004**, *108*, 295-308.

157. Matheson, M.; Mulac, W.; Weeks, J.; Rabani, J., *J. Phys. Chem.* **1966**, *70*, 2092-2099.

158. Gombár, M.; Lente, G.; Fábián, I., At *European Colloquium on Inorganic Reaction Mechanisms*, Debrecen, Hungary, **2014**. Poster 10

159. Das, A. B.; Nauser, T.; Koppenol, W. H.; Kettle, A. J.; Winterbourn, C. C.; Nagy, P., *Free Radic. Biol. Med.* **2014**, *70*, 86-95.

160. Di Bilio, A. J.; Crane, B. R.; Wehbi, W. A.; Kiser, C. N.; Abu-Omar, M. M.; Carlos, R. M.; Richards, J. H.; Winkler, J. R.; Gray, H. B., *J. Am. Chem. Soc.* **2001**, *123*, 3181-3182.

161. Morimoto, A.; Tanaka, M.; Takahashi, S.; Ishimori, K.; Hori, H.; Morishima, I., *J. Biol. Chem.* **1998**, *273*, 14753-14760.

162. Pattison, D. I.; Lam, M.; Shinde, S. S.; Anderson, R. F.; Davies, M. J., *Free Radicals in Biology and Medicine* **2012**, *53*, 1664-1674.

163. Reece, S. Y.; Stubbe, J.; Nocera, D. G., *Biochim. Biophys. Acta, Bioenerg.* **2005**, *1706*, 232-238.

164. Stevenson, K. L.; Papadantonakis, G. A.; LeBreton, P. R., *J. Photochem. Photobiol., A* **2000**, *133*, 159-167.

165. Pileni, M.; Bazin, M.; Santus, R., *Chem. Phys. Lett.* **1977**, *51*, 61-64.

166. Kohen, E.; Santus, R.; Hirschberg, J. G. *Photobiology*; Academic Press, **1995**.

167. Tsentalovich, Y. P.; Snytnikova, O. A.; Sagdeev, R. Z., *J. Photochem. Photobiol., A* **2004**, *162*, 371-379.

168. Redpath, J. L.; Santus, R.; Ovadia, J.; Grossweiner, L. I., *Int. J. Radiat. Biol.* **1975**, *27*, 201-204.

169. Marquez, L. A.; Dunford, H. B., *J. Biol. Chem.* **1995**, *270*, 30434-30440.

170. Nagy, P.; Kettle, A. J.; Winterbourn, C. C., *Free Radic. Biol. Med.* **2010**, *49*, 792-799.

171. Kraljić, I., *Int. J. Radiat. Phys. Chem.* **1970**, *2*, 59-68.

172. Kumar, A.; Neta, P., *J. Am. Chem. Soc.* **1980**, *102*, 7284-7289.

173. Fronaeus, S., *Acta Chem. Scand.* **1986**, *40*, 572-578.

174. Matthews, R.; Sworski, T., *J. Phys. Chem.* **1975**, *79*, 681-686.

175. Buxton, G. V.; Wang, J.; Salmon, G. A., *Phys. Chem. Chem. Phys.* **2001**, *3*, 2618-2621.

176. Bansal, K. M.; Fessenden, R. W., *Radiat. Res.* **1976**, *67*, 1-8.

177. Fornier de Violet, P.; Bonneau, R.; Logan, S. R., *J. Phys. Chem.* **1974**, *78*, 1698-1701.

178. Treinin, A.; Hayon, E., *J. Am. Chem. Soc.* **1975**, *97*, 1716-1721.

179. Lilie, J.; Hanrahan, R.; Henglein, A., *Radiat. Phys. Chem.* **1978**, *11*, 225-227.

180. Zuo, Z.; Cai, Z.; Katsumura, Y.; Chitose, N.; Muroya, Y., *Radiat. Phys. Chem.* **1999**, *55*, 15-23.

181. Tsona, N. T.; Bork, N.; Vehkamäki, H., *Atmospheric Chemistry and Physics* **2015**, *15*, 495-503.

182. Turing, A. M., *Philos. Trans. R. Soc., B* **1952**, *237*, 37-72.

183. Miura, T.; Maini, P. K., *Anat. Sci. Int.* **2004**, *79*, 112-123.

184. Vanag, V. K.; Epstein, I. R., *Chaos* **2007**, *17*, 037110.

185. Horváth, J.; Szalai, I.; De Kepper, P., *Science* **2009**, *324*, 772-775.

186. Gáspár, V., *Káosz és rend kémiai rendszerekben: káoszszabályozás és mintázatképződés*, MTA Doktori Értekezés, Debreceni Egyetem, Debrecen, Hungary, **2000.** and references therein

187. Csörgeiné Kurin, K.; Gáspár, V.; Horváth, D.; Orbán, M.; Szalai, I.; Tóth, Á., *Nemlineáris dinamika: Önszerveződés kémiai és biológiai rendszerekben*, Szegedi Tudományegyetem, Szeged, Hungary, **2013.**
http://www2.sci.u-szeged.hu/physchem/nld/ejegyzet/nld.html, 17 Dec 2015

188. Kovács, B., *Semilinear parabolic problems*, Master's Thesis, ELTE:**2011.** and references therein

189. *Wolfram MathWorld*; http://mathworld.wolfram.com/FiniteDifference.html; accessed: 17 Dec 2015

190. *The finite difference method*; http://www.ann.jussieu.fr/~frey/cours/UdC/ma691/ma691_ch6.pdf; accessed: 17 Dec 2015

191. Faragó, I.; Horváth, R. *Numerikus módszerek* Budapest, Hungary, **2011**.

List of publications

(in reverse chronological order)

Publications connected to this dissertation

4. Éva Dóka, Gábor Lente
Modelling studies of inhomogeneity effects during laser-flash photolysis experiments: a reaction-diffusion approach
manuscript in preparation

3. Éva Dóka, Gábor Lente, István Fábián
The reactivity of the sulfate ion radical
manuscript in preparation

2. Éva Dóka, Gábor Lente, István Fábián
Kinetics of the autoxidation of sulfur(IV) co-catalyzed by peroxodisulfate and silver(I) ions
Dalton Transactions, **2014**, *43*, 9596-9603. IF: 4.197

1. József Kalmár, Éva Dóka, Gábor Lente, István Fábián
Aqueous photochemical reactions of chloride, bromide, and iodide ions in a diode-array spectrophotometer. Autoinhibition in the photolysis of iodide ions
Dalton Transactions, **2014**, *43*, 4862-4870. IF: 4.197

Publications not connected to this dissertation

5. Éva Dóka, Irina Pader, Adrienn Bíró, Katarina Johansson, Qing Cheng, Krisztina Ballagó, Justin R. Prigge, Daniel Pastor-Flores, Tobias P. Dick, Edward E. Schmidt, Elias S. J. Arnér, Péter Nagy
Novel persulfide detection method reveals protein persulfide and polysulfide reducing functions of thioredoxin- and glutathione-systems
Science Advances, **2016**, *2*, e1500968. IF: N/A

4. Anita Vasas, Éva Dóka, István Fábián, Péter Nagy
Kinetic and thermodynamic studies on the disulfide-bond reducing potential of hydrogen sulfide
Nitric Oxide, **2014**, *46*, 93-101. IF: 3.521

3. D. Peralta, A.K. Bronowska, B. Morgan, É. Dóka, K. v. Laer, P. Nagy, T.P. Dick
A proton relay enhances H_2O_2 sensitivity of GAPDH to facilitate metabolic adaptation
Nature Chemical Biology, **2015**, *11*, 156-63. IF: 12.996

2. Éva Dóka, Gábor Lente
Stochastic mapping of the Michaelis-Menten mechanism
Journal of Chemical Physics, **2012**, *136*, 054111. IF: 3.164

1. Éva Dóka, Gábor Lente
Mechanism-Based Chemical Understanding of Chiral Symmetry Breaking in the Soai Reaction. A Combined Probabilistic and Deterministic Description of Chemical Reactions
Journal of the American Chemical Society, **2011**, *133*, 17878-17881. IF: 9.907